ELECTROCHEMICAL INVESTIGATIONS OF THERMODYNAMIC AND STRUCTURAL ASPECTS OF THE INTERFACE BETWEEN TWO IMMISCIBLE ELECTROLYTE SOLUTIONS

by

HAILEMICHAEL ALEMU

A Dissertation

Submitted to the School of Graduate Studies

Addis Ababa University

In Partial Fulfillment for the

Degree of Doctor of Philosophy in Chemistry

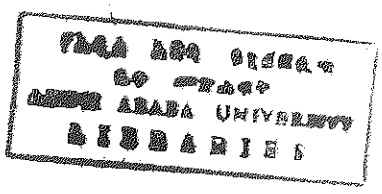

Department of Chemistry

Faculty of Science

February 1991

To Menbere and Simret

ADDIS ABABA UNIVERSITY

ABSTRACT

FACULTY OF SCIENCE

CHEMISTRY

Doctor of Philosophy

ELECTROCHEMICAL INVESTIGATIONS OF THERMODYNAMIC AND STRUCTURAL ASPECTS OF THE INTERFACE BETWEEN TWO IMMISCIBLE ELECTROLYTE SOLUTIONS.

by Hailemichael Alemu

Simple ion transfer across the immiscible water/o-nitrotoluene, water/benzonitrile and water/o-dichlorobenzene interfaces has been studied using ac and dc cyclic voltammetry. The standard Gibbs energies of transfer from water to the organic solvents for several ions have been determined. The results are compared with theoretical values calculated using the model of ionic solvation.

The transfer across the immiscible water/nitrobenzene interface of transition metal (Fe, Co, Ni, Cu and Zn)-terpyridine complexes has been studied using ac and dc cyclic voltammetry, linear sweep voltammetry and absorption spectroscopy. From the voltammetric measurements and convolution integral analysis, thermodynamic and transport properties have been evaluated. The transfer behaviour of cuprous ion across the water/1,2-dichloroethane interface facilitated by 2,2'-biquinoline has been studied and the mechanisms for the transfer process are proposed.

The structure of the electrical double layer at the water/o-nitrotoluene and water/o-dichlorobenzene interfaces containing different base electrolytes with different concentrations has been studied by impedance measurements. The capacitance values obtained from experiments have been compared with the values calculated from the Gouy-Chapman theory. Analysis of the results has indicated the absence of specific adsorption at the water/o-nitrotoluene interface.

ACKNOWLEDGEMENTS

I would like to thank my supervisor, Dr. Theodros Solomon for his sustained interest, continued help and advice throughout this period of study. I would also like to thank Dr. B. Hundhammer for his participation and constant advice on all aspects of the research.

I also wish to thank Professor D.J. Schiffrin, currently, professor of physical chemistry, Department of Chemistry, University of Liverpool, who gave me the opportunity to work in his laboratory at the Department of Chemistry, the University Southampton (UK).

My thanks must also go to Professor K. Juttner, Institute of Physical chemistry and Electrochemistry, Karlsruhe University for his unreserved encouragement, help and advice during my studies in F R.G.

I am grateful to Dr. Y. Cunnane, Dr. L. Berlouis, Mr. Yufei Cheng, Mr. S. Kaufman and Ato Demeke Kifle for their assistance and good friendship during my stay in Southampton.

I would also like to thank members of the Chemistry Department of Addis Ababa University for the kindness which they have shown towards me throughout the period of this work. In particular the help of Dr. Wondimagegn Mamo and Ato Tekle Habte is greatly appreciated.

The financial support by Swedish Agency for Research Co-operation with Developing Countries (SAREC) is greatly acknowledged.

CONTENTS

TABLES

FIGURES

CHAPTER ONE

LITERATURE REVIEW

1.1 INTRODUCTION

In the first decade of this century, Nernst and Riesenfeld [1,2] began their studies of the water/phenol/water interfaces in an attempt to model biological membranes. Using electrolytes partitioned in the two liquids they observed the transfer of ions during the passage of current through the system. They theoretically predicted, and experimentally demonstrated, the accumulation and depletion of the transported ions at the interface depending on the direction of the current and on the values of the transport numbers. Their main interest was in determining the transport number of an ion in the organic phase. Following this innovative work, investigations of the interface between two immiscible electrolyte solutions, ITIES, raised special interest in the area of physiology [3]. For several decades thereafter research on ITIES was focused on the study of equilibria or steady state electrical potential differences between aqueous and organic phases in the presence of different electrolytes [4].

Bauer and Kronman [5] investigated the ITIES by adding a picrate or tetramethylammonium salts in the aqueous phase. The potential differences were interpreted as ionic adsorption potentials. Such types of studies were extended to show the dependence of the equilibrium potential differences on the partition coefficients of salts dissolved between water and the organic liquid [6]. However, the measured potential differences across the water /oil / water interfaces did not show significant changes when the concentration of the salts were varied in one of the aqueous components. Consequently, this observation had been the subject of significant contention for several years. Beutner [4,6] explained the phenomena in terms of the free charge at the oil / water interface, which arose as a consequence of unequal distribution of the ions across the interface, whereas Bauer [5,7,8], Ehrensvärd and Sillen [9,10] viewed the potential differences as adsorption

potentials or surface potential differences arising due to specific ionic adsorption.

Dean et al. [11,12] demonstrated theoretically that Beutner's proposal was correct and that the measured potential difference was a volta potential difference (outer potential difference).

Kahlweit et al. [13,14] estimated the concentration gradient of different ions in quinoline/HCl system and quantified many components of the membrane potential by splitting it into a phase boundary potential and diffusion potential.

Davies and Rideal [15,16] determined surface and diffusion potentials and justified the idea of Beutner by illustrating that the adsorption potential would not be observable for a water/polar-organic solvent system since interfacial double layers could be formed. They indicated, however, that this potential would be inevitable if the organic solvent used were non-polar. The results of these investigations settled the long-lived dispute of Beutner and Bauer concerning the principle and origin of the electrical potential differences at the ITIES.

In the mid - 1950's, new investigations on ITIES started under the flow of current. A change in the interfacial tension of ITIES was observed during the flow of current across the interface [17]. This alteration of the interfacial tension was believed to be due to electroadsorption. It was assumed that it was induced by the electric field arising at the electrode during the process of current flow.

Watanabe et al. [18,19] studied electroadsorption phenomena and obtained electrocapillary curves for different systems. These authors observed changes in the interfacial tension with changes in the type of anions and cations present in the systems. Blank and Feig [20] did experiments to reveal the difference between electrocapillarity and electroadsorption. In a subsequent investigation Blank [21] studied the effects due to the flow of current across a

water/nitrobenzene interface in the presence of a cationic surface active agent. He illustrated that the effect of electroadsorption was exclusively due to the accumulation or depletion of surface active electrolytes at the interface and concluded that electroadsorption was due to migrational mass transfer control.

Dupeyrat and Michel [22,23] investigated the mechanism of electroadsorption at ITIES and drew a conclusion that the variation in the interfacial tension as a function of applied potential could not be described only by electrocapillary adsorption. A similar approach was utilized by Joos et al. [24,25], who interpreted the shift of the interfacial tension during the flow of current as being due to a difference in transport numbers of the cations in both phases.

D'Epenoux et al. [26,27] also carried out similar investigations and accounted for the variation of the interfacial tension in terms of the change of the ionic concentration in the interfacial layer due to the ion transfer between the two immiscible solutions. All these investigations on the electroadsorption phenomena endorsed the interpretation introduced by Blank.

The electrical phenomena of the current-potential relationship at ITIES were carefully examined by Gavach and co-workers [28,29]. These authors showed for the first time that ITIES is polarizable when the salt dissolved in the organic phase is hydrophobic and the salt in the aqueous phase is hydrophilic. Afterwards these authors investigated the ITIES in much detail [30-32]. The overpotential of the ITIES was studied by splitting it into the ion transfer overvoltage and the diffusion overvoltage. The results obtained were qualitatively identical to those obtained for metal/electrolyte solution systems under mass transfer control for the ion studied [31,32]. They also estimated kinetic parameters for the transfer of tetraalkylammonium ions [33].

Guastalla [34,35] proceeded with the polarizability of ITIES with a four-electrode set up and measured the current flowing across the ITIES as a function of an applied triangular voltage wave. However, the obtained current

potential curves were severely distorted due to the absence of potentiostatic control. These preliminary investigations on the polarization of the ITIES were the basis which led to an improvement of the currently used electrochemical techniques.

The contemporary interest on ITIES, that it could serve as a simple model representing one-half of a biological membrane, and that it can have analytical applications, was initiated by Koryta et al. [36]. A comprehensive review of the ITIES, comparing it to the metal/electrolyte solution interface, was presented for the first time [37] in 1979. In the same year a mathematical relationship between the Galvani potential and the current for a charge transfer reaction at ITIES was derived [38]. The equilibrium conditions and the Galvani potential difference across the ITIES was also examined by different authors [39-42].

The irreversible ion transfer behavior at ITIES for a single ion [43] and for two ions [44,45] was treated by Melroy and Buck. These workers pointed out the differences between the process of ion transfer at ITIES and electron transfer at the metal/electrolyte solution interface, namely : (i) diffusion and migration of ions should be treated with the help of the Nernst-Planck equation, (ii) because of salt equilibria, interfacial transport of ions of opposite signs must be considered and (iii) partition equilibrium is a non-linear ionic process that can lead to equations without analytical solutions.

In the last two decades most of the investigations on ITIES were focused on the development of electrochemical techniques and cell designs.It has been shown that most standard electrochemical techniques could be applied without any complications, once a defined and accurate potential difference could be set up at the interface, and the iR drop in the organic phase could be properly compensated.

An electrolyte dropping electrode (EDE) was designed and tested for polarographic investigation of the ITIES [36,46] by Koryta et al.. Samec et al.

[47-49] demonstrated that the charge transfer processes across ITIES could be well observed using cyclic voltammetry with a four-electrode potentiostat coupled with a positive feedback for the elimination of the ohmic drop. A six electrode cell arrangement was also proposed [50] For most ITIES studies, however, the four-electrode potentiostat has been found to be satisfactory. Other experimental methods employed for the electrochemical investigation of the ITIES include : (i) the use of convolution potential sweep voltammetry (CPSV) as applied to the quantitative analysis of the linear sweep or cyclic voltammetric data on ion or electron transfer [51,52]; (ii) the use of three-electrode system with a hanging electrolyte drop electrode [53]; (iii) potential-step chronopotentiometry [54]; (iv).current scan polarography at the ascending water electrode (AWE) [55]; (v) alternating current cyclic voltammetry [56]; (vi) ac impedance with a phase-selective ac polarography [57]; (vii) ac bridge impedance [58]; (viii) maximum bubble pressure method [59]; (ix) video image digitizing technique for measuring the interfacial tension of a pendant (sessile) drop [60,61]; (x) fast performance galvanostatic pulse method for the evaluation of both capacitance and ohmic potential drop in the studies of the double layer and kinetics of ion transfer [62-64].

The classical streaming method has been extended for the determination of the potential of zero charge at ITIES [65]. The technique of chronopotentiometry with cyclic linear current scanning was fully developed, (both theoretically and experimentally), for the investigation of ion transfer at ITIES [66-67]. A polyvinyl chloride/nitrobenzene gel electrode and an agar/water gel electrode was introduced for the analytical application of ITIES [68]. A hydrophilic cellulose membrane was employed to separate the aqueous electrolyte phase from the organic phase in ITIES investigations [69]. A liquid / liquidmicroelectrode analogous to a metallic micro electrode was developed and used for the studies of facilitated ion transfer and ion transfer kinetics

[70,71]. Further a liquid/liquid multi-micro electrode was designed and used by employing a membrane with well-defined pore size [72]. Semi-differential cyclic voltammetry was applied by coupling a semi-differential transformer to a four electrode potentiostat [73]. An amperometric detector based on a membrane stabilized ITIES was developed and tested in a flow injection system for the determination of ionic species [74]. Very recently, a silver/silver tetraphenyl borate reference electrode was introduced for electrochemical studies of ITIES [75].

1.2 ION TRANSFER AND ION TRANSFER KINETICS

Simple ion transfer is one kind of charge transfer process across ITIES which has been thoroughly studied by many investigators. The phenomena of ion transfer and ion transfer kinetics have been examined experimentally with the aid of various electrochemical methods which have been discussed in the previous part of this chapter. The purpose of this section is to mention the different types of ions which have been investigated in a variety of water/organic solvent systems .Details have been given in literature reviews [37,76-84]. The rate of ion transfer across ITIES is fast enough to be classified as reversible [83,84]. In some instances, the kinetics of the ion transfer have been determined. Studies of diffusion controlled ion transfer allow the evaluation of diffusion coefficients, the determination of thermodynamic quantities such as standard Gibbs energy of transfer, and also the analytical determination of transferable ions.

1.2.1 *REVERSIBLE ION TRANSFER*

The process of ion transfer is rather fast as shown by many experimental results. Under proper conditions electrochemical measurements can be carried out for reversible diffusion controlled transfer process with the help of electroanalytical methods developed for metallic electrodes [47], since the boundary conditions at ITIES can be approximated to those applicable to the metal / electrolyte solution interface.

With a help of a four electrode potentiostat, and cyclic voltammetry Samec et al. [48] studied the diffusion controlled reversible transfer of TMA^+ ion across the water/ nitrobenzene interface. The transfer of Cs^+ ion was also investigated [48]. The transferred ions showed reversible behaviour by fulfilling the commonly used criteria for reversible charge transfer processes.

The transfer of the picrate ion was similarly shown to behave reversibly [49]. However, such investigations for anions like ClO_4^-, SCN^-, and NO_3^- showed only voltammetric peaks due to the transfer of these ions from the organic phase to water, while the reverse peaks were accompanied by the simultaneous transfer of the base electrolyte tetrabutylammonium ion (TBA^+). The introduction of a more hydrophobic base electrolyte like the cation of crystal violet (CV^+) in the organic phase eliminated this limitation and enabled the studies of n-octoate, picrate, laurylsulphate, SCN^-, ClO_4^-, I^-, Br^- and NO_3^-, ions [85,86].

The water/nitrobenzene interface has received much attention for the following reasons : the very low solubility of water in nitrobenzene (0,34 % by weight); very low electrical resistance; relatively high solubility of electrolytes; high dielectric constant (35), large specific density (1.2 g/cm^3) and low vapor pressure. As a consequence many ion transfer investigations has been made in this system. Some of these include the transfer of fifteen different alkylammonium ions [87] for which the reversible half wave potentials and the standard Gibbs energies of transfer have been determined. Apart from these, other ions that have been studied include acetylcholine and choline [88], dialkylviologen cations, tris-(2,2`-bipyridine) ruthenium (II) [89,90], and CV^+ ion, [86]. For the anions ,in addition to the previous ones, tetrafloroborate (BF_4^-), F^-, IO_4^-, ClO_3^-, BrO_3^-, [91,92], I^- and its complexes (I_3^- and I_5^-) [93], the acidic dye bromophenol blue (BPB), bromocresol green [94], and different types of acidic and basic dyes [95], 12-tungstosilicate ($[SiW_{12}O_{40}]^{4-}$)[96], and very recently, the 12-molybdophosphate ($[PMo_{12}O_{40}]^{3-}$) and 18-molybdophosphate ($[P_2Mo_{18}O_{62}]^{6-}$) [97] have been investigated across the water/nitrobenzene interface.

Makrlik and Hung [98] studied the transfer of several univalent cations (H^+, Li^+, Na^+, K^+, Rb^+, Cs^+, and TMA^+) and the dipcrylaminate (DPA^-)

anion as a function of temperature in the range 5-65 ^{0}C and calculated the associated changes in the enthalpy and entropy of the transfer. The results indicated that the transfer of all ions from the aqueous to the organic was accompanied by an entropy drop.

The transfer of ions at the water/1,2-dichloroethane (1,2-dce) interface was also investigated by many workers. The transfer of the cations tetraalkylammonium and Cs^+ and of the anions: Pi^-, IO_4^-, ClO_4^-, BF_4^-, I^-, SCN^-, and NO_3^- was studied using different electrochemical techniques [91,99,100]. Similar ion transfer studies for halides, their oxo-acid anions and other polyatomic anions were also carried out [92].

Very recently Samec et al. [101] made revised experiments for the transfer of alkali metal ions (Li^+, Na^+, K^+, Rb^+, and Cs^+) both at the water/nitrobenzene and water/1,2-dce interfaces. These authors claimed that the values of the standard Gibbs energies of transfer from water to nitrobenzene agree well with those data in the literature, while their values from water to 1,2-dce deviate from the literature values. They have remarked that the already reported data should be amended.

The water/isobutyl methyl ketone interface was examined by Koczorowski et al. [102] for the reversible transfer of TEA^+, tetrapropylammonium ($TPrA^+$) and I^- ions. However the applicable potential window of this system is too narrow to extend the investigation to other ions.

Solomon et al. [103] investigated the transfer of several ions at the water/acetophenone interface and demonstrated that this system does provide a reasonable polarization window; however, the mutual solubility of the two phases imposes a limitation. The water/mixed-organic-solvents system, where the organic mixtures were nitrobenzene and benzonitrile[104]; nitrobenzene and benzene [102]; nitrobenzene and chlorobenzene [105] were also studied. It has been suggested that studies of systems containing organic mixtures could assist in fully understanding the ion and electron transfer mechanisms across

ITIES [84].

In addition to the above solvent systems, investigations of ion transfer across the water/dichloromethane [106], water/chloroform [92] , water/o-nitrophenyloctyl ether [107], water/o-nitrotolune and water/benzonitrile [108,109] (the latter two in the course of the present work) and, very recently, the water/nitroethane [110] interfaces were carried out.

The transfer of acetylcholine, methyl viologen, Cs^+, Pi^-, and ClO_4^- ions across a polyvinyl chloride+nitrobenzene gel/water interface were examined by Marecek and Colombini [111]. These authors accounted for the observed shift in the half wave potentials of the ion transfer in terms of the low values of the diffusion coefficient of the ions in the gel phase, but other researchers claim that such variation arises mainly due to changes in the Gibbs hydration energy rather than changes in transport parameters [112].

Geblewicz et al. [113] studied the increase in the polarization window of electrified liquid interfaces due to salting out effects of the organic electrolyte by varying the aqueous base electrolyte concentration. This kind of analysis could help in determining the optimum concentration of the base electrolyte to be used in order to provide the widest possible polarization window.

Certain electroneutral species are capable of accepting protons to form cations which may then transfer across the ITIES. Such transfers have been detected for aniline [114], benzylamine, 2-phenylethylamine and related compounds [115], tetracycline, tetracycline derivatives, and terramycin [116]. Such investigations have very important applications in pharmaceutical analysis.

1.2.2 *ION TRANSFER KINETICS*

Studies of ion transfer kinetics were started by Gavach and Henry

[30,33], who investigated the transfer of tetraalkylammonium ions across the water/nitrobenzene interface with the help of chronopotentiometry. They determined the kinetic parameters of the transferred ions by employing the theoretical treatment established for electron transfer at the metal/electrolyte solution interface.

Samec [117] attempted to elucidate the fundamentals of the kinetics of ion and electron transfer processes at ITIES. Convolution potential sweep voltammetry experiments were carried out to analyze the potential dependence of the rate constant [52]. The apparent rate constant was corrected for the double layer effect using the capacity data and the Gouy-Chapman theory. From the obtained result it was concluded that the corrected rate constant of Cs^+ ion transfer was independent of the applied Galvani potential difference.

Melroy et al. [45,118,119] analyzed ion transfer kinetics obtained by chronopotentiometry in relation to the structure of the ITIES. From their observations they pointed out that the transfer coefficients do depend on the potential and on the non-aqueous supporting electrolyte concentration, a behavior which is not common to a metal/electrolyte solution interface. Further, Samec et al. [120] evaluated kinetic parameters for the transfer of choline and acetylcholine cations across the water/nitrobenzene interface using convolution potential sweep voltammetry. In order to single out the factors which control the ion transfer kinetics they used a semiphenomenological theory [120]. This theory is based on the following assumptions: the temperature dependence of the rate constant has the form of the Arrehnius equation; it is assumed that the reaction site is located in the outer Helmholtz plane (OHP); and it is presumed that a Bronsted type relationship exists between the true activation Gibbs energy and the reaction Gibbs energy for the ion transfer from the OHP in water to that in the organic solvent phase. The values obtained of the charge transfer coefficient were accounted for in terms of an asymmetric potential energy barrier for the ion transfer step.

The kinetics of TMA^+, and Pi^- ion transfer across the water/nitrobenzene interface was investigated with the help of ac polarography [57]. The results obtained demonstrated that both the observed rate constants and the apparent transfer coefficient values are potential dependent. This observation indicates that the double-layer corrections alone could not explain the potential dependence of the ion transfer at ITIES [84].

A new formalism for the analysis of the kinetics of ion transfer across ITIES was presented based on the activated migration and diffusion transport models for homogeneous media [121]. Two types of transfer coefficients were defined namely, chemical and electrical. By employing a primitive diffuse layer model, it was shown that the electrical component of the transfer coefficient is strongly potential dependent. It was suggested that (i) the formalism of homogeneous ion mobility can be applicable to the case of ion transfer at ITIES, (ii) the commonly used transfer coefficient for electron transfer kinetics cannot be used in the same way for ITIES, and (iii) the direct application of electron transfer theories of the electrode/electrolyte solution interface to the ITIES seems to be incorrect.

Samec and Marecek [64] re-examined the transfer kinetics of some tetraalkylammonium ions with the galvanostatic pulse technique. The data obtained indicated that, on crossing the interface, the ion must overcome a symmetric potential energy barrier. Gurevich and Kharkhats [122] by considering ion transfer as a transport phenomena, used a stochastic approach and drew a conclusion that there exists an activated step in which the shape of the activation energy barrier is influenced by the applied potential.

Further work on the ion transfer kinetic was carried out by Samec et al. [123] by taking into account the reorganization of the solvent molecules and based on the model given in ref. 122. The results showed that the activation energy of the transfer of tetraalkylammonium ions across the water/nitrobenzene interface was found to be in the range between 20 and 30

$kJ\ mol^{-1}$.

Kinetics of salt extraction into high-permitivity oil phase has been presented by Koryta et al. [124,125]. From such analysis an extraction potential can be evaluated, provided the rate constants and the form of the kinetic equation are known.

The kinetics of ion transfer across adsorbed phospholipid layers was investigated by Cunnane et al. [126] by taking TEA^+ as a probe. The observed decrease of the rate constant of the ion transfer was explained in terms of the work of pore formation. The kinetics of K^+ ion transfer at the water/1,2-dce interface has been recently analyzed by Kontturi et al. [127]. These authors observed Tafel slope of 40 mV/decade which corresponds to a value of β, the transfer coefficient of the transfer of the ion pair components from the adsorbed state to the bulk of both phases, of 1/2.

Recently Girault [128] presented a general formalism which allows to express the apparent rate constant as a function of the applied Galvani potential difference, the standard rate constant and the charge transfer coefficient. The facilitated transfer of K^+ ion across the water/1,2-dce interface supported at the tip of a micropipette was studied [71]. The apparent rate constant and the apparent charge transfer coefficient were determined by analyzing quasi-reversible steady state waves.

Wang et al. [129] examined the equilibrium Galvani potential difference at ITIES and pointed out some of the factors that influence the rate of ion transfer. Very recently a kinetic study of ion transfer facilitated by crown ethers has been reported [130], in which it has been observed that the potential dependence of the rate constant is highly sensitive to the stability constant of the complex in the organic phase.

1.3. FACILITATED ION TRANSFER

The number of transferable ionic species across ITIES is limited by the transfer of the base electrolytes dissolved in either of the two phases at the extreme ends of the potential window. However, in the presence of a hydrophobic ligand (ion carrier or ionophore) in the organic phase, the transfer of hydrophilic ions from the aqueous phase to the organic phase can be facilitated if complex formation between the two takes place. The details of the mechanism of complexation have been given in review articles [83,84].

The introduction of this idea to ITIES was pioneered by Koryta et al. [49,131,132], who studied in their original work the transfer of alkali metal ions facilitated by macrotetrolide nonactine, dibenzo-18-crown-6, and valinomycin across the water/nitrobenzene interface. When the concentration of the alkali metal ions in the aqueous solution was higher than that of the ionophore in the organic phase, reversible transfer behavior was observed, but these early investigations were limited by the transfer of the tetraphenylborate (TPB^-) anion in the positive potential range. From such studies stability constants of the complexes formed could be evaluated.

The transfer of Ca^{2+} facilitated by synthetic neutral macrocyclic polyether diamide (7,19-dibenzyl-2,3-dimethyl-7,19-diazo-1,4,10,13,16-penta-oxacycloheneicosane-6,20-dione) was studied by Homolka et al. [133]. These workers applied the theory of CPSV to analyze the partial kinetic controlled transfer process. The transfer of monovalent, divalent, and trivalent cations facilitated by the above ionophore was also observed to a lesser extent.

A theory for single scan voltammetry curves due to assisted ion transfer for the complex formed from 1:1, 1:2, or 1:3 cation to ligand ratios was worked out [134]. Application of the theoretical results was illustrated for the transfer of Li^+ and Ca^{2+} ions facilitated by the neutral macrocyclic polyether diamine across the water/nitrobenzene interface. A continuation of

this work later appeared for the facilitated transfer of proton, alkali and alkaline earth metal cations [135].

Makrlik et al. [136] reported proton transfer across ITIES facilitated by 2,4-dinitro-N-picryl-1-naphthylamine. Na^+ and H^+ ion transfer across the water/nitrobenzene interface facilitated by the presence of monensin (a carboxylic ionophore) in nitrobenzene was studied by Koryta et al. [137] who obtained two different association constants depending on the Na^+ ion and H^+ concentrations.

The transfer of Mg^{2+}, Ca^{2+}, Sr^{2+} and Ba^{2+} ions facilitated by a macrocyclic polyether diamide (N,N'-di/(11'-ethoxycarbonyl)undecyl/-N,N'-5-tetramethyl-3,6-dioctane diamide) was studied using differential pulse stripping voltammetry with a hanging electrolyte drop electrode [138] This communication revealed the analytical application of the method in determining micro-molar concentrations of the metals.

The site of complex formation and dissociation between a metal cation and an ionophore at liquid/liquid interface has remained a point of discussion. According to Koryta [37] complexation takes place in the organic phase in the presence of a hydrophobic carrier or ionophore, whereas Yoshida and Freiser believe that the complex formation occurs in the aqueous phase, following the transport of the carrier from the organic to the aqueous phase even with ionophores having low water solubility [55,139]. In a latter communication Koryta et al. [140] described the observed voltammogarams of ref. 139 to have been due to, not facilitated ion transfer, but rather simple ion transfer.

The transfer of proton facilitated by dipicrylaminate, erythromycin B, 2,2'-bipyridine, the irreversible transfer of Ni^{2+} by 2,2'-bipyridine and the reversible transfer of synthesized rare earth complexes with crown ether across the water/nitrobenzene interface has been reported [141,142]. The transfer of transition metal ions such as Fe(II), Fe(III), Ni(II) and Zn(II) complexed by bidentate nitrogen ligands in the aqueous phase has been studied

by Homolka and Wendt [143]. These authors showed that complexation of Ni(II) by successive molecules of ligands change the Gibbs energy of transfer by approximately the same value. Sinru et al. [144,145] examined the K^+ ion transfer at the water/1,2-dce interface facilitated by urushiol ether and dibenzo 18-crown-6. They formulated a mechanism whereby, for low K^+ ion concentrations, the complexation reaction occurs in the aqueous phase, whereas, for high concentration of K^+ ion, the interfacial region is the site of complexation.

The facilitated transfer of Cd(II) by 1,2-bipyridine has been reported by Wang and Liu [146] who observed the peak to peak separation of the cyclic voltammogram of the complex to be larger than the one expected for a simple reversible behaviour. The transfer of alkali metals and alkaline earth metals assisted by polyoxyethylene ethers of Triton X (with flexible structures) was investigated and the values of the Gibbs energy of transfer were reported [147]. Transfer of the H^+ ion facilitated by 18-crown-6 [148] and by acridine chloride [149] was also studied. The transfer of trisbipyridine transition metal complexes across the water/1,2-dce interface has been investigated and the observed changes due to ligand dissociation and solvolysis reactions have been explained [150].The transfer of Li^+ ion facilitated by mydecamycin was also reported [151].

Liu and Wang [152] studied the transfer behavior of Co(II) ion across the water/nitrobenzene interface facilitated by 2,2'-bipyridine. They interpreted the results obtained in terms of coupled chemical reactions occurring both in the aqueous and in the organic phase. However these authors did not pay attention to the possible formation of Co(III)/2,2'-bipyridine complex while working with air saturated solutions.

Very recently Baruzzi and Wendt [153] reported the transfer of Ni(II) complexed with some selected substituted ethylene diamines across the water/nitrobenzene interface. These workers gave a clear evidence for the fast

formation of tris-complexes in the reaction layer of both phases and the enhancement of the extraction of Ni(II) in the organic phase. Moreover the obtained stability constants of the complexes in the organic phase are higher by five orders of magnitude than those in the aqueous phase.

In a recent publication the transfer behaviour of Pb(II) facilitated by polyethlyne glycols has been reported [154]. The transfer Gibbs energy and the dissociation constant of the complex in the aqueous phase have been determined.

1.4 ELECTRON TRANSFER

The other type of charge transfer process occurring at ITIES is the transfer of electron(s) from one phase to the other due to the presence of redox couples confined in each phase. This kind of charge transfer process has incited great interest since it is believed that it may shed some light to certain bioelectrochemical phenomena taking place at the membrane/electrolyte solution interface [77].

Electron transfer at ITIES was first detected by Guainazzi et al. [155] who studied the reduction of aqueous Cu(II) by tetrabutylammonium hexacarbonylvanadate dissolved in the organic phase. Later, Samec [38] derived the relationship between the current and the Galvani potential difference due to electron transfer at ITIES. In an ensuing investigation the electron transfer reaction between hexacyanoferrate redox couple in water and ferrocene in nitrobenzene was reported [156]. However at a later stage a revised experiment on the above system [157] indicated the interference due to the transfer of the ferrocenium cation with the electron transfer reaction between ferrocene in nitrobenzene and hexacyanoferrate(III) in water. Therefore electron transfer reactions which have been reported for the system between Fe(III)/Fe(II) or Cu(II)/Cu(I) redox couple in water and ferrocene or acetylferrocene in nitrobenzene [158] have to be reconsidered.

Theoretical potential-time curves for electron transfer processes proceeding at ITIES under galvanostatic conditions were derived by Makrlik [159]. A similar formulation for an electron transfer reaction preceding homogeneous chemical reactions under the conditions of electrolyte dropping electrode was presented [160] and the possible use of the theory of linear sweep voltammetery for a reversible electron transfer was discussed [161].

A general theory of electron transfer at ITIES was presented by Girault and Schiffrin [162]. In a subsequent work Geblewicz et al. [163] studied the

electron transfer between a very hydrophobic organic compound (lutetium diphthalocyanine) in 1,2-dce and an aqueous hexacyanoferrate couple. Such investigation was extended to tin(IV) diphthalocyanine in the organic phase [164]. In this latter study emphasis was made on the important applications in redox phase transfer catalysis .

The electrochemical measurement of a photocurrent across the ITIES was carried out using a ruthenium 2,2′-bipyrindinium complex and heptyl-4,4′-bipyridinium di-cation [165,166]. The observed photocurrents were interpreted as either the result of the transfer of the photoexcited electron between a sensitizer in one solvent phase and an electron acceptor in the other solvent phase, or to the transfer of an ionic product of the homogeneous photoassociated electron transfer reaction.

Electron transfer at ITIES studied by current scan polarography has been reported [167]. In this study different types of redox couples have been examined and their reversible half-wave potentials have been determined. Very recently, a theory for cyclic voltammetry of electron transfer at ITIES has been presented [168]. The theory has been used to show how the voltammograms vary when the ratios of the redox couples in both phases are changed.

From the above literature review it is readily seen that the studies made on electron transfer at ITIES are very few in number as compared to ion transfer studies. The limitation is due to certain requirements which should be satisfied for such investigations. These are: (i) the possibility of having strong hydrophilic and hydrophobic redox agents in the respective phases; (ii) the need to have both species electroactive in the available potential window with very close half wave potentials; and (3) the non-interference of the redox products with the process of the electron transfer (i.e. the redox products should not be transferable across the interface).

1.5 THE DOUBLE LAYER AT ITIES

Another aspect of studies at the ITIES has focused on the structure of the double layer at such an interface. Electrical double layers exist at all boundaries between two phases, one of which at least must be an ionic or an electronic conductor. The variation of the electrical potential between two liquids is closely related to the distribution of the ionic and dipolar components across the liquid/liquid interfaces [83]. The structure of the double layer at ITIES has remained a controversial topic and quite a large number of investigations have been carried out

In many respects the treatment of the double layer at ITIES is similar to that of the metal/electrolyte solution interface [79,80,83] The first theoretical approach of the double layer at ITIES was presented by Verwey and Niessen as cited in ref. 83 According to their model the interface is represented by a back-to-back diffuse double layer with charges distributed in the two phases. This theory was based on the Gouy and Chapman model [169].

Analogous to Stern's model [169], Gavach et al. [170] introduced the concept of an ion-free layer between the two immiscible phases, similar to the inner layer at a metal/electrolyte solution interface, with two diffuse layers penetrating the respective phases. This model is known as the modified Verwey-Niessen (MVN) model. A simple representation of this model is shown in Fig. 1.5.1.

The authors of ref. 170 carried out interfacial tension measurements using alkylammonium cations(C_2 to C_5) and interpreted their results in terms of specific adsorption of the cations. In a subsequently work, interfacial tension measurements for different tetraalkylammonium ions led to electrocapillary curves comparable to the curve obtained with the classical mercury/aqueous solution system [171]. A further extension of the study led the investigators to suggest that the interfacial charge distributions are only

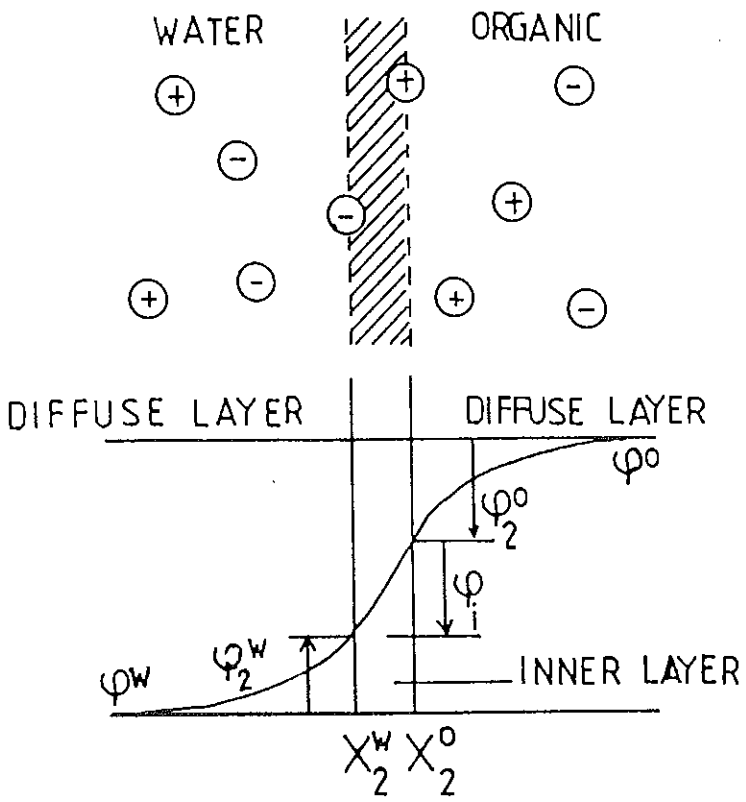

Fig. 1.5.1. Modified Verwey-Niessen model of an ITIES. Full circles represent the point-charge ions, and X_2^w or X_2^o are positions of ions in planes of closest approach (outer Helmholtz planes) to the hypothetical plane of contact in the phase w or o, respectively.

spread within the diffuse layers, showing a continuity of the electrical potential across the central layer [27].

Other workers [172] neglected the diffuse double layer approach and proposed that the electric field is formed by ions of opposite signs specifically adsorbed on the respective sides of the interface. A similar treatment based on adsorption of ions up to a monolayer thickness was presented by Joos and Bogaert [24].

In the last decade many investigations were carried out to analyse the structure of the double layer at ITIES by measuring the differential capacitance. Samec et al. [58] employed ac impedance measurements to estimate the capacity of the water/nitrobenzene interface as a function of the Galvani potential difference. These investigators observed that the capacity of the inner layer at ITIES is greater than that of the inner layer at a metal/electrolyte solution interface, and this was accounted for in terms of the smaller effective thickness of the inner layer at ITIES. Furthermore the potential drop across the inner compact layer remained constant and very close to zero when the total potential drop across the interface was varied. The invariance of the potential drop across the compact layer had also been reported by Gavach et al. [171] and Girault and Schiffrin [61]. The magnitude of the potential drop reported in ref. 58 was, however, different from the values reported by other workers.

Reid et al. [173] measured the interfacial tension at the water/nitrobenzene interface in order to test the applicability of the MVN model. The comparison of the charges calculated theoretically with those determined experimentally indicated that the potential difference across the interface is concentrated in the diffuse layers of each phase and that the surface potential drop at the interfacial compact layer is near to zero.

Homolka et.al.[174] measured the capacitance of the water/nitrobenzene interface for different aqueous and organic base electrolytes. From their observations they concluded that the formation of an ion-free layer at the

interface is associated with the presence of certain ions in the double layer.

Girault and Schiffrin [61] suggested that the concept of an interfacial compact layer of oriented solvent dipole may not be valid due to mixed solvation and interfacial mixing. These authors further indicated that the inner layer thickness as obtained from measurements of surface excess of water depends upon the polarity of the organic solvent and the nature of the electrolyte. The thickness for most electrolytes corresponds to only a fraction of the solvent monolayer. Figure 1.5.2 illustrates the mixed solvent layer model of ITIES.

The ac impedance method was used to study the water/1,2-dce interface [175]. The behaviour of this system was found to be the same as that of the water/nitrobenzene except for the difference in the degree of ion association and the value of the capacitance minimum for a given base electrolyte. Using an impedance bridge and a two electrode cell arrangement, admittances of the water/nitrobenzene system were measured for" blocked liquid/liquid interface" (polarized interface) [176]. In a subsequent publication [177], the results of impedance measurements at "unblocked interface" (non-polarized interface) were presented. In both cases the authors claimed that the capacitance calculated from experimental observations agreed well with the values obtained from the Gouy and Chapman theory. Qualitatively very similar results were reported independently by Osakai et al. [57] who used ac polarography for the water/nitrobenzene interface.

The thermodynamics of a polarized ITIES was presented and the difference between the surface charge density of a polarized ITIES and that of a metal/electrolyte solution interface was discussed [178]. The difference was accounted for in terms of interfacial mixing and ion pairing at ITIES. In this study [178], electrocapillary curve for the water/1,2-dce system was obtained and it was in good agreement with integrated capacitance data as measured from galvanostatic pulse experiment.

In a preliminary note [179] the use of the mean spherical approximation

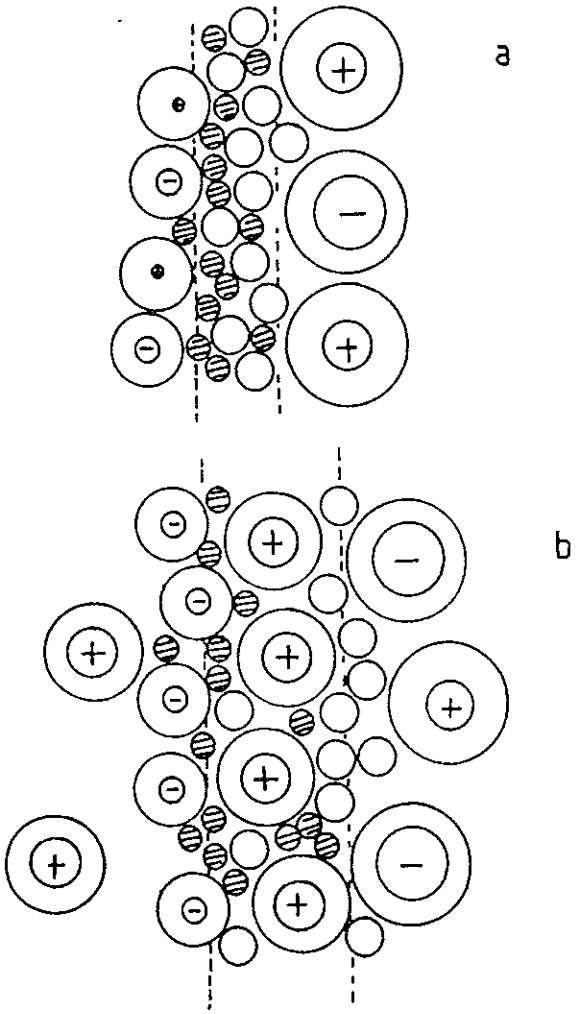

Fig. 1.5.2. Mixed solvent layer model at a polarisable (a), and non-polrisable (b), water/1,2-dichloroethane interface. System (a) : KCl (w)/TBATPB (o), system (b): TBACl (w)/TBATPB (o).

in the calculation of the double layer capacitance at ITIES has been discussed by assuming that the ITIES consists of two ion and dipole mixtures facing each other and separated by a hypothetical plane of contact. However the existence of a fitting parameter limits the applicability of the procedure.

A study of the impedance of the water/1,2-dce interface was carried out in the presence and absence of Pi^- ion in the organic phase [180]. It was found that the capacity of the polarizable interface has a higher value than the one calculated from the Gouy and Chapman theory. The observed discrepancy was believed to be either due to the surface charge transfer reactions or to the limited applicability of the Gouy and Chapman theory.

Silva and Moura [181] measured the impedance at the water/nitrobenzene and water/1,2-dce interfaces to confirm the possible existence of a surface charge transfer process of very low rate, which was indicated by the results of other workers [175,180]. From their findings they concluded that it is not the surface charge transfer which causes the appearance of a semi-circle at the high frequency region of the impedance plot, but rather the impedance of the Luggin capillaries of the reference electrodes. Very recently [182], this phenomenon has been fully scrutinized and the origin of the experimental high frequency artifacts has been discussed. It has been clarified that the main cause of the observed high frequency dispersion is the high value of the resistance of the Luggin capillary in the organic phase. It has been recommended that the application of a silver/silver tetraphenylborate reference electrode in the organic phase could obviate the problems. The construction of a four-electrode potentiostat/voltage clamp of novel design has also been reported very recently [183]. Its simple construction, low noise, and good frequency response has been suggested to be suitable for use in ac impedance measurements, particularly with high resistive systems.

Fast-galvanostatic pulse method was applied to the study of the electrical double layer at ITIES [184]. In this study the MVN model was used and the

following assumptions made : (i) the approximations of the Poisson-Boltzmann equation by Gouy and Chapman are removed; and (ii) the boundary between the space-charge region and the inner layer is considered to be diffuse rather than sharp. In a further work, the applicability of the above method for the evaluation of the ohmic potential drop, the minimization of the resistance inside the reference electrode connected to the organic phase, and the introduction of a computer controlled pulse was fully described [63].

Koczorowski [185] determined the volta and zero charge potentials at ITIES . These data provide useful information for the analysis and modeling of the electrical double layer at ITIES.

The structure of the water/nitrobenzene interface was further studied in the presence of 1:1 and 2:2 electrolytes [186] The capacitance of the interface was evaluated as a function of potential difference. At zero surface charge a comparison was made with a theoretical capacitance calculated using the mean spherical approximation for a model consisting of two ion and dipole mixtures facing each other. The results were interpreted in terms of ion penetration into the inner layer which is believed to be a function of ion solvation.

A different approach of the double layer structure was presented by Torrie and Valleau [187] who claimed, from the results of their Monte Carlo simulation, that the MVN theory is misleading and that it presents quite an unrealistic structure of the ITIES.

Other more sophisticated double layer theories [188,189] of the ITIES have shown that the Gouy and Chapman theory does fail at high surface charge densities. Samec et al. [190] also observed certain discrepancies with the MVN theory from capacitance measurements of the water/1,2-dce system. Eventually the absence of an ion free layer (inner layer) at the water/organic solvent interface is likely, as shown by surface excess measurements [61]. A similar investigation has been carried out very recently, at the water/1,2-dce interface in the presence and absence of a transferring ion [191]. In this study

the double layer capacity and the Warburg coefficient for the system containing only the supporting electrolytes as well as with added transferable ion (TMA^+) have been determined. The observed decrease in the double layer capacity in the presence of TMA^+ ion is, however, opposite to that observed in ref. 180.

In summary, the amount of information collected during the last two decades has helped to elucidate to a certain extent the structure of the electrical double layer at ITIES. From the above review it is evident that measurements of interfacial tension and capacitance have provided access to important interfacial quantities.

The use of the Gouy and Chapman theory has indeed confirmed that the Galvani potential difference between the two phases is spread entirely within the two back to back double layers. The theory gives very good approximate capacitance values for very low electrolyte concentrations. The MYN theory has been applied by many researchers [192] and it has been pointed out that the model can be used provided that ions are allowed to penetrate into the inner layer over some distance. The inner layer is thus pictured as partly populated by oriented solvent molecules and partly by disarrayed solvent molecules with ions present in it [83].

The interface on the other hand is regarded as a mixed solvent layer, no more than two or three molecular diameter thick, which ions from both sides can penetrate partially [178]. Girault [193] suggested that the expression "inner layer", which is linked to the Stern layer in the classical double layer model of metal/electrolyte solution interface, is not an appropriate term for ITIES. It has been indicated that, at the present time, there is a fundamental difficulty in modeling the interface of the mixed solvent region using the methods of molecular dynamics [84].

1.6 GIBBS ENERGY OF IONIC SOLVATION

Since the Gibbs energy of ion transfer at ITIES is the difference of the solvation free energies of an ion in the two phases, it is essential to have theoretical estimates of the values of the solvation free energy in order to make comparisons with experimental results.

For many years there has been considerable interest in the behaviour of electrolytes in aqueous, non-aqueous and mixed solvents with a view to investigate changes in the solvation of ions. The solvation process for a solute, according to Ben-Naim and Marcus [194,195], is its transfer from a fixed point in vacuum (an ideal gas phase) to a fixed point in the solution. It is considered that the solution is infinitely dilute; thus solute-solute interactions are absent. To understand and quantify the solvation process, the sum of all structural and energy changes occurring in the system when ions pass from the gaseous phase into the solution have to be determined [196]. Ion solvent interactions are divided into electrostatic, non-electrostatic, and specific chemical interactions[197].

Current theories of ionic solvation are conventionally classified as discontinuous and continuous models [198-200]. In the discontinuous model the environment of the ion is considered to consist of individual particles with the real or a simplified structure of the solvent. The ordinary procedure in such calculations is to find the free energy of interaction of an ion with N molecules whose spatial configuration is fixed and then to determine the optimum configuration which corresponds to the minimum energy of the system. In the continuous model the solvent is regarded as a continuum of given dielectric constant i.e.,the ionic environment is viewed as a structureless dielectric continuum.

The simplest continuous model of ionic solvation was first proposed by Born as cited in ref. 201, who regarded the ion as a rigid sphere of fixed

radius, with a uniformly distributed charge and immersed in a continuous medium of dielectric constant. The solvation energy calculated using this model is not satisfactory except for rough estimates . There are two obvious flaws in this model [202]. In the vicinity of an ion the solvent may be oriented by the electric field of the ion, and its dielectric constant there will be much lower than the bulk value (dielectric saturation). A further uncertainty arises in using the crystallographic radii of ions in solution.

Webbs [203] presented a model of ionic solvation aimed at making two corrections to Born's theory. His theory was based on two points : (i) the dielectric constant near the ion is less than that of the bulk solution, and (ii) the solvent undergoes compression near the ion, thus an allowance must be made for the work used up in this process. The results of the solvation free energy of individual ions obtained in this way are higher than experimental values. However the theory is principally of interest because of its analysis of the continuous dielectric model applied to polarization problems in electrolyte solutions. It also gives a method of calculating the variation of dielectric constant with field strength.

The first attempt to carry out calculation of the free energy of solvation based on the discontinuous model was made by Bernal and Fowler [204], who considered the free energy of solvation as a sum of the energies which arise due to ion-dipole interaction, the Born term for the primarily solvated complex and from the electrostatic energy of the solvent molecules. The calculated values from this theory were, however, incorrect due to certain missing terms such as ion-solvent repulsion etc.

The other approach of the discontinuous theory was by Eley and Evans [205]. The solvation energy was considered to have five components, namely, (i) the energy associated with the transfer of solvent molecules from the bulk to the gas phase, (ii) the dissociation energy of solvent molecules, (iii) the energy which arises due to the coordination of the gaseous ion with the solvent

molecules, (iv) the energy due to cavity formation, and (v) energy related to the condensation of uncomplexed solvent molecules. This model (structural theory), however, suffers from the mixing of heat and free energy terms and as a consequence it introduces an ambiguity in the calculated free energy values.

Gould and Laidler made calculations on the basis of both the discontinuous and continuous models [206,207]. In spite of the fact that their discontinuous model was greatly over-simplified, the agreement between theoretical values and experiment values, were reasonable. On the other hand their continuous model treatment had helped in the interpretation of the main trends of the solvation energy.

Beveridge and Schnuelle [208,209] solved the electrostatic problem of a multipole in the centre of a spherical cavity surrounded by a shell of solvent molecules. Abraham and Liszi have successfully applied this model to the calculation of the energies of solvation of a number of simple ions in aqueous and non-aqueous solvents [199,210-212]. The continuous model of Abraham and Liszi has two kinds of approaches.

(a) One-layer continuous model: The model considers an ion of radius a surrounded by an organized, dielectrically saturated, solvent layer of thickness (b-a); beyond this organized layer lies only the bulk solvent. The breakdown of the total energy involved is accomplished by regarding the solvation process as carried out in two stages. These are creation of a cavity in the solvent, and insertion of an ion from the gas phase into the cavity. The associated energy terms are thus: (i) the energy needed to make an appropriate cavity in the bulk solvent; (ii) the energy required to reorganize the solvent molecules round the cavity into various layers; (iii) the electrostatic energy of interaction of the ion with the solvent in the layers and with the bulk solvent; (iv) the non-electrostatic energy of interaction of the ion with its near neighbour solvent molecules, and (v) some correction term for different standard states. The non-ionic solvation energy includes the energy terms of

(i), (ii), (iv) and (v). Its value is calculated from an empirical equation based on the assumption that it is equal to the free energy of solvation of a non-polar gaseous solute of the same size as the ion in question. By combining the electrostatic and neutral contribution, the solvation free energies of several ions in different solvents of varied polarity have been calculated and very good agreement with experimental values have been obtained.

(b) Two-layer model: In this model the electrostatic energy contains a term due to the interaction of the ion with the first layer; a second term containing the dielectric constant of the second layer; and a third term due to the contribution of the bulk solvent outside the layers.[199,213]. The solvation energy calculated with the help of this model agree well with the observed ones However this model shows no marked improvement over the one layer model.

The other continuous model is due to Marcus [214], which is similar in many respects to the model used by Abraham and Liszi [210]. It involves the cavity in which the ion is situated in the water, a completely immobilized first hydration shell, and then surroundings, in which, on the one hand, the structure of the water is modified, and, on the other, the water behaves as a dielectric continuum. According to this model the transfer of the ion from a fixed position in the gas phase to a fixed position in water is considered as proceeding in three stages: (i) the ion is discharged; (ii) it is transferred as a neutral species having the same size as the (bare) ion in the solution; and (iii) it is recharged up to its original charge. This model has been tested only for water, but the calculated values of the hydration energies for several ions are in excellent agreement with experimental data. The model also enables the estimation of hydration energies of multivalent ions.

The very recent theoretical approach known as the non-local electrostatic theory [215-217] refers to the continuum models, but the effective parameters needed for calculation are chosen by analyzing the solvent

structure. That is, an allowance for the non-linear dielectric effects, as well as analysis of the correlation between the solvent polarization vectors at small distances with the help of a non-local electrostatic theory, are made. According to this model the solvation energy has two components, namely the electrostatic and the solvophobic, in which the latter arises due to cavity formation and entropy effects. These two contributions depend upon the size of the ion under consideration. For small ions the electrostatic contribution dominates. With the increase of ionic size, the electrostatic term decreases, and becomes comparable to the rising solvophobic contribution. This theoretical model furnishes physical expressions for a qualitative understanding of the features of ionic solvation; however, for quantitative estimations the method is impeded by the lack of information on the details of non-local screening in liquids.

In summary , the above models are some of the most relevant theoretical approaches to estimating the free energy of solvation. It is worth mentioning that there are also other types of models which have not been raised here due to their restricted applications. As an example the quantum chemical theory of solvation [218] is regarded as the most modern but, because of its complexity, the necessity of many approximations and simplifications, it is applied to only limited systems. The Abraham-Liszi`s relation has proved to be very useful and convenient for practical applications. The predictive power of the model has been used effectively by many authors; however, it is criticized for its inability to fully explain the physical principles and for its utilization of a step-wise profile for the dielectric constant.

References

1. W. Nernst and E.H. Riesenfeld, Ann. Physik., 8 (1902) 600.
2. E.H. Riesenfeld, Ann. Physik.,8(1902) 600.
3. M. Cremer, Z. Biol., 47 (1906) 562.
4. R. Beutner, J. Am. Chem. Soc., 35 (1913) 344.
5. E. Bauer and S. Kronman, Z. Phys. Chem., 92 (1917) 819.
6. R. Beutner, Z. Phys. Chem., 87 (1917) 385.
7. E. Bauer, Z. Phys. Chem., 103 (1922) 39.
8. E. Bauer, Z. Phys. Chem., 106 (1923) 157.
9. G. Erhensvärd and L.G. Sillen, Nature 141 (1938) 788.
10. G. Erhensvärd and L.G. Sillen, Nature 142 (1938) 396.
11. R.B. Dean, O. Gatty, and E.K. Rideal, Trans. Faraday Soc., 36 (1940) 161.
12. R.B.Dean, Trans. Faraday Soc., 36 (1940) 166.
13. K.F. Bonhoeffer, M. Kahlweit and H. Strehlow, Z. Phys. Chem., 1 (1954) 21.
14. M. Kahlweit, H. Strehlow and C:S. Hocking, Z. Phys. Chem., 4 (1955) 212.
15. J. T. Davies and E.K. Rideal. Can. J. Chem., 33 (1955) 947.
16. J.T. Davies, Z. Elektrochem., 55 (1951) 559.
17. J. Guastalla, J. Chem. Phys., 53 (1956) 607.
18. A. Watanabe, M. Matsumoto, H. Tamai and R. Gotoh, Kolloid Z.Z. Polym. 220 (1967) 152.
19. A. Watanabe, H. Tamai, and K. Higashitsiyi, J. Colloid. Interface Sci., 43 (1973) 548.
20. M. Blank and S. Feig, Science, 141(1963)1173.
21. M. Blank, J. Colloid. Interface Sci., 22 (1966) 51.
22. M. Dupeyrat and J. Michel, C.R. Acad. Ser. C., 264(1967)1240.
23. M. Dupeyrat and J. Michel, J. Colloid. Interface Sci., 29 (1969) 605.

24. P. Joos and R. Vanden Bogaert, J. Colloid. Interface Sci., 56 (1976) 206.
25. P. Joos and M. Van Bockstaele, J. Phys. Chem., 80 (1976) 1573.
26. B.D. Epenoux and C. Gavach, J. Colloid. Interface Sci., 56 (1976) 139.
27. B.D. Epenoux, P. Seta, G. Amblard and C.Gavach, J. Electroanal. Chem., 99 (1979) 77.
28. C. Gavach, T. Mlodnicks, and J. Guastalla, C.R. Acad. Ser. C., 266 (1968) 1196.
29. C. Gavach, C.R. Acad. Ser. C., 269(1969)1356
30. C. Gavach, J. Chim. Phys., 70 (1973)1478.
31. C. Gavach and F. Henry, J. Electroanal. Chem., 54 (1974)361.
32. C. Gavach and B.D. Epenoux, J. Electroanal. Chem., 55 (1974) 59.
33. C. Gavach, B.D. Epenoux, and F. Henry, J. Electroanal. Chem., 64 (1975) 107.
34. J. Guastala, Nature, 227 (1970) 485.
35. J. Guastala, Experimentia Suppl., 18 (1971) 333.
36. J. Koryta, P. Vanysek and M. Brezina, J. Electroanal. Chem., 67 (1976) 263.
37. J. Koryta, Electrochim. Acta, 24 (1979) 293.
38. Z. Samec, J. Electroanal. Chem., 103 (1979) 1.
39. Q. Le Hung, J. Electroanal. Chem., 115 (1980) 159.
40. Q. Le Hung, J. Electroanal. Chem., 149 (1983) 1.
41. E. Makrlik, Electrochim. Acta, 28 (1983) 573.
42. Z. Koczorowski, J. Electroanal. Chem., 127 (1981) 11.
43. O.R. Melroy and R.P. Buck, J. Electroanal. Chem., 136 (1982) 19.
44. O.R. Melroy and R.P. Buck, J. Electroanal. Chem., 143 (1983) 23.
45. O.R. Melroy and R.P. Buck, F. S. Stover and H.C. Hughes J. Electroanal. Chem., 121 (1981) 93.
46. J. Koryta, P. Vanysek and M. Brezina, J. Electroanal. Chem., 75 (1977) 211.

47. Z. Samec, V. Marecek, J. Koryta and M.W. Khalil, J. Electroanal. Chem., 83 (1977) 393.
48. Z. Samec, V. Marecek, and J. Weber , J. Electroanal. Chem., 100 (1979) 841.
49. D. Homolka, Le Q. Hung, A. Hofmanova, M.W. Khalil, J. Koryta, V. Marecek, Z. Samec.,S.K. Sen, P. Vanysek, J. Weber, M. Brezina, M. Janda and I.Stibor, Anal. Chem.,52 (1980) 1606.
50. Le Q. Hung, Chem. Listy, 74 (1980) 1089.
51. Z. Samec, J. Electroanal. Chem., 111 (1980) 211.
52. Z. Samec, V. Mareck, J. Weber and D. Homolka, J. Electroanal. Chem., 126 (1981) 105.
53. V. Marecek and Z. Samec, Anal. Chim. Acta, 141 (1982) 65.
54. T. Kakutani, T. Osakai and M. Senda, Bull. Chem. Soc. Jpn., 56 (1983) 991.
55. Z. Yoshida and H. Freiser, J. Electroanal. Chem., 162 (1984) 307.
56. B. Hunhammer, T. Solomon and H. Alemu, J. Electroanal. Chem., 149 (1983) 179.
57. T. Osakai, T. Kakutani and M. Senda, Bull. Chem. Soc. Jpn., 57 (1984) 370.
58. Z. Samec, V. Mareck, and D. Homolka, J. Electroanal. Chem., 126 (1981) 121.
59. T. Kakiuchi and M. Senda, Bull. Chem. Soc. Jpn., 56 (1983) 1322.
60. H.H. Girault, D.J. Schiffrin and B. Smith, J. Electroanal. Chem., 137 (1982) 207.
61. H.H. Girault, and D.J. Schiffrin, J. Electroanal. Chem., 150 (1983) 43.
62. V. Marecek and Z. Samec, J. Electroanal. Chem., 149 (1983) 185.
63. V. Marecek and Z. Samec, J. Electroanal. Chem., 185 (1985) 263.
64. Z. Samec, and V. Mareck, J. Electroanal. Chem., 200 (1986) 17.
65. H.H. Girault, and D.J. Schiffrin, J. Electroanal. Chem., 161 (1984) 415.

66. E. Wang and Z. Pang, J. Electroanal. Chem.,189 (1985) 1.
67. E. Wang and Z. Pang, J. Electroanal. Chem.,189 (1985) 21.
68. T. Osakai, T. Kakutani and M. Senda, Bunseki Kagaku, 33 (1984) E371.
69. B. Hundhammer, S.K. Dhawan, A. Bekele and H.J. Seidlitz, J. Electroanal. Chem., 217 (1987) 253.
70. G. Taylor and H.H. Girault , J. Electroanal. Chem.,208 (1986) 197.
71. J.A. Campbell, A.A. Stewart and H.H. Girault , J. Chem. Soc., Farad. Trans. 1, 85 (1989) 843.
72. J.A. Campbell and H.H. Girault , J. Electroanal. Chem.,266 (1989) 465.
73. R. Fan and X. Wang, J. Electroanal. Chem.,261 (1989) 77.
74. B. Hundhammer and S. Wilke, J. Electroanal. Chem.,266 (1989) 133.
75. D. Clarke, D.J. Schiffrin and M.C. Wiles, Electrochim. Acta, 34 (1989) 767.
76. J. Koryta, Hungarian Sci. Instr., 49 (1980) 25.
77. J. Koryta and P. Vanysek, in H. Gerisher and C.W. Tobias (Eds.), Advances in Electrochemistry and Electrochemical Engineering, Vol.12, Wiley Interscience, New York, 1981.
78. J. Koryta, Electrochimica Acta, 29 (1984) 445.
79. J.D. Reid, O.R. Melroy, W.E. Bronner, H.C. Hughes, P. Vanysek and R.P. Buck, in A.F. Silva (Ed.), Trends in Interfacial Electrochemistry, NATO ASI Series, Reidel Publishing Comp.,1984.
80. P. Vanysek, Electrochemistry at Liquid/Liquid Interfaces, Springer-Verlag, Berlin, 1985.
81. J. Koryta, Electrochim. Acta, 32 (1987) 419.
82. J. Koryta, Electrochim. Acta, 33 (1988) 189.
83. V. Marecek, Z. Samec and J. Koryta, Advances in Colloid and Interface Science, 29 (1988) 1.
84. H.H.Girault and D.J. Schiffrin, in A.J. Bard (Ed.), Electroanalytical Chemistry, Vol.15, Marcel Dekker, Inc., New York, 1989.

85. P. Vanysek, J. Electroanal. Chem., 121 (1901) 149.
86. B. Hundhammer, T. Solomon and B. Alemayehu, J. Electroanal. Chem., 135 (1982) 301.
87. T. Osakai, T. Kakutani, Y. Nishiwaki and M. Senda, Bunseki Kagaku 32 (1983)) E8
88. P. Vanysek and M. Behrendt, J. Electroanal. Chem., 130 (1981) 287.
89. Z. Samec, D. Homolka, V. Marecek and L. Kavan, J. Electroanal. chem. 145 (1983) 213.
90. J. Hanzlik and Z. Samec, Coll. Czech. Chem. Commun., 52 (1987) 830.
91. B. Hundhammer and T. Solomon, J. Electroanal. Chem.,157 (1983) 19.
92. S. Kihara, M. Suzki, K. Maeda, K. Ogura and M. Matsiu, J. Electroanal. Chem., 210 (1986) 147.
93. Z. Pang and E. Wang, J. Electroanal. Chem.,252 (1988) 245.
94. E. Wang and Z. Sun, J. Electroanal. Chem.,220 (1987) 235.
95. Z. Sun and E. Wang, Electrochim. Acta, 33 (1988) 603.
96. E. Wang and Y. Liu, J. Chem. Soc., Faraday I , 84 (1988) 2289.
97. L. Yuqing and E. Wang, J. Electroanal. Chem.,277 (1990) 291.
98. E. Makrlik and Le Q. Hung, Electroanal. Chem.,158 (1983) 269.
99. Z. Koczorowski and G. Geblewicz, J. Electroanal. Chem., 152 (1983) 55.
100. G. Geblewicz, and Z. Koczorowski, J. Electroanal. Chem., 158 (1983) 37.
101. Z. Samec, V. Marecek and M.P. Colombini, J. Electroanal. chem. 257 (1988) 147.
102. Z. Koczorowski ,G. Geblewicz and I. Paleska, J. Electroanal. Chem., 172 (1984) 327.
103. T. Solomon, H Alemu and B. Hundhammer, J. Electroanal. Chem. 169 (1984) 303.
104. Z. Koczorowski, I. Paleska and G. Geblewicz J. Electroanal. Chem., 164 (1984) 201.

105. T. Solomon, H. Alemu and B. Hundhammer, J. Electroanal. Chem., 169 (1984) 311.

106. Z. Samec, D. Homolka,V. Marecek and L. Kavan, J. Electroanal. chem. 145 (1983) 213.

107. O. Valent, J. Koryta, and M. Panoch, J. Electroanal. Chem., 226 (1987) 21.

108. H. Alemu and T. Solomon, J. Electroanal. Chem., 237 (1987) 113.

109. H. Alemu and T. Solomon, J. Electroanal. Chem., 261 (1989) 261.

110. I. Paleska, J. Kotowski, Z. Koczorowski, E. Nakache and M. Duperat, J. Electroanal. Chem., 278 (1990) 129.

111. V. Marecek and M.P. Colombini, J. Electroanal. Chem., 241 (1988) 133.

112. Y. Sao and H.H. Girault, J. Electroanal. Chem.,282 (1990) 59.

113. G. Geblewicz, A.A. Kontturi, K. Kontturi and D.J. Schiffrin, J. Electroanal. Chem., 217 (1987) 261.

114. E. Makrlik, W. Ruth and P. Vanysek, J. Colloid Interface Sci., 96 (1983) 548.

115. D. Homolka, V. Marecek, Z. Samec, K. Base and H. Wendt, J. Electroanal. Chem., 163 (1984) 159.

116. E. Wang and Y. Liu, J. Electroanal. Chem.,214 (1986) 459.

117. Z. Samec, J. Electroanal. Chem., 99 (1979) 77.

118. O.R. Melroy, W.E. Bronner and R.P. Buck, J. Electroanal. Chem., 130 (1983) 373.

119. W.E. Bronner, O.R. Melroy and R.P. Buck, J. Electroanal. Chem., 162 (1984) 263.

120. Z. Samec, V. Marecek and D. Homolka, J. Electroanal. Chem., 158 (1983) 25.

121. H.H. Girault and D.J. Schiffrin, J. Electroanal. Chem.,195 (1985) 213.

122. Y. Y. Gurevich and Y. I. Kharkats, J. Electroanal. Chem., 200 (1986) 3.

123. Z. Samec, Y. I. Kharkats, and Y. Y. Gurevich, J. Electroanal. Chem.,

204 (1986) 257.

124. J. Koryta, J. Electroanal. Chem., 213 (1986) 323.

125. J. Koryt and M. Skalicky, J. Electroanal. Chem., 229 (1987) 265.

126. V.J. Cunnane, D.J. Schiffrin, M.Fleishmann G. Geblewicz and D. Williams, J. Electroanal. Chem., 243 (1988) 455.

127. A.A. Kontturi, K. Kontturi and D.J. Schiffrin, J. Electroanal.Chem., 255 (1988) 331.

128. H.H. Girault, J. Electroanal. Chem., 257 (1988) 47.

129. C.A. Chang, E. Wang and Z. Pang, J. Electroanal. Chem., 266 (1989) 143.

130. M. Seno, K. Iwamoto and Q. Chen, Electrochim. Acta, 35 (1990) 127.

131. P. Vanysek, W. Ruth and J. Koryta, J. Electroanal. Chem., 148 (117) 1983.

132. E. Makrlik, L.Q. Hung and A. Hofmanova, Electrochim. Acta, 28 (1983) 847.

133. D. Homolka, V. Marecek and Z. Samec, J. Electroanal. Chem., 125 (1981) 243.

134. D. Homolka, K. Holub and V. Marecek, J. Electroanal. Chem., 138 (1982) 29.

135. Z. Samec, D. Homolka, and V. Mareck, J. Electroanal. Chem., 135 (1982) 265.

136. E. Makrlik, W. Ruth and P. Vanysek, Electrochim. Acta, 28 (1983) 575.

137. G. Du, J. Koryta, W. Ruth and P. Vanysek, J. Electroanal. Chem. 159 (1983) 413.

138. V. Marecek and Z. Smec, Anal. Chim. Acta, 151 (1983) 265.

139. Z. Yoshida and H. Freiser, J. Electroanal. Chem., 179 (1984) 31.

140. J. Koryta, Y.N. Kozlov and M. Skalicky, J. Electroanal. Chem., 234 (1987) 355.

141. E. Makrlik, J. Colloid and Interface. Sci., 108 (1985) 551.
142. E. Wang and Z. Sun, Extended Abstracts, 169th Meeting of the Electrochemical Society, Boston, 1986, p. 867.
143. D. Homolka and H. Wendt, Ber. Bunsenges. Phys. Chem. 89 (1985) 1075.
144. L. Sinru and H. Freiser, J. Electroanal. Chem., 191 (1985) 437.
145. L. Sinru, Z. Zaofan and H. Freiser, J. Electroanal. Chem., 210 (19886) 137.
146. E. Wang and Y. Liu, J. Electroanal. Chem.,214 (1986) 465.
147. Z. Yoshida and S. Kihara, J. Electroanal. Chem., 227 (1987) 171.
148. E. Makrlik, A. Hofmanova and L.Q. Hung, J. Colloid Interface Sci., 107 (1985) 1.
149. Y. Liu and E. Wang, J. Electroanal. Chem., 234 (1987) 85.
150. J. Hanzlik, J. Hovorka and A.M. Camus, Coll. Czech. Chem. Commun. 52 (1987) 838.
151. R. Fan and Y. Cheng, J. Electroanal. Chem., 256 (1988) 207.
152. Y. Liu and E. Wang, J. Electroanal. Chem., 277 (1990) 305.
153. A.M. Baruzzi and H. Wendt, J. Electroanal. Chem., 279 (1990)19.
154. Z. Sun and P. Vanysek, Anal. Chim. Acta, 228 (1990) 241.
155. M. Guainazzi, G. Silvstri and G. Survalle, J. Chem. Soc. Chem. Commun., (1975) 200.
156. Z. Samec, V. Marecek, and J. Weber, J. Electroanal. Chem., 103 (1979)
157. J. Hanzlik, Z. Samec and J. Hovorka, J. Electroanal. Chem., 216 (1987) 303.
158. E. Makrlik, Z. Phys. Chem. Leipzig, 268 (1987) 212.
159. E. Makrlik, J. Electroanal. Chem., 158 (1983) 295.
160. E. Makrlik, Z. Phys. Chem. Leipzig, 268 (1987) 200.
161. E. Makrlik, Z. Phys. Chem. Leipzig, 268 (1987) 826.
162. H.H. Girault and D.J. Schiffrin, J. Electroanal. Chem., 244 (1988) 15.
163. G. Geblewicz and D.J. Schiffrin, J. Electroanal. Chem., 244 (1988) 27.

164. C.A. Beltran, Y.J. Cunnane, G. Geblewicz, D.J. Schiffrin, and T. Solomon, J. Electroanal. Chem., 247 (1988) 203.

165. F.L. Thomoson, L.J. Yellowless, and H.H. Girault, J. Chem. Soc., Chem. Commun., (1988) 1547.

166. Z. Samec, A.R. Brown, L.J. Yellowless and H.H. Girault, J. Electroanal. Chem.,259 (1989) 309.

167. S. Kihara, M. Suzuki, K. Maeda, K. Ogura, M. Matsui and Z. Yoshida, J. Electroanal. Chem., 271 (1989) 107.

168. A.A. Stewart, J.A. Campbell, H.H. Girault and M. Eddowes, Ber. Bunsenges. Phys. Chem., 94 (1990) 83.

169. P.H. Rieger, Electrochemistry, Prentice-Hall, Inc., New Jersey, 1987.

170. C. Gavach, P. Seta and B. Depenoux, J. Electroanal. Chem., 83 (1977) 225.

171. M. Gros, S. Gromb and C. Gavach, J. Electroanal. Chem., 89 (1978) 29.

172. V. Krylov, L. Boguslavsky and M. Manvelyan, Soviet Electrochem., 13 (1977) 707.

173. J. Reid, O. Melroy and R. Buck, J. Electroanal. Chem., 147 (1983) 71.

174. D. Homolka, P. Hajkova, V. Marecek and Z. Samec, J. Electroanal. Chem., 159 (1983) 233.

175. P. Hajkova, D. Homolka, V. Marecek and Z. Samec, J. Electroanal. Chem., 151 (1983) 277.

176. J.D. Reid, P. Vanysk and R.P. Buck, J. Electroanal. Chem., 161 (1984) 1.

177. J.D. Reid, P. Vanysk and R.P. Buck, J. Electroanal. Chem., 170 (1984) 109.

178. H.H. Girault and D.J. Schiffrin, J. Electroanal. Chem., 170 (1984) 127.

179. Z. Samec, V. Marecek and D. Homolka, J. Electroanal. Chem., 170 (1984) 383.

180. G. Geblewicz, Z. Figaszewski and Z. Koczorowski, J. Electroanal. Chem., 177 (1984) 1.

181. F. Silva and C. Moura, J. Electroanal. Chem., 177 (1984) 317.
182. M.C. Wiles, D.J. Schiffrin, T.J. Vander Noot and A.F. Silva, J. Electroanal. Chem., 278 (1990) 151.
183. T.J. Vander Noot, D.J. Schiffrin and R.S. Whiteside, J. Electroanal. Chem., 278 (1990) 137.
184. Z. Samec, V. Marecek, and D. Homolka, Faraday Discuss. Chem. Soc., 77 (1984) 197.
185. Z. Koczorowski, J. Electroanal. Chem., 190 (1985) 257.
186. Z. Samec, V. Marecek and D. Homolka, J. Electroanal. Chem., 187 (1985) 31.
187. G.M. Torrie and J.P. Valleau, J. Electroanal. Chem., 206 (1986) 69.
188. C.W. Outhnaite, L.B. Bhuiyan and S. Levine, J. Chem. Soc. Faraday. Trans. II 76 (1980) 1388.
189. S.L. Carnie, D.Y.C. Chan, D.J. Mitchell and B.W. Ninham, J. Chem. Phys., 74 (1981) 1472.
190. P. Hajokova, J. Electroanal. Chem., 225 (1987) 65.
191. Z. Figaszewski and I. Paleska, J. Electroanal. Chem., 266 (1989) 253.
192. Z. Samec, Chem. Rev,. 88 (1988) 617.
193. H.H. Girault, Electrochim. Acta, 32 (1987) 383.
194. J.I. Padova, in B.E. Conway and J.O'M. Bockris (Eds.), Modern Aspects of Electrochemistry, Vol.7, Butterworths, London, 1987.
195. A. Ben-Naim and Y. Marcus, J. Chem. Phys., 81 (1984) 2016.
196. V.S. Markin and A.G. Volkov, J. Electroanal. Chem., 235 (1987) 23.
197. O. Popovcyh and R. Tomkins, Non-aqueous Solution Chemistry, Wiley-Interscience, New York, 1981.
198. J.O'M. Bockris and P.P.S. Saluj, J. Phys. Chem., 76 (1972) 2298.
199. M.H. Abraham, J. Liszi and L. Meszaros, J. Chem. Phys., 70 (1979) 2491.
200. R.R. Dogonadze and A.A. Kornyshev, J. Chem. Soc., Faraday. Trans. II, 7 (1974) 1121.

201. B.E. Conway and J.O'M. Bockris, in B.E. Conway and J.O'M. Bockris (Eds.), Modern Aspects of Electrochemistry, Vol. 7, Butterworths, London, 1954.
202. R.M. Noyes, J. Am. Chem. Soc., 84 (1962) 513.
203. T.J. Webb, J. Am. Chem. Soc., 48 (1926) 2589.
204. J.D. Bernal and R.H. Fowler, J. Phys. Chem., 1 (1933) 515.
205. D.D. Eley and M.G. Evans, Trans. Faraday Soc., 34 (1938) 1093.
206. J.S. Muirhead-Gould and K.J. Laidler. Trans. Faraday Soc., 63 (1967) 944.
207. J.S. Muirhead-Gould and K.J. Laidler. Trans. Faraday Soc., 63 (1967) 958.
208. G.W. Schnuelle and D.L. Beveridge, J. Phys. Chem., 79 (1975) 2562.
209. G.W. Schnuelle and D.L. Beveridge, J. Phys. Chem., 79 (1975) 2566.
210. M.H. Abraham and J. Liszi, J. Chem. Soc. Farad. Trans., I, 74 (1978) 1604.
211. M.H. Abraham and J. Liszi, J. Chem. Soc. Farad. Trans., I, 74 (1978) 2858.
212. M.H. Abraham and J. Liszi, J. Chem. Soc. Farad. Trans., I, 76 (1980) 1219.
213. J. Liszi, L. Meszaros and I.Ruff, J.Chem. Phys., 74 (1981) 6896.
214. Y. Marcus, Pure and Appl. Chem., 59 (1987) 1093.
215. A.A Kornyshev and A.G. Volkov, J. Electroanal. Chem., 180 (1984) 363.
216. V.S. Markin and A.G. Volkov, J. Electroanal. Chem., 235 (1987) 23.
217. V.S. Markin and A.G. Volkov, Electrochim. Acta, 34 (1989) 93.
218. H.L. Friedman, in B.E. Conway and J.O'M. Bockris (Eds.), Modern Aspects of Electrochemistry, Vol. 6, Plenum Press, New York, 1971.

CHAPTER TWO

THEORETICAL

2.1 THERMODYNAMICS OF THE ITIES

The electrochemical behaviour of ITIES depends on the ionic composition of the two electrolyte solutions. It is characterized by different types of polarisabilities depending on the extent to which it is permeable to the charged species present in the system [1].

(i) Ideally polarisable interface:- When the system contains a strongly hydrophilic electrolyte of the type B_1A_1 (e.g, LiCl) dissolved in the aqueous phase and a strongly hydrophobic electrolyte B_2A_2 (e.g, tetraphenylarsonium tetraphenylborate) dissolved in the organic phase, then the properties of the ITIES become analogous to that of a polarisable electrode, i.e., charged species cannot pass through the interface [1,2].

(ii) Non-polarisable interface:- When the system contains at least one common ion in both phases(e.g, TBACl in the aqueous phase and TBATPB in the organic phase) which can freely passes across the interface, such an interface is called non-polarisable [1,2].

In a system consisting of water (phase α) in contact with an immiscible organic solvent (phase β) and containing an ion i of charge Z, which is transferred from one phase to another, the condition for equilibrium can be stated as follows. The electrochemical potential of the ion in phase α must be the same as that in phase β [1,3]. That is

$$i(\alpha) \rightleftharpoons i(\beta) \qquad (I)$$

$$\bar{\mu}_i^{\alpha} = \bar{\mu}_i^{\beta} \qquad (2.1.1)$$

Using the definition of the electrochemical potential this can be rewritten in the form [3]

$$\mu_i^{o,\alpha} + RT\ln a_i^{\alpha} + ZF\phi^{\alpha} = \mu_i^{o,\beta} + RT\ln a_i^{\beta} + ZF\phi^{\beta} \qquad (2.1.2)$$

where $\mu_i^{o,\alpha}$, and $\mu_i^{o,\beta}$ stand for the standard chemical potentials of the ion i in phase α and β respectively, a_i^{α} and a_i^{β} are the activities of the ion i in the two phases, ϕ^{α} and ϕ^{β} are the inner potentials of i in the respective phases and R,F,T stand for the gas constant, Faraday constant and temperature (K),respectively.

From Eq.(2.1.2) one can derive the dependence of the Galvani potential difference between the two phases on the activities of the ion in the two phases [3]. Thus,

$$\Delta^{\alpha}_{\beta}\phi = \phi^{\alpha} - \phi^{\beta} = (\mu_i^{o,\beta} - \mu_i^{o,\alpha})/ZF + (RT/ZF)\ln(a_i^{\beta}/a_i^{\alpha}) \qquad (2.1.3)$$

$$= \Delta^{\alpha}_{\beta}\phi^{o} + (RT/ZF)\ln(a_i^{\beta}/a_i^{\alpha})$$

where $\Delta^{\alpha}_{\beta}\phi^{o}$ is the standard Galvani potential difference defined as:

$$\Delta^{\alpha}_{\beta}\phi^{o} = (\mu_i^{o,\beta} - \mu_i^{o,\alpha})/ZF = (\Delta G_t^{o,\alpha\rightarrow\beta})/ZF \qquad (2.1.4)$$

where $\Delta G_t^{o,\alpha\rightarrow\beta}$ is the standard Gibbs energy of transfer of the ion i from phase α to phase β. Eq.(2.1.3) shows that the Galvani potential difference can be calculated from the values of the standard potential and the activity of any ion participating in the equilibrium distribution.

For an electron transfer reaction at ITIES of the type

$$O_1(\alpha) + R_2(\beta) \rightleftharpoons R_1(\alpha) + O_2(\beta) \qquad (II)$$

where O_1, R_1, O_2, and R_2 represent the oxidized and reduced forms of the species in the respective phases, the equilibrium condition is

$$\bar{\mu}_{O_1}^{\alpha} + \bar{\mu}_{R_2}^{\beta} = \bar{\mu}_{R_1}^{\alpha} + \bar{\mu}_{O_2}^{\beta} \qquad (2.1.5)$$

and the equilibrium Galvani potential difference is [4,5]

$$\Delta^{\alpha}_{\beta}\phi = \Delta^{\alpha}_{\beta}\phi_e^{\circ} + (RT/nF)\ln[(a_{R_1}^{\alpha} a_{O_2}^{\beta})/(a_{O_1}^{\alpha} a_{R_2}^{\beta})] \qquad (2.1.6)$$

where n stands for the number of transferred electrons. The standard Galvani potential difference $\Delta^{\alpha}_{\beta}\phi_e^{\circ}$ is related to the standard potentials of the redox couples [4,5],

$$\Delta^{\alpha}_{\beta}\phi_e^{\circ} = (\mu_{R_1}^{\circ,\alpha} + \mu_{O_2}^{\circ,\beta} - \mu_{O_1}^{\circ,\alpha} - \mu_{R_2}^{\circ,\beta})/nF \qquad (2.1.7)$$

$$= \Delta G_e^{\circ}/nF = E^{\circ,\beta}_{O_2/R_2} - E^{\circ,\alpha}_{O_1/R_1} + \Delta^{\alpha}_{\beta}\phi^{\circ}_{e,H^+}$$

where $E^{\circ,\beta}_{O2/R2}$ and $E^{\circ,\alpha}_{O1/R1}$ are the standard potentials of the redox couples in phase β and phase α, respectively (both related to the same reference electrode in each particular phase [e.g., the standard hydrogen electrode]) [4].

2.1.1 *NON-POLARISABLE INTERFACE*

(i) ITIES Reversible with Respect to Single Ion.

For a system containing MX_1 and MX_2 electrolytes (e.g, TBACl and TBATPB) in the aqueous phase and organic phase respectively, as shown by the following scheme [1,6]

$$\underset{(\alpha)}{M^+X_1^-} \;\;||\;\; \underset{(\beta)}{M^+X_2^-} \qquad \text{(III)}$$

the interface is reversible with respect to the common cation M^+ under the following conditions;

$$\Delta G^{0,\alpha->\beta}_{t,X_1} >> 0,\ \Delta G^{0,\alpha->\beta}_{t,X_2} << 0, \text{ and}$$

$$\Delta G^{0,\alpha->\beta}_{t,X_2} < \Delta G^{0,\alpha->\beta}_{t,M} < \Delta G^{0,\alpha->\beta}_{t,X_1}$$

At equilibrium the Galvani potential difference at the interface is given by the Nernst-Donnan potential equation [1,7],

$$\Delta^{\alpha}_{\beta}\phi = \Delta^{\alpha}_{\beta}\phi^{0}_{M^+} + (RT/F)\ln(a_{M^+}{}^{\beta}/a_{M^+}{}^{\alpha}) \qquad (2.1.8)$$

$$= \Delta^{\alpha}_{\beta}\phi^{0}_{M^+} + (RT/F)\ln[[M^+]^{\beta}(\gamma_{M^+}{}^{\beta})/[M^+]^{\alpha}(\gamma_{M^+}{}^{\alpha})]$$

When $[M^+]^{\alpha} = [M^+]^{\beta}$,

$$\Delta^{\alpha}_{\beta}\phi = \Delta^{\alpha}_{\beta}\phi^{0}_{M^+} + (RT/F)\ln(\gamma_{M^+}{}^{\beta}/\gamma_{M^+}{}^{\alpha}) = \Delta^{\alpha}_{\beta}\phi^{\theta}_{M^+} \qquad (2.1.9)$$

Eq.(2.1.9) is frequently used in the investigation of ITIES.

(ii) ITIES Reversible with Respect to Both Ions.

For a 1:1 valent electrolyte of the type MX dissolved in both phases as represented by the following scheme [1,7],

$$\underset{(\alpha)}{M^+X^-} \;\|\; \underset{(\beta)}{M^+X^-} \qquad \text{(IV)}$$

the Galvani potential difference (distribution potential) is expressed by the equation [1,4],

$$\Delta^{\alpha}_{\beta}\phi_{MX}=(\Delta^{\alpha}_{\beta}\phi^{o}_{M^+}+\Delta^{\alpha}_{\beta}\phi^{o}_{X^-})/2+(RT/2F)\ln[(\gamma_{M^+}{}^{\beta}\gamma_{X^-}{}^{\alpha})/(\gamma_{M^+}{}^{\alpha}\gamma_{X^-}{}^{\beta})] \qquad (2.1.10)$$

which is independent of salt concentration, and the supply of a charge from an external source cannot result in a change in $\Delta^{\alpha}_{\beta}\phi$ [4]. The standard Galvani potential is given as

$$\Delta^{\alpha}_{\beta}\phi^{o}_{MX} = 1/2F(\Delta G^{o,}{}_{t,X^-}{}^{\alpha\to\beta} - \Delta G^{o,}{}_{t,M^+}{}^{\alpha\to\beta}) \qquad (2.1.11)$$

2.1.2 *IDEALLY-POLARISABLE INTERFACE*

If a system is composed of a strongly hydrophilic 1:1 electrolyte M_1X_1 in phase α and a strongly hydrophobic 1:1 electrolyte M_2X_2 in phase β as shown below,

$$M_1X_1 \;\|\; M_2X_2 \qquad (v)$$
$$(\alpha) \qquad (\beta)$$

corresponding to the following condition regarding the standard Gibbs energy of transfer

$$\Delta G^{o,}{}_{t,M_1^+}{}^{\alpha->\beta} \text{ and } \Delta G^{o,}{}_{t,X_1^-}{}^{\alpha->\beta} >> 0$$

and

$$\Delta G^{o,}{}_{t,M_2^+}{}^{\alpha->\beta} \text{ and } \Delta G^{o,}{}_{t,X_2^-}{}^{\alpha->\beta} << 0$$

then there exists a potential window in which $\Delta^{\alpha}{}_{\beta}\phi$ is controlled by the electrical charge in the electrical double layer rather than by the activities of the ions. Such an interface has the properties of an ideally polarisable electrode in which the interface behaves as a capacitor [4]. For equal volumes of the two phases and $\gamma_i{}^{\alpha} = \gamma_i{}^{\beta}$ the Galvani potential difference can be given as [4,8],

$$\Delta^{\alpha}{}_{\beta}\phi = \frac{(RT/2F)\ln\left(n_{X_1}\exp(F/RT)\Delta^{\alpha}{}_{\beta}\phi^{o}{}_{X_1} + n_{M_2}\exp(F/RT)\Delta^{\alpha}{}_{\beta}\phi^{o}{}_{M_2} \right)}{n_{M_1}\exp(-F/RT)\Delta^{\alpha}{}_{\beta}\phi^{o}{}_{M_1} + n_{M_2}\exp(-F/RT)\Delta^{\alpha}{}_{\beta}\phi^{o}{}_{M_2}}$$

(2.1.12)

where n_i stands for the number of moles of the i species in the system.

2.1.3 *FACILITATED ION TRANSFER*

In the presence of a hydrophobic ligand (L) in the organic phase and a

metal cation (M^{Z+}) in the aqueous phase the cross transfer reaction is

$$M^{Z+,\alpha} + mL^{\beta} \rightleftharpoons ML_m^{Z+,\beta} \qquad (VI)$$

For a 1:1 metal cation (M^+) to ligand ratio the stability constant K_{ML^+} of the complex in the organic phase (β) is represented by the equation,

$$K_{ML^+} = (a^{\beta}_{ML^+})/(a^{\beta}_{M^+}a^{\beta}_{L}) \qquad (2.1.13)$$

The Galvani potential difference between phases α and β for a reversible facilitated transfer is [1,4] (see Eq. 2.1.8),

$$\Delta^{\alpha}_{\beta}\phi = \Delta^{\alpha}_{\beta}\phi^{0}_{M^+} + (RT/F)\ln(a^{\beta}_{M^+}/a^{\alpha}_{M^+}) \qquad (2.1.14)$$

Substituting Eq.(2.1.13) into Eq.(2.1.14) leads to

$$\Delta^{\alpha}_{\beta}\phi = \Delta^{\alpha}_{\beta}\phi^{0}_{M^+} + (RT/F)\ln(a^{\beta}_{ML^+}/K_{ML^+}a^{\beta}_{L}a^{\alpha}_{M^+}) \qquad (2.1.15)$$

Thus, the facilitated ion transfer depends on the magnitude of the stability constant and of the ligand concentration in the organic phase [4].

Experimentally, in using the technique of voltammetry, certain conditions have to be imposed in order to solve the equations for $\Delta^{\alpha}_{\beta}\phi_{1/2}$ or $\Delta^{\alpha}_{\beta}\phi^{0}$. Thus two important cases are considered [1,4].

(i) In the case of very high concentration of the metal ion in the aqueous phase (α) and very low concentration of the ligand in the organic phase (β), the electric current due to ion transfer from the aqueous to the organic phase

and back is controlled by diffusion of the ligand to the ITIES and by diffusion of the complex formed from the ITIES, or by the reverse processes. The free metal ion in the aqueous phase is considered constant. At the half-wave potential the following condition applies provided the chemical reaction processes are rapid with fast ion transfer [4,5],

$$(D^{\beta}_{LM^+})^{1/2}(a^{\beta}_{LM^+})_{X=0} = (D^{\beta}_{L})^{1/2}(a^{\beta}_{L})_{X=0} \qquad (2.1.16)$$

where D stands for diffusion coefficient. The reversible half-wave potential difference is then given by the equation [4,5],

$$\Delta^{\alpha}_{\beta}\phi_{1/2} = \Delta^{\alpha}_{\beta}\phi^{o}_{M^+} + (RT/F)\ln[(D^{\beta}_{L}/D^{\beta}_{ML^+})^{1/2}(\gamma^{\beta}_{ML^+}/\gamma^{\beta}_{L})] - (RT/F)\ln(K_{ML^+}a^{\alpha}_{M^+}) \qquad (2.1.17)$$

and thus the stability constant of the complex in the organic phase can be determined.

(ii) For very high concentration of the ligand in the organic phase and very low concentration of the metal ion in the aqueous phase, the concentration of the ligand is considered to be constant. In this case the rate determining steps are the diffusion of the free metal ion from the aqueous phase to the ITIES and of the complex to the bulk of the organic phase from the ITIES (and vice versa for the reverse process). The reversible half-wave potential difference is given by the relationship [4,5],

$$\Delta^{\alpha}_{\beta}\phi_{1/2} = \Delta^{\alpha}_{\beta}\phi^{o}_{M^+} + (RT/F)\ln[(D^{\alpha}_{M^+}/D^{\beta}_{ML^+})^{1/2}(\gamma^{\beta}_{ML^+}/\gamma^{\alpha}_{M^+})] - (RT/F)\ln(K_{ML^+}a^{\beta}_{L}) \qquad (2.1.18)$$

From Eq. (2.1.18) it can be seen that the stability constant of the complex in

the aqueous phase can be obtained.

2.1.4 *DETERMINATION OF STANDARD GIBBS ENERGIES OF TRANSFER.*

The standard Gibbs energy of transfer of an ion i from pure solvent α to pure solvent β is defined as the difference of the standard Gibbs energy of solvation of i in the two phases. This thermodynamic quantity is normally determined from solubility experiments and is different from the Gibbs energy of partition, which refers to the transfer from the solvent α to solvent β when the two solvents are mutually saturated with each other [9].

The standard Gibbs energy of transfer of individual ions are not accessible to a direct measurement unless an extra thermodynamic assumption is made. The most often used is the "tetraphenylarsonium tetraphenylborate (TPAsTPB) assumption", which states that the standard Gibbs energies of transfer of $TPAs^+$ cation and TPB^- anion are equal in any pair of solvents [9]. This assumption is based on the fact that the cation and the anion are symmetrical species of much the same size and shape with the charge "buried" under the phenyl groups. Thus, the same standard Gibbs energy of transfer from an arbitrary solvent α to another solvent β holds for both ions [10].

$$\Delta G^{0,\alpha\rightarrow\beta}_{t,(TPAs^+)} = \Delta G^{0,\alpha\rightarrow\beta}_{t,(TPB^-)} = 1/2(\Delta G^{0,\alpha\rightarrow\beta}_{t,(TPAsTPB)}) \qquad (2.1.19)$$

On the basis of this assumption a scale for standard Gibbs energies of partition of ions from one solvent to another can be obtained.

In voltammetric experiments, the TPAsTPB assumption can be employed in order to get absolute values for the standard Galvani potential of ion transfer. If TPAsTPB is used as the base electrolyte in the organic phase and Li_2SO_4, or LiF in the aqueous phase, the voltammogram will be limited by the transfer of $TPAs^+$ cation and TPB^- anion at the negative and positive ends of the

potential window respectively. Thus the zero point of the Galvani potential can be fixed from the relationship

$$(\Delta^{\alpha}_{\beta}\phi_{1/2,\,TPAs^+} + \Delta^{\alpha}_{\beta}\phi_{1/2,\,TPB^-})/2 = \Delta^{\alpha}_{\beta}\phi = 0 \qquad (2.1.20)$$

Theoretically $\Delta G^0_{t}{}^{,\alpha\rightarrow\beta}$ can be estimated from the standard Gibbs energies of solvation of an ion in the two solvents:

$$\Delta G^0_{t}{}^{,\alpha\rightarrow\beta} = \Delta G^0_{s} - \Delta G^0_{h} \qquad (2.1.21)$$

where ΔG^0_{s} and ΔG^0_{h} are the standard Gibbs energy of solvation and hydration of the ion respectively. According to Abraham and Liszi [11,12], ΔG^0_{s} may be split into an electrostatic term and a neutral term

$$\Delta G^0_{s} = \Delta G^0_{el} + \Delta G^0_{n} \qquad (2.1.22)$$

where ΔG^0_{n}, the neutral term, is the Gibbs energy of solvation of a non-polar gaseous solute of the same size as the ion of interest. In the one-layer continuum model the electrostatic energy term ΔG^0_{el} refers to an ion of radius a and dielectric constant $\varepsilon_i = 1$, surrounded by a solvent layer of thickness (b-a) and dielectric constant ε_1 and immersed in the bulk solvent dielectric constant ε_0. It is given by:

$$\Delta G^0_{el} = [N(Ze)^2/(8\pi\varepsilon^0)][[(1/\varepsilon_1)-1][(1/a)-(1/b)]+[(1/\varepsilon_0)-1]1/b] \qquad (2.1.23)$$

where N is the Avogadro number, ε^0 is the perimitivity of vacuum, a is the radius of the ion, and b is the solvent molecule radius plus a. In Eq.(2.1.23)

the first term is determined by the interaction of the ion with the first layer, and the second term is due to the long range polarization of the bulk of the liquid. ΔG^0_{el} for ions which are fully hydrated in the organic phase is calculated using the two-layer model in which a fully hydrated ion in a wet organic solvent is surrounded by a layer of water molecules. This is given by

$$\Delta G^0_{el} = [N(Ze)^2/(8\pi\varepsilon^0)][[(1/\varepsilon_1) - 1][(1/a) - (1/b) + [(1/\varepsilon_m)-1][(1/b)-(1/c)] + [(1/\varepsilon_0)-1]1/c] \quad (2.1.24)$$

where $\varepsilon_1=2$, $b-a=1.6$ Å (radius of H_2O molecule). In Eq.(2.1.24) the first term yields the contribution from the first layer; in the second term, ε_m is the dielectric constant of the second layer ($\varepsilon_m=(\varepsilon_b+\varepsilon_c)/2=29$) and $(c-b)$ is the thickness of this second layer. The third term gives the contribution of the bulk solvent outside the layers. The neutral contribution of the solvation energy is given by

$$\Delta G^0_n = ma + c \quad (2.1.25)$$

where m and c are constants the values of which are known for several solvents [11]. Eq.(2.1.25) is valid for ions of radius less than or equal to 3 Å. For a>3 Å, ΔG^0_n can be obtained using the data collected by Abraham [13].

2.2 THE ELECTRICAL DOUBLE LAYER AT ITIES

An electrochemical system is an impedance to a perturbing electrical signal with a small amplitude. The electrical behaviour of an interface can therefore be represented by an electrical equivalent circuit, a circuit of resistors and capacitors that pass current with the same amplitude and phase as the real system would under the same excitation [14,15].

A purely sinusoidal voltage can be expressed as [14],

$$e = E\sin\omega t \qquad (2.2.1)$$

and

$$\omega = 2\pi f, \qquad (2.2.2)$$

where E is the amplitude of the ac voltage and f is the conventional frequency in hertz. The sinusoidal current is analogously represented by the relationship

$$i = I\sin(\omega t + \delta) \qquad (2.2.3)$$

where I is the amplitude of the ac current and δ is the phase angle which is constant for a given frequency.

In the classical impedance measurement, a small sinusoidal voltage or current signal is applied to an electrochemical interface and the electrical current or voltage response is measured. From the complex voltage ($\mathbf{E}$) and the complex current ($\mathbf{I}$) the complex impedance ($\mathbf{Z}$) can be determined as [14],

$$\mathbf{Z} = \mathbf{E}/\mathbf{I} \qquad (2.2.4)$$

For a liquid / liquid electrochemical system the simplest circuit which can

represent the whole cell is;

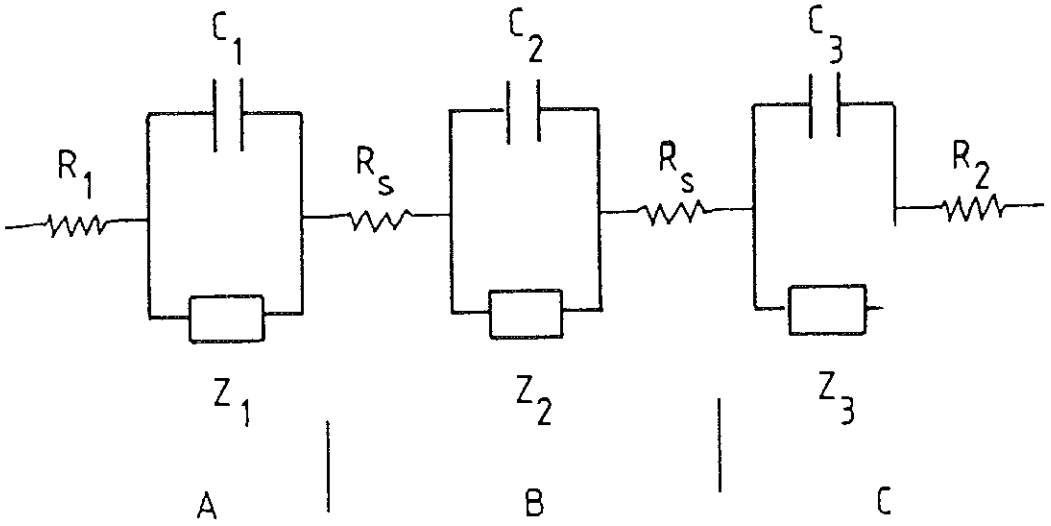

where A and C stand for the counter-electrodes and lead contributions to the overall impedance and B represents the electrochemical interface. In practice the impedances of A and C can be ignored by employing large surface area electrodes.

In an ideal potentiostatic arrangement, the circuit becomes,

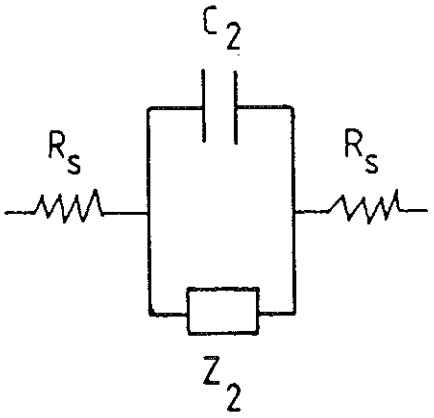

If the interface is ideally polarised it can be represented as a pure capacitor, and the Nyquist plot (the imaginary component of the impedance Z'' *vs* the real component Z') will be a perpendicular line displaced from the origin by the value of the solution resistance. For an interface which is not ideally polarisable the shape of the Nyquist plot becomes dependent on the impedance Z_2 [14-16].

Z_2 is often considered as a combination of a charge transfer resistance, R_{ct}, and a Warburg impedance, Z_W. The later is related to the impedance associated with the finite rate of diffusion. The relative magnitudes of R_{ct}, Z_W and C_2 determine the shape of the complex impedance plot. When the rate of transfer is slow, R_{ct} is greater than Z_W, and as a result one obtains a parallel RC circuit giving a semi-circle. On the other hand, if $R_{ct} << Z_W$, then a parallel Z_W and C_2 circuit exists. As shown in Fig. 2.2.1 both types of behaviour can exist in a Nyquist plot as the ratio of R_{ct} and Z_W can be frequency dependent. At high frequencies the kinetic control determines the impedance behaviour and the impedance plot is shown by a semicircle. As the measuring frequency decreases, the mass transfer control becomes more important and the impedance plot is characterised by a line with a slope of 45°, a typical case of the Warburg impedance [14,17].

For a fast, diffusion controlled, ion transfer process,

$$X^z(\alpha) \rightleftharpoons X^z(\beta)$$

where z is the charge number of the ion X, the impedance Z_2 becomes the Warburg impedance [17].

$$Z_2 = Z_W = (1-J)\sigma\omega^{-1/2} \qquad (2.2.5)$$

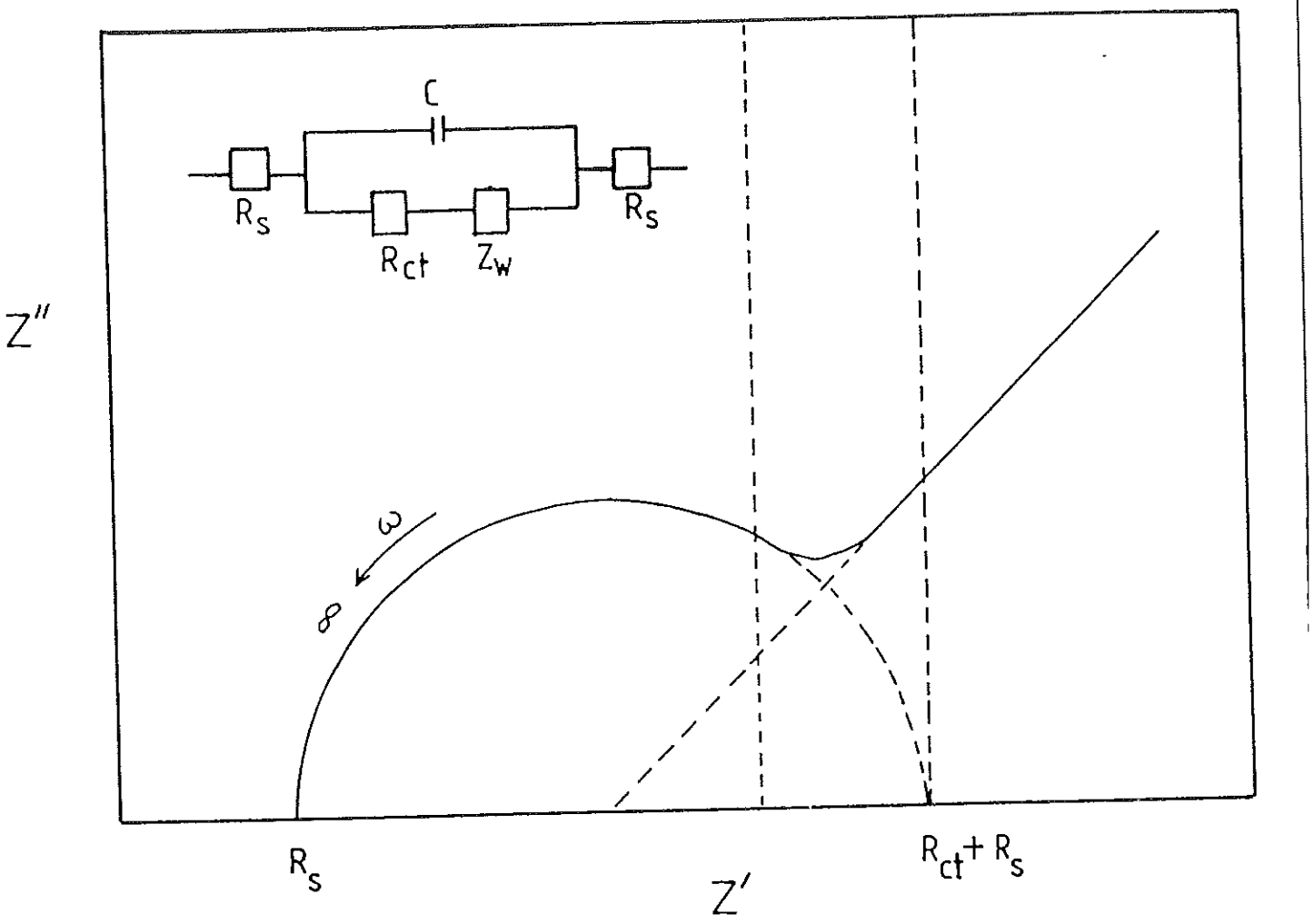

Fig. 2.2.1. Nyquist plot which shows the frequency dependent character. Regions of mass transfer and kinetic control are found at high and low frequencies, respectively.

where σ is a characteristic parameter of the faradaic process and is given as

$$\sigma = [4RT/(ZF)^2AC^0(2D)^{1/2}]\cosh^2[ZF(\Delta^{\alpha}_{\beta}\phi-\Delta^{\alpha}_{\beta}\phi_{1/2})/2RT] \qquad (2.2.6)$$

where A is the interfacial area, C^0 is the bulk concentration, D is the diffusion coefficient, and $\Delta^{\alpha}_{\beta}\phi_{1/2}$ is the reversible half-wave potential. Z' and Z'' then become [17],

$$Z' = |Z|\cos\delta = R_s+Z_cX[(X+1)^2+1]^{-1} \qquad (2.2.7)$$

$$Z'' = |Z|\sin\delta = Z_cX(X+1)[(X+1)^2+1]^{-1} \qquad (2.2.8)$$

The capacitive reactance Z_c is given by ,

$$Z_c = 1/\omega C \qquad (2.2.9)$$

and the parameter X is expressed as [17]

$$X = (Z_W/Z_c)2^{1/2} = 2\sigma C\omega^{1/2} \qquad (2.2.10)$$

If $X>>1$ (high frequency limit), then

$$Z' = R_s+Z_cX^{-1} = R_s+(2C^2\sigma)^{-1}\omega^{-3/2} \qquad (2.2.11)$$

and

$$Z'' = (\omega C)^{-1} \qquad (2.2.12)$$

The plot of Z'' vs Z' is not very informative. On the other hand, if $X<<1$ (low frequency limit), then

$$Z' = R_s + Z_W 2^{1/2} \qquad (2.2.13)$$

and

$$Z'' = Z' - R_s \qquad (2.2.14)$$

The impedance plot is a straight line with a slope of 1 . R_s can be evaluated from the high frequency limit of Eq.(2.2.11) and the value of X and C can be obtained from Eqs.(2.2.7) and (2.2.8).

In the ac impedance technique a sinusoidal voltage of small amplitude (≈ 5 mV peak to peak) and frequency ranging from 10 Hz to 1 KHz is superimposed on a small triangular voltage pulse (continuous method) or constant potential (point by point method). The alternating current flowing through the interface is analysed as a function of the dc potential E by means of phase sensitive detection. The in-phase $I(0^0)$ and quadrature $I(90^0)$ components of the current signal are transformed into the impedance Z and the phase shift according the relationships [18],

$$|Z| = E/[I(0^0)^2 + I(90^0)^2)]^{1/2} \qquad (2.2.15)$$

$$\delta = \tan^{-1}[I(90^0)/I(0^0)] \qquad (2.2.16)$$

In the modified Verwey-Niessen Model the Galvani potential difference is the sum of three components [19],

$$\Delta^{\alpha}_{\beta}\phi = \phi^{\alpha}_{\infty} - \phi^{\beta}_{\infty} \qquad (2.2.17)$$

$$= (\phi^{\alpha}_{\infty} - \phi^{\alpha}_{2}) + (\phi^{\alpha}_{2} - \phi^{\beta}_{2}) + (\phi^{\beta}_{2} - \phi^{\beta}_{\infty}) \qquad (2.2.18)$$

where $\phi_2 - \phi_\infty = \Delta\phi_2$, represents the potential drop in the diffuse layers of both

phases, respectively and $\phi^{\alpha}_{2} - \phi^{\beta}_{2} = \Delta^{\alpha}_{\beta}\phi_i$, stands for the potential drop across the inner layer.

From electroneutrality requirements [4,19],

$$q^{\alpha} = - q^{\beta} \qquad (2.2.19)$$

where q^{α} and q^{β} are the surface charge densities on both sides of the interface. In the absence of specific adsorption in the inner layer, the double layer capacity C can be expressed as a series combination of the inner layer capacity C_i and the diffuse layer capacities C_{α} and C_{β} [4,20,21],

$$C^{-1} = C_i^{-1} + C_{\alpha}^{-1} + C_{\beta}^{-1} \qquad (2.2.20)$$

where $C_i = dq^{\alpha}/d\Delta^{\alpha}_{\beta}\phi_i$, $C_{\alpha} = -dq^{\alpha}/d\Delta\phi^{\alpha}_{2}$, and $C_{\beta} = dq^{\alpha}/d\Delta\phi^{\beta}_{2}$.

Using the Gouy and Chapman relationship for a symmetrical (z:z) electrolyte the surface charge densities are [4,20,21],

$$q^{\alpha} = - 2A^{\alpha}\sinh(ZF\Delta\phi^{\alpha}_{2}/2RT) \qquad (2.2.21)$$

$$q^{\beta} = - 2A^{\beta}\sinh(ZF\Delta\phi^{\beta}_{2}/2RT) \qquad (2.2.22)$$

and

$$A^{\alpha(\beta)} = (2RT\varepsilon^{\alpha(\beta)}C^{0})^{1/2} \qquad (2.2.23)$$

where $\varepsilon^{\alpha(\beta)}$ is the permitivity of the solvent, and the capacity of the diffuse layer of each phase is [4,20]

$$C_{\alpha} = -\partial q^{\alpha}/\partial\Delta\phi^{\alpha}_{2} = (ZFA^{\alpha}/RT)\cosh(ZF\Delta\phi^{\alpha}_{2}/2RT) \qquad (2.2.24)$$

$$C_{\beta} = -\partial q^{\beta}/\partial \Delta\phi^{\beta}{}_{2} = (ZFA^{\beta}/RT)\cosh(ZF\Delta\phi^{\beta}{}_{2}/2RT) \qquad (2.2.25)$$

Using Eq.(2.2.19) the following relationship can be obtained [4],

$$\Delta\phi^{\alpha}{}_{2}=(RT/ZF)\ln\{[1+(\epsilon^{\beta}C^{0,\beta}/\epsilon^{\alpha}C^{0,\alpha})^{1/2}\exp(-ZF/2RT(\Delta^{\alpha}{}_{\beta}\phi-\Delta^{\alpha}{}_{\beta}\phi_{1}))]/[1+ (\epsilon^{\beta}C^{0,\beta}/\epsilon^{\alpha}C^{0,\alpha})^{1/2}\exp(ZF/2RT(\Delta^{\alpha}{}_{\beta}\phi-\Delta^{\alpha}{}_{\beta}\phi_{1}))]\} \qquad (2.2.26)$$

If $\Delta^{\alpha}{}_{\beta}\phi_{1}$ = constant, then $\Delta\phi^{\alpha}{}_{2}$ and $\Delta\phi^{\beta}{}_{2}$ can be calculated as the functions of $\Delta^{\alpha}{}_{\beta}\phi$. By substituting the values of $\Delta\phi^{\alpha}{}_{2}$ and $\Delta\phi^{\beta}{}_{2}$ into Eq.(2.2.24) or (2.2.25) respectively the theoretical diffuse double layer capacitance can be estimated.

References

1. J. Koryta, Electrochim. Acta, 24 (1978) 293.
2. S. Trasatti and R. Parsons, J. Electroanal. Chem., 205 (1986) 359.
3. J. Koryta, in V.E. Kazarinov (Ed.), The Interface Structure and Electrochemical Processes at the Boundary Between Two Immiscible Liquids, Springer-Verlag, Berlin, 1987, p.3.
4. V. Marecek, Z. Samec and J. Koryta, Advances in Colloid and Interface Science, 29 (1988) 1.
5. H.H.Girault and D.J. Schiffrin, in A.J. Bard (Ed.), Electroanalytical Chemistry, Vol.15, Marcel Dekker, Inc., New York, 1989.
6. Z. Koczorowski, in V.E. Kazarinov (Ed.), The Interface Structure and Electrochemical Processes at the Boundary Between Two Immiscible Liquids, Springer-Verlag, Berlin, 1987, p.77.
7. V.S. Markin and A.G. Volkov, Advances in Colloid and Interface Science, 31 (1990) 111.
8. LeQ. Hung, J. Electroanal. Chem., 115 (1980) 159.
9. A.J. Parker, Chem. Rev., 69 (1969) 1.
10. J. Koryta, Ions, Electrodes and Membranes, Wiley Interscience, New York, 1982.
11. M.H. Abraham and J. Liszi, J. Chem. Soc. Faraday Trans. 1, 74 (1978) 1604.
12. M.H. Abraham and J. Liszi, J. Inorg. Nucl. Chem. 43 (1981) 143.
13. M.H. Abraham, J. Am. Chem. Soc., 101 (1979) 5477.
14. A.J. Bard and L.R. Faulkner, Electrochemical Methods, Fundamentals and Applications, Wiley, New York, 1980.
15. M. Sluyters-Rehbach, J.H. Sluyters, in A.J. Bard (Ed.), Electroanalytical Chemistry, Vol. 4, Marcel Dekker, New York, 1970, p.1.
16. D.D. MacDonald, Transient Techniques in Electrochemistry, Plenum Press,

New York, 1977.

17. P. Haj kova, D. Homolka, V. Marecek and Z. Samec, J. Electroanal. Chem., 151 (1983) 277.
18. V. Marecek and Z. Samec, J. Electroanal Chem., 149 (1983) 185.
19. M. Gros, S. Gromb and C. Gavach, J. Electroanal. Chem., 89 (1978) 29.
20. Z. Samec, V. Marecek and D. Homolka, J. Electroanal. Chem., 126 (1981)121.
21. J. D. Reid, P. Vanysek and R.P. Buck, J. Electroanal. Chem., 161 (1984) 1.

CHAPTER THREE

SCOPE OF THE PRESENT WORK

3.1 SIMPLE ION TRANSFER STUDIES

Numerous electrochemical studies of ion transfer across immiscible water/organic solvent interfaces have been made in the past. The organic solvents that were studied were mainly nitrobenzene and 1,2-dichloroethane [1]. The importance and applications of such investigations in the fields of chemistry and biology have been fully described elsewhere [1,2]. The importance of ion transfer studies across such systems lies in the improvement in the understanding of the processes occurring at the interfaces, collection of thermodynamic and kinetic data for the transfer, development of new electroanalytical tools, and improvement in the understanding of liquid/liquid extraction processes. However, certain difficulties are encountered in extending such studies to many other water/organic solvent systems. This is due to the low dielectric constant of most organic solvents that are immiscible with water resulting in very low conductivity of electrolyte solutions. As a result the systems which were investigated so far are few in number. Thus a search for organic solvents which satisfy the above requirement is essential if the field of liquid/liquid electrochemistry is to be to widened.

In the present work the organic solvents chosen were o-nitrotoluene, benzonitrile and o-dichlorobenzene. o-nitrotoluene has a fairly high dielectric constant (ε_0=27.4), low solubility in water (0,065%w) and higher density than water (1.16 g cm^{-1}) [3]. On the other hand benzonitrile is a strongly polar aromatic solvent which dissolves many organic substances, anhydrous inorganic salts and organometallic compounds. A number of electrochemical investigations have been carried out in benzonitrile [4]. This solvent enables voltammetric investigations to be carried out over a wide potential range. It has a relatively high dielectric constant (25.2 at 15 °C), low miscibility with water (0,2%w benzonitrile in water and 1%w water in benzonitrile) [3]. It is not a strongly coordinating solvent as seen from its Gutman donor-acceptor number of 15 [4].

o-dichlorobenzene is a stable solvent for many organic salts as compared with halogenated alkyl solvents and possesses some excellent characteristics as a solvent in synthetic and extraction processes [3]. It has a dielectric constant of 9.93 (at 20 °C), with density of 1.31 g cm^{-3} and very low miscibility with water (0.02%w o-dichlorobenzene in water and 0.31%w water in o-dichlorobenzene).

In the present work, the transfer of several ions across the immiscible liquid/liquid interface was investigated using water and the above organic solvents. The results of the experimentally determined standard Gibbs energies of transfer are compared with theoretically calculated values.

3.2 COMPLEX ION TRANSFER AND FACILITATED ION TRANSFER STUDIES

There has been appreciable interest in the bidentate and terdentate analogues of the pyridine molecules as ligands for transition metal complex formation. These compounds are very similar to the biologically important heterocyclic ligands such as the porphyrines and pyrines [5-8].

The chemistry of the terdentate ligand 2,2′,2″-terpyridine (**1**; terpy) and its metal complexes has been investigated widely (see, for example, ref. 5 and references cited therein). The ligand readily forms stable one-to-one and one-to-two (metal to ligand) complexes with transition metals. This ligand and its derivatives have been widely proposed as analytical reagents for the detection of metal ions in biological and other samples, as photometric reagents and as masking agents. Their metal chelates are also used as redox indicators [9-11].

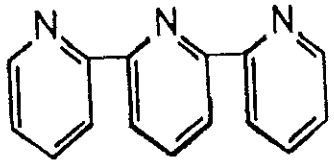

1

Numerous studies on the photochemical, photophysical, electrochemical and kinetic properties of many transition metal-terpyridine complexes have been carried out [12-19]. Some complexes of terpyridine have been reported as effective catalysts for the electrocatalytic oxidation of alcohols, aromatic hydrocarbons and olefins [20-23]; as oxygen transfer catalysts for the oxidation of thiosulphate to sulphate [24]; and as catalysts for the hydrolysis of fluorophosphate esters [25].

The complexes of some transition metals with terpyridine have attracted attentions as photosensitizers, the redox properties of which satisfy the thermodynamic requirements for the photodecompostion of water [26,27].

Although very few complex ion transfer studies were made using transition metal complexes of bidentate nitrogen containing ligands [28-30], no terdentate ligand complexed metal transfer has up to now been investigated. Complex ion transfer studies at ITIES can provide information about the relative stability of complexes, the type of complexation, transport and thermodynamic parameters. Phase transfer of complexed transition metal ions is also very important in solvent extraction processes, which are frequently used in hydrometallurgy, metal extraction, and metal winning. In the first part of this work the transfer of the terpyridine complexes of Fe^{2+}, Fe^{3+}, Co^{2+}, Co^{3+}, Ni^{2+}, Zn^{2+} and Cu^{2+} across the water/nitrobenzene interface is discussed.

The nitrogen base ligand 2,2′-biquinoline (2) shows remarkable selectivity towards Cu^{+} ions [31]. In the presence of other metal cations the ligand forms coloured complexes selectively with Cu^{+}. This is understood to be due to the steric hindrance of the substituent groups on the carbon atoms adjacent to the ring nitrogen atoms [31,32].

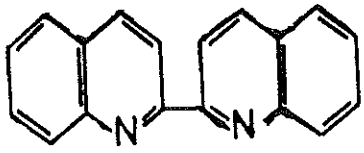

2

The characteristics of the Cu(I)-biquinoline complex in various non-aqueous solvents have been studied by several investigators [33-35]. The ligand is used for spectrophotometric micro-detection and quantitative determination of Cu^{+}. It also serves as masking reagent for the separation of other metal ions

in the presence of Cu^{+}. Various anions can be extracted into immiscible solvents as an ion-pair with Cu(I)-biquinoline chelate. Based on this principle, the extraction and photometric determination of colorless anions and anionic complexes can be conducted [31].

No work has been reported on the transfer of Cu(I) facilitated by biquinoline across ITIES. Thus a study has been made on biquinoline-assisted transfer of Cu^{+} across the water/1,2-dichloroethane interface.

3.3 THE ELECTRICAL DOUBLE-LAYER AT ITIES

The electrical double-layer at the ITIES has been investigated by many workers using various electrochemical methods (see refs. 1,2 and 36 and references cited therein). The most frequently used technique is the ac impedance measurement. Such studies have so far been made mainly on the water/nitrobenzene and water/1,2-dichloroethane interfaces. The quantity which can be obtained from the impedance measurements and which is related to the double layer structure is the interfacial capacitance. Extension of such studies to other solvent systems seems to be very important since it can contribute to the general understanding of the structure of the electrical double layer at liquid/liquid interfaces.

In the present investigation, the electrical double-layer at the water/o-dichlorobenzene,and water/o-nitrotoluene interfaces has been studied using different types of supporting electrolytes. The double-layer capacitances were measured at different concentrations using the ac impedance technique.The results are compared with those of the water/nitrobenzene and water/1,2-dichloroethane interfaces.

References

1. V. Marecek, Z. Samec and J. Koryta, Advances in Colloid and Interface Science, 29 (1988) 1.
2. H.H. Girault and D.J. Schiffrin, Electroanalytical Chemistry, A.J. Bard Ed., Vol. 15, Marcel Dekker Inc., New York, 1989.
3. J.A. Riddick and W.B. Bunger, Organic Solvents, Wiley and Sons, New York, 1986.
4. K. Kadish and J. Anderson, Pure Appl. Chem., 59 (1987) 704.
5. E.C. Constable, Adv. Inorg. Chem. Radiochem., 30 (1986) 69.
6. W.W Brandt, F.P. Dwyer and E.C. Gyarfas, Chem. Rev., 54 (1954) 959.
7. E.C. Constable, Polyhedron, 2 (1983) 551.
8. F.P. Dwyer and D.P. Mellor, Chelating Agents and Metal Chelates, Academic Press, New York, 1964.
9. D.W. Fink, J.V. Pivnichny and W.E. Ohnesorge, Anal. Chem., 41 (1969) 833.
10. S. Hadsovic, B. Nikolin and P. Stern, Eur. J. Pharmacol., 1 (1967) 15.
11. J.L. Lin, L.F. Chang and M. Satake, Bull. Chem. Soc. Jpn, 56 (1983) 2739.
12. M.C. Hughes, D.J. Macero and J.M. Rao, Inorg. Chim. Acta, 49 (1981) 241.
13. D.E. Morris, K.W. Hanck and M.K. DeArmond, J. Electroanal. Chem., 149 (1983) 115.
14. S. Musumece, E. Rizzarcelli, S. Sammartano and R.p. Bonomo, J. Inorg. Nucl. Chem., 36 (1974) 853.
15. J. Prasad and D.B. Scaife, J. Electroanal. Chem., 84 (1977) 373.
16. J.M. Rao, M.C. Hughes, and D.J. Macero, Inorg. Chim. Acta, 16 (1976) 231.
17. J.M. Rao, D.J. Macero and M.C. Hughes, Inorg. Chim. Acta, 41 (1980) 221.
18. T. Saji and S. Aoyagui, J. Electroanal. Chem., 58 (1975) 401.
19. T. Saji and S. Aoyagui, J. Electroanal. Chem., 108 (1980) 223.
20. B.A. Moyer, M.S. Thompson and T.J. Myer, J. Am. Chem. Soc.,

102 (1980) 2310.

21. M.S. Thompson, W.F. DeGiovani, B.A. Moyer and T.J. Meyer, J. Org. Chem., 49 (1984) 4972.
22. M.S. Thompson and T.J. Meyer, J. Am. Chem. Soc., 104 (1982) 4106.
23. M.S. Thompson and T.J. Meyer, J. Am. Chem. Soc., 104 (1982) 5070.
24. M. Chandra, K.F. O'Driscoll and G.L. Rempel, J. Mol. Catal., 8 (1980) 339.
25. T. Wagner-Jauregg, B.E. Hackley, T.A. Lies, O.O. Owens and R. Proper, J. Am. Chem. Soc., 77 (1955) 922.
26. Y.W.D. Chen, K.S.V. Santhanam and A.J. Bard, J. Electrochem. Soc., 129(1982)61.
27. Y.W.D. Chen, K.S.V. Santhanam and A.J. Bard, J. Electrochem. Soc., 128(1981)1460.
28. Z. Samec, D. Homolka, V. Marecek and L. Kavan, J. Electroanal. Chem., 145 (1983) 213.
29. D. Homolka and H. Wendt, Ber. Bunsenges. Phys. Chem., 89(1985)1075.
30. E. Wang and Y. Liu, J. Electroanal. Chem., 214 (1986) 465.
31. K.L. Cheng, K. Ueno and T. Imamura, Handbook of Organic Analytical Reagents, CRC Press, Florida, 1982.
32. G.F. Smith, Anal, Chem., 26 (1954) 1534.
33. R.T. Pflaum and W.W. Brandt, J. Am. Chem. Soc., 77 (1955) 2019.
34. J. Hoste, Anal. Chim. Acta, 4 (1950) 23.
35. J. Gillis, Anal. Chim. Acta, 8 (1953) 97.
36. Z. Samec, Chem. Rev., 88 (1988) 617.

CHAPTER FOUR

EXPERIMENTAL

4.1 CHEMICALS AND PREPARATION OF REAGENTS

4.1.1 *SOLVENTS AND THEIR PURIFICATION*

The organic solvents used in these studies were purified using the methods given in [1,2].

Benzonitrile (bn)- The commercially obtained benzonitrile (BDH, 98%) was washed successively with concentrated hydrochloric acid (MERCK), water, saturated potassium bicarbonate solution and finally twice with water. This pre-wash treatment was for the removal of isonitriles and amines which are the common impurities in this solvent [1,2]. The benzonitrile was then pre-dried with calcium chloride. The calcium chloride was decanted and the benzonitrile was transferred to a distillation apparatus containing phosphorous pentoxide. It was distilled under reduced pressure. The middle half of the distillate was stored over finely divided activated alumina and withdrawn as required.

O-nitrotoluene (o-nt)- The main impurities of o-nitrotoluene are believed to be o-and p-nitrophenols [1]. O-nitrotoluene (MERCK, Schuchardt) was washed several times with concentrated sulphuric acid (MERCK) until the acid layer became colourless, then washed twice with 20% sodium hydroxide solution, and finally washed several times with water until a neutral pH was obtained. The solvent was pre-dried over calcium chloride, followed by distillation from phosphorous pentoxide at reduced pressure. The middle half of the distillate was stored over activated alumina and kept in the dark to avoid exposure to light.

1,2-dichloroethane (1,2-dce)-The common impurities found in 1,2-dichloroethane are water, hydrogen chloride as well as other chlorinated hydrocarbons [2]. The commercially obtained 1,2-dichloroethane (Fluka, 98%) was purified following the procedure used for o-nitrotoluene.

Table 4.1.1

Selected Physical Properties of the Organic Solvents [a].

Property	Solvent				
	bn	1,2-dce	o-dcb	nb	o-nt
Density (ρ) (g cm^{-3}) (20 °C)	1.01 (15 °C)	1.25	1.31	1.2	1.16
Viscosity (η) (g m^{-1} s^{-1}) (25 °C)	1.45	0.887	1.32	2.17	2.37
Dielectric Constant (ε) (25 °C)	25.2	10.37	9.93	34.78	27.4
Refractive Index (n_D) (25 °C)	1.53	1.44	1.55	1.55	1.55
Solubility in water (%) (w/v)	0.2	0.81	0.02	0.19	0.07
Solubility of H_2O in solvent (w/v)	1	0.19	0.31	0.24	

[a] Taken from [1,3].

Nitrobenzene (nb)- The same purification procedure as for o-nitrotoluene was adopted for nitrobenzene (BDH)).

O-dichlorobenzene (o-dcb)- (Aldrich, 99% spectrophotometric grade) was used as received without further purification.

Throughout the experiments an all-glass doubly-distilled water was utilized for the preparations of all inorganic electrolyte solutions.

4.1.2 *CHEMICALS AND PREPARATION OF REAGENTS*

Crystalviolet tetraphenylborate (CVTPB) - was prepared by mixing equimolar amounts of crystalviolet chloride (CVCl),(Aldrich), and sodium tetraphenylborate (NaTPB) (Fluka), both dissolved in methanol (Analar,BDH). After evaporating the solvent, the CVTPB was extracted with benzene (Analar, BDH) and precipitated from the benzene solution by addition of n-hexane (spectroscopic grade, MERCK). The melting point of the obtained violet powder was 114-115 ^{0}C.

Tetraphenylarsonium tetraphenylborate (TPAsTPB) - was prepared by mixing equimolar aqueous solution of tetraphenylarsonium chloride (TPAsCl) (Fluka), with an aqueous solution of sodium NaTPB. The white precipitate was washed several times with water and then recrystillised twice from acetone (Analar, BDH).

Tetraphenylarsonium tetrakis(4-chlorophenyl)borate (TPAsTPBCl)-was prepared by mixing equimolar aqueous solution of TPAsCl and methanol solution of potassium tetrakis(4-chlorophenyl)borate (KTPBCl) (selectophore, Fluka). The white precipitate was filtered and washed thoroughly with water and recrystallised twice from acetone.

μ-nitrido-bis(triphenylphosphorus)3,3-como-bis(undecahydro-1,2-dicarba-3-cobalta-closododecabor)ate (PNPDCC) - was prepared by mixing

equimolar amounts of acetone solutions of PNPCl [4] and CsDCC. CsCl was precipitated and filtered out of the solution. The acetone was evaporated at reduced pressure until an orange residue was left, which was then recrystallised twice from n-propanol (spectroscopic grade, MERCK). Yellow needles of PNPDCC were finally obtained with melting point of 186-186.5 °C.

μ-nitrido-bis(triphenylphosphorus) tetraphenylborate (PNPTPB) and tetraphenylarsonium 3,3- como - bis (undecahydro-1,2-dicarba-3-cobalta-closododecabor)ate (TPAsDCC) - were prepared by following the procedure used for the PNPDCC.

Tetrabutylammonium tetraphenylborate (TBATPB)-(Fluka, 99%), was used as received.

Li_2SO_4 (BDH), LiCl (Fluka, water free), LiF (BDH) were recrystallised from their supersaturated aqueous solutions for the impedance measurements.

$NaClO_4$ (BDH), $NaIO_4$ (BDH), KSCN (BDH), sodium picrate (NaPi, BDH), tetramethylammonium chloride (TMACl, BDH), tetraethylammonium chloride (TEACl, BDH), tetrapropylammonium chloride (TPrACl, Fluka), tetrabutylammonium chloride (TBACl, Fluka), tetrapentylammonium chloride (TPACl, Fluka), 2,2′,2″-terpyridine (Fluka, 99%), 2,2′-biquinoline (Fluka, 99%), $CoSO_4$ (Analar, BDH), $ZnSO_4$ (Analar, BDH), $FeSO_4$ (Analar, MERCK), $Fe_2(SO_4)_3$ (Analar, MERCK), $CuSO_4$ (Analar, BDH), $NiSO_4$ (Analar, BDH), CuCl (Fluka), ,30% H_2O_2 (MERCK), NaOH (BDH), $CaCl_2$ (BDH), $KHCO_3$ (MERCK), P_2O_5 (BDH) were used as such without further purification.

Stock solutions of the base electrolytes were prepared at concentrations of 10 mM and 50 mM and then diluted as required. CVTPB, PNPDCC, TPAsDCC, TBATPB, TPASTPBCl and PNPTPB were used independently as base electrolytes in the organic phase, whereas TPAsTPB was mainly employed to fix the zero of the Galvani potential difference. LiCl, LiF, and Li_2SO_4 were used as base electrolytes in the aqueous phase.

For all studied electrolytes, stock solutions were prepared at a

concentration of 50 mM and diluted as necessary, immediately prior to use. In the case of the complex-ion transfer studies, solutions of the metal cations were prepared in the aqueous phase together with the complexing ligand terpyridine outside the electrochemical cell. The ligand was found to be very slightly soluble in water, but in the presence of transition metal ions it readily forms coloured solutions. The prepared metal to ligand ratios were 5:1, 2:1, 1:1, 1:2, 1:3, 1:4 and 1:5. When it was necessary to avoid air oxidation of the solutions fresh solutions of the complexes were prepared daily under nitrogen atmosphere. When excess amount of $[Co(terpy)_2]^{+3}$ was required, it was prepared by oxidising the solution of Co^{+2} and terpyridine with 10% H_2O_2 solution followed by boiling of the solution until the test for H_2O_2 was negative. In all experiments, the organic and the aqueous phase were equilibrated with each other before use. The measured Galvani potential differences are aqueous with respect to organic. All measurements were made at a laboratory temperature of 22±1 ^{0}C.

4.1.3 *MEASUREMENT OF pH*

A Phillips pH meter (PW 9418) with a combined glass electrode was used for pH measurements. The pH meter was calibrated for every set of experiments using standard buffer solutions of pH 4 and pH 7. All pH measurements were carried out at room temperature 22±1 ^{0}C.

4.1.4 *UV/VISIBLE ABSORPTION MEASUREMENTS*

The absorption measurements of the complex species were carried out using a computerized Beckman Model DU-65 spectrophotometer. One centimeter

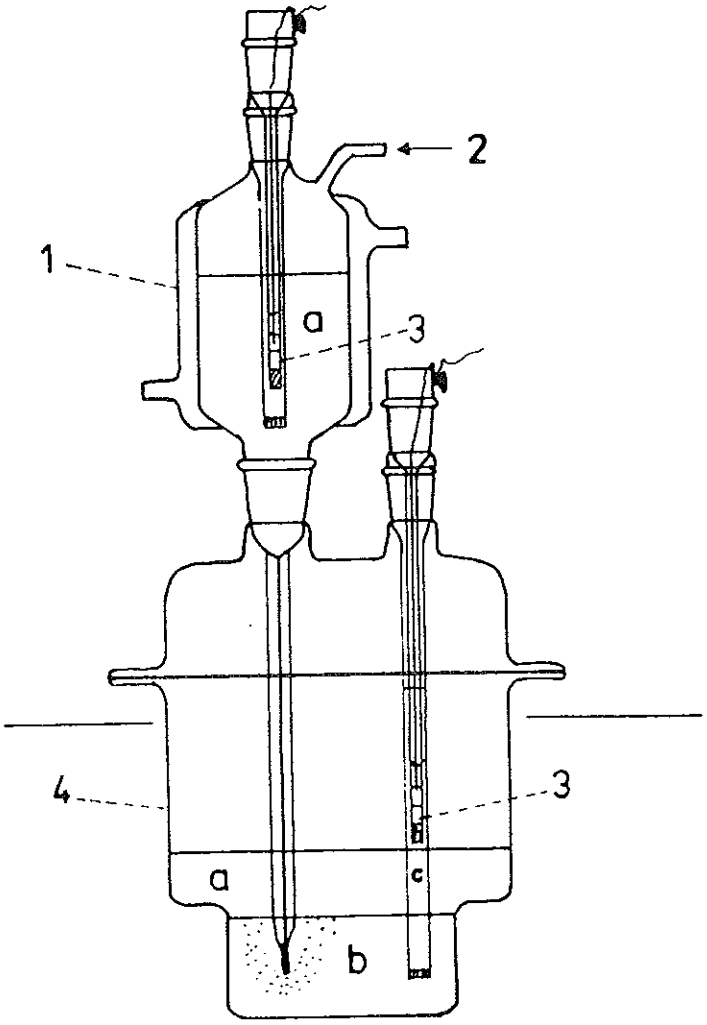

Fig. 4.1.1. Diagram of the cell used for the measurement of the point of zero charge at ITIES. (a) Aqueous solution; (b) organic solution; (c) aqueous tetrabutylammonium bridge. (1) Jacketed aqueous solution reservoir; (2) N_2 pressure inlet; (3) saturated calomel reference electrodes; (4) streaming electrode reservoir.

path length quartz cuvettes were employed. The measurements were carried out at room temperature, 22±1 °C.

4.1.5 *MEASUREMENT OF POTENTIAL OF ZERO CHARGE*

The streaming jet method was used for the potential of zero charge measurement. The cell used was similar to that described in ref. 5 and is shown in Fig.4.1.1. The streaming jet was made with the aqueous solution. The reference electrodes used were calomel electrodes. The solutions employed were 10 mM LiCl, 10 mM TBACl in water and 10 mM TBATPB in o-nitrotoluene. Due to very low solubility of TBATPB in o-dichlorobenzene the experiment was not carried out for this solvent system. The cell was thermostated and the temperature was kept at 22 °C. The cell arrangement was as shown below [5].

SCE | 10 mM TBACl(w) | 10 mM TBATPB(O) | 10 mM LiCl(w) | SCE

4.2 ELECTROCHEMICAL CELL ARRANGEMENTS

As shown in Figure 4.2.1 and 4.2.2 the electrochemical cells employed in these studies contained four electrodes and were generally similar to that used by Samec et al. [6]. Cell (I) was mainly used for the simple ion transfer studies of the dc cyclic experiments whereas cell (II) was employed for the ac-impedance experiments.

Cell (I) had an interfacial area of 0.283 cm^2, with aqueous and organic compartments of 5 cm^3 volume respectively. The two current supplying and withdrawing counter electrodes were circular Pt gauze (10 mm diameter) positioned parallel with respect to the interface in both phases. The potential difference at the interface was monitored by means of two reference electrodes connected via Luggin capillaries to each phase. The reference electrodes in each phase were immersed in aqueous solutions of the corresponding base electrolytes. A Ag/AgCl electrode served as the reference electrode for both phases, and was repeatedly renewed by anodic polarization in 0.1 M KCl solution with a current density of 5 mA/cm^2 for two hours.

Cell (II) had an interfacial area of 0.69 cm^2, with volumes of 0.5 cm^3 (organic) and 2 cm^3 (aqueous). The two current supplying and withdrawing counter electrodes were similar to those of cell (I). The reference electrode used in the aqueous phase was either a Ag/AgCl electrode immersed directly in to the solution (when LiCl was employed as the base electrolyte) or a calomel electrode (when Li_2SO_4 or LiF was used as a base electrolyte) connected with an agar bridge to the test solution.

Prior to each experiment the cell was washed with a solution of chromic acid, then with acetone and doubly distilled water and finally dried in an oven. This washing procedure was used also to clean the glassware in every experiment.

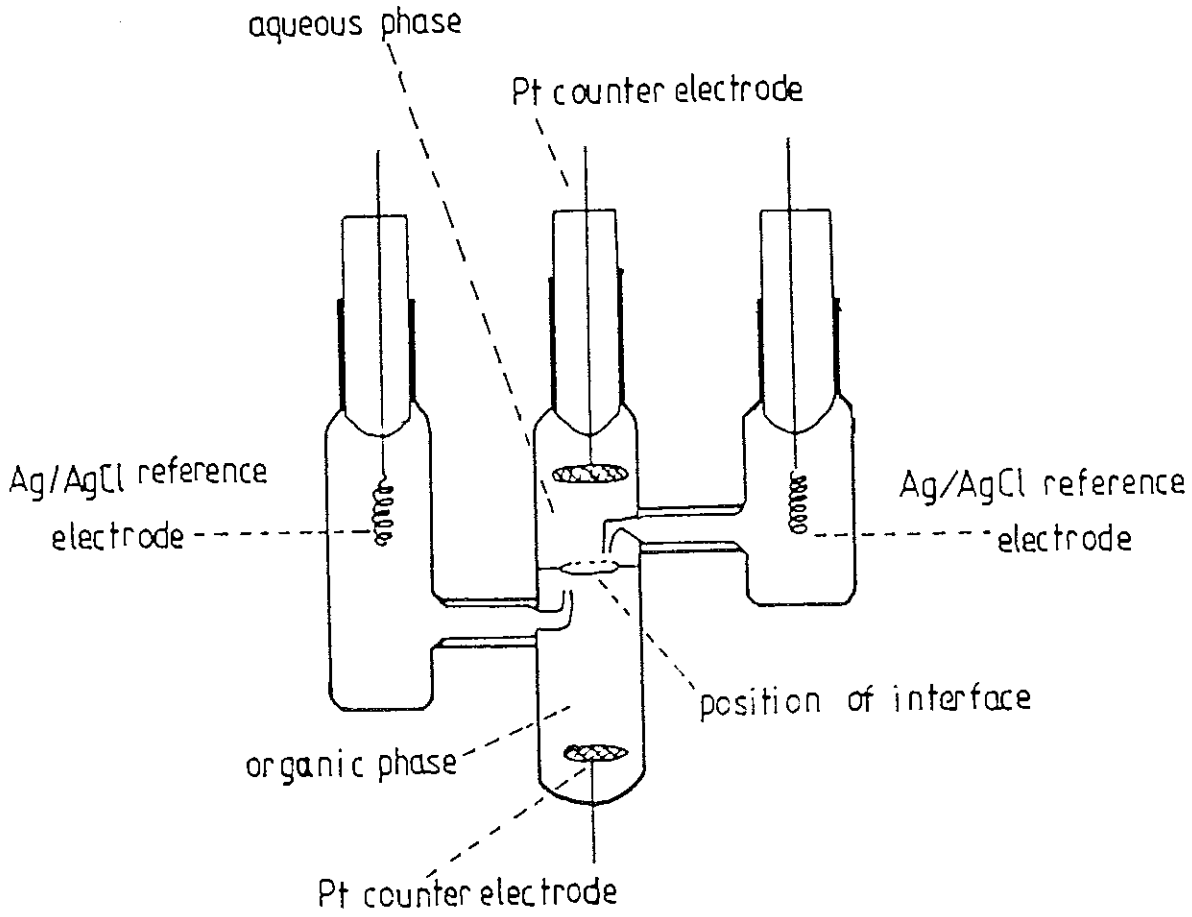

Fig. 4.2.1. ELECTROCHEMICAL CELL (I)

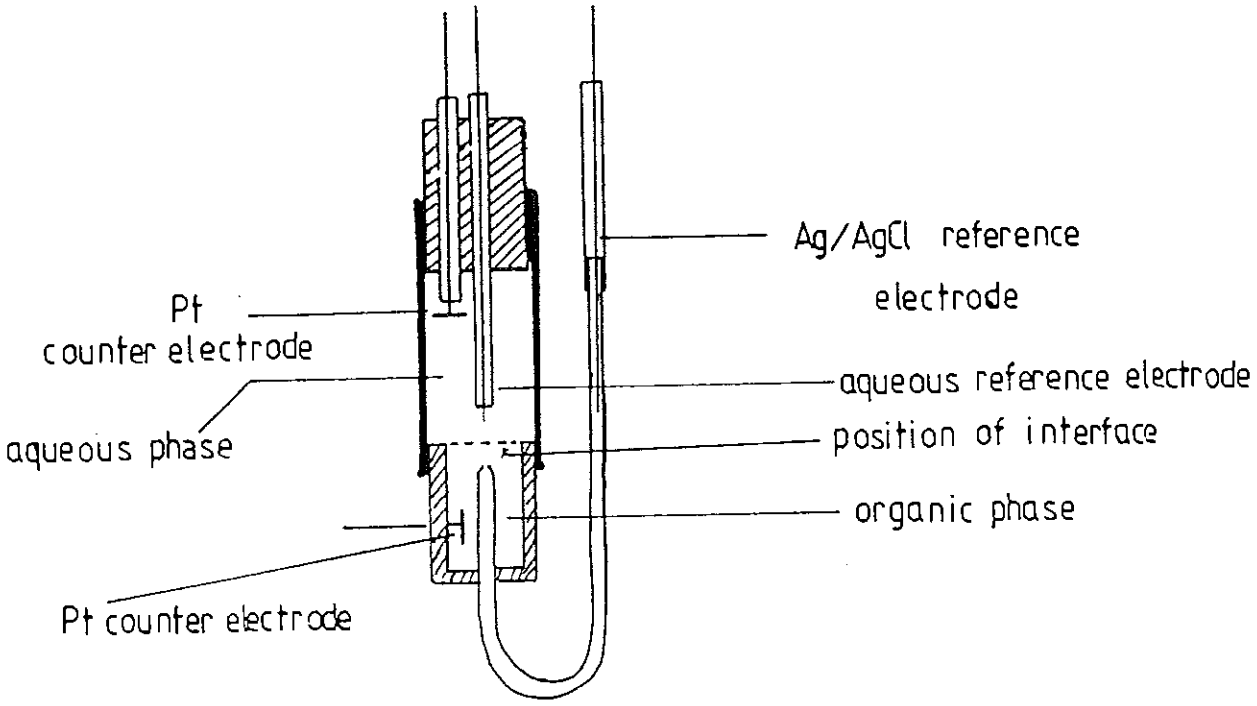

Fig. 4.2.2. ELECTROCHEMICAL CELL (II)

Schematic representations of the interfaces are presented as follows.

Ag|AgCl| 10 mM TPAsCl(w)| 10 mM TPAsTPB(O)|6| 10 mM LiCl(w)|AgCl|Ag

Ag|AgCl| 10 mM TPAsCl(w)| 10 mM TPAsTPB(O)|6| 5 mM Li_2SO_4(w)|SCE

where, 6 is the interface under investigation.

4.3 ELECTRONIC INSTRUMENTATION

The electronic set-up used for the dc cyclic experiments and impedance measurements are represented by the block diagrams of Fig. 4.3.1 and 4.3.2. A four electrode potentiostat with automatic IR compensation similar to that described in ref. 6 was constructed and employed. To regulate the proper compensation of the ohmic drop across the interface, the current output of the potentiostat was connected to an oscilloscope (Tektronix Model 501).

For the dc cyclic and linear sweep voltammetric experiments, linear and triangular voltage ramps were supplied from a scan generator (YSG 72, Bank). The current output of the potentiostat was connected directly to a storage oscilloscope (Tektronix Model 5441) and an X-Y recorder (LLOYD Instruments PLC-3).

For the ac-impedance experiments the superimposed sinusoidal potential was of magnitude ΔE=5 mV peak to peak and was fed from a frequency generator (Tektronix FG 501) while the triangular voltage ramp (5 mV/s) was generated using MP-1502 Electroanalyzer (McKee Pedersen Instruments). The current output of the potentiostat was connected to the input of a lock-in analyzer (PAR Model 5204) which was used for the continuous measurement of the in-phase and quadrature components of the ac-current. The outputs were detected using the storage oscilloscope and X-Y recorder. The real and imaginary parts of the impedance were then calculated from the in-phase and quadrature components using an ATARI (1040ST) micro computer.

A simple RC parallel circuit was used to test the frequency response of the potentiostat and the lock-in analyser. The observed impedance spectra of the dummy cell were as expected. The values of the resistance and the capacitance were accurately determined from the impedance plot at $R_{ct}/2$ using the equation [7]:

$$\omega = 1/(R_{ct}\, C) \qquad (4.3.1)$$

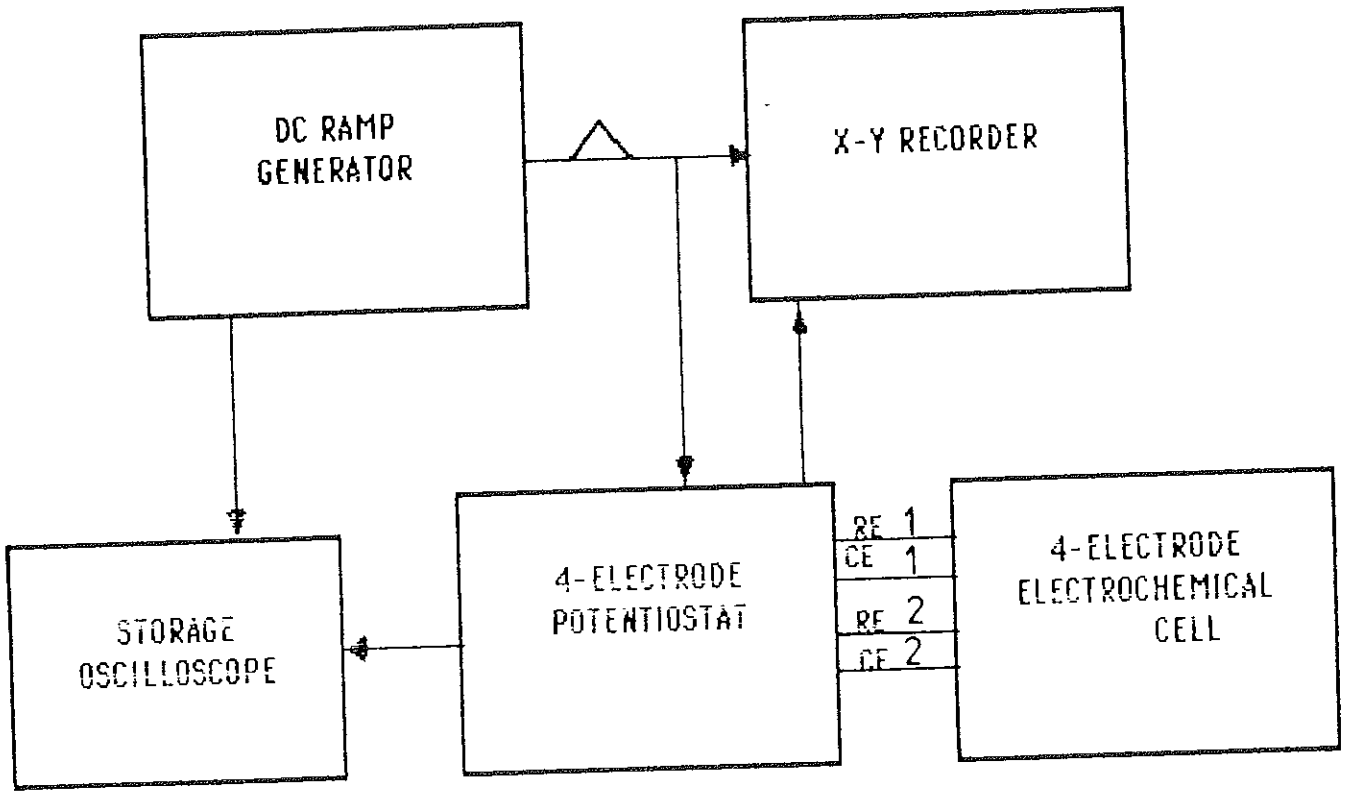

Fig. 4.3.1. Block diagram of the electrical set-up used for dc cyclic voltammetric studies.

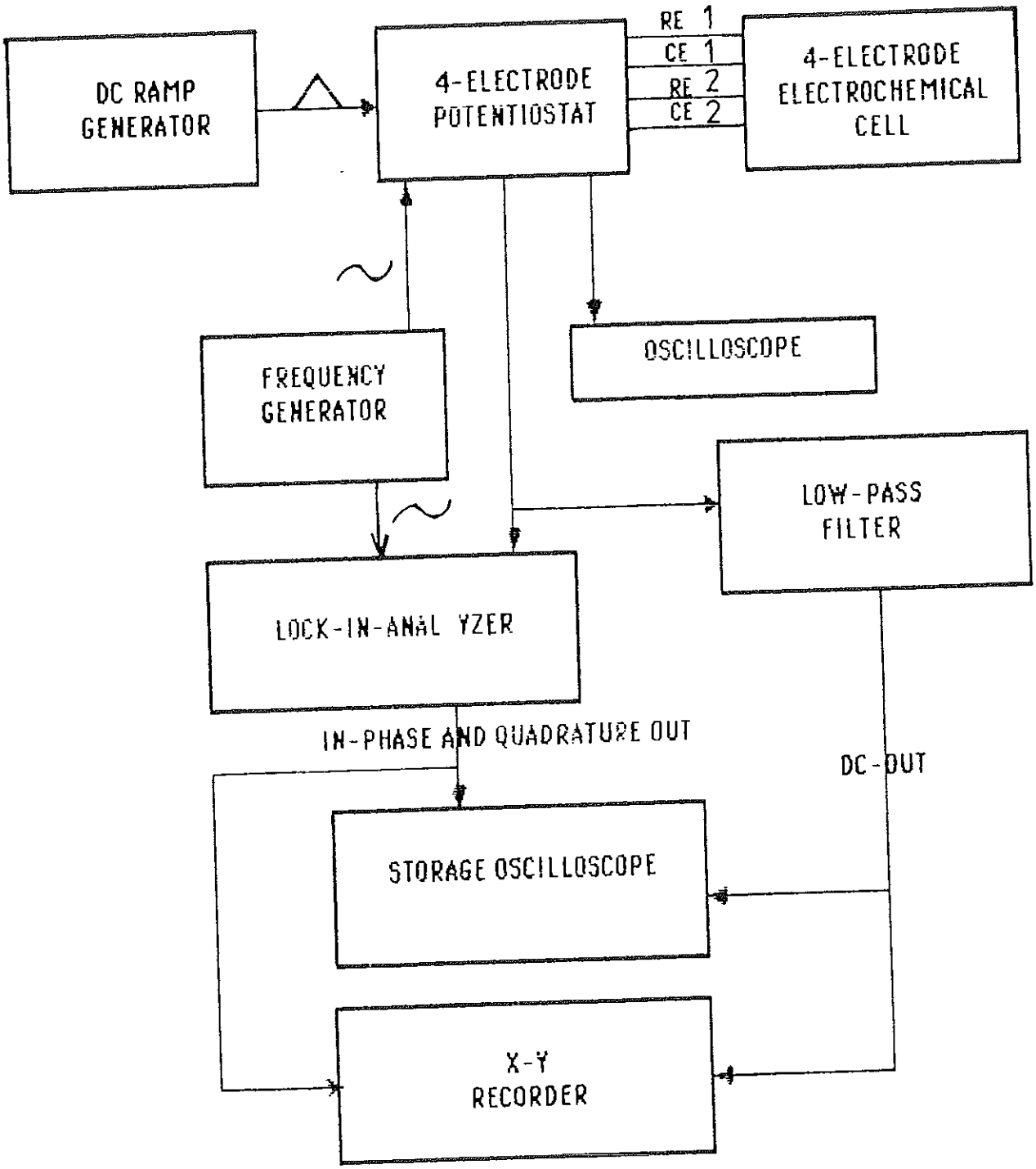

Fig. 4.3.2. Block diagram of the electrical set-up used for ac cyclic and impedance studies.

References

1. J.A. Riddick and W.B. Bunger, Organic Solvents, 4th ed., Wiley and Sons, New York, 1986.
2. K. Kadish and J. Anderson, Pure Appl. Chem., 59(1987)704.
3. N.A. Lange, Handbook of Chemistry, McGraw-Hill, New York, 1967.
4. J.K. Ruff and W.J. Schlientz, Inorganic Synthesis, Ed. G.W. Parshall, Vol.15, McGraw-Hill, New Yok, 1974.
5. H.H. Girault and D.J. Schiffrin, J. Electroanal. Chem., 161(1984)415.
6. Z. Samec, V. Marecek and J. Weber, J. Electroanal. Chem., 100(1979)841.
7. A.J. Bard and L.R. Faulkner, Electrochemical Methods, Fundamentals and Applications, John Wiley and Sons, New York, 1980.

CHAPTER FIVE

RESULTS AND DISCUSSION

5.1 SIMPLE ION TRANSFER STUDIES

5.1.1 *ION TRANSFER ACROSS THE IMMISCIBLE WATER/o-NITROTOLUENE INTERFACE*

Figure 5.1.1 shows dc cyclic voltammograms obtained at the water/o-nitrotoluene interface for 10 mM base electrolytes of LiCl (a), LiF (b), and Li_2SO_4 (c) in the aqueous phase and 10 mM PNPDCC in the organic phase. As can be seen from the voltammograms the potential windows are reasonably wide, allowing the study of the transfer of almost all ions which were investigated across the water/nitrobenzene or water/1,2-dichloroethane interface [1,2]. Comparison of the potential windows of the voltammograms illustrates that the potential limit in the negative potential range is controlled by the transfer of Cl^- (a), F^- (b), and by either SO_4^{-2} or PNP^+ ions (c), whereas, in all cases, the positive range is limited by the transfer of Li^+ [3]. The maximum polarization window is observed for the electrolyte couple Li_2SO_4 / PNPDCC.

Fig. 5.1.2 compares the potential windows of base electrolytes obtained by using 10 mM LiCl in the aqueous phase and 10 mM PNPTPB (d) or PNPDCC (e) in the organic phase. For the voltammogram shown in (d) the positive and negative potential ranges are limited by the transfer of TPB^- and Cl^- respectively. These comparisons were made in order to see the degree of polarisability of the water/o-nitrotoluene interface by applying different base electrolytes.

Ac and dc voltammograms for the transfer of ClO_4^- and TMA^+ ions across the water/o-nitrotoluene interface are shown in Fig. 5.1.3. The ac voltammograms were recorded from the in phase component of the ac current. As seen from the dc voltammograms the forward and reverse peaks are separated by 60 mV indicating the reversible behaviour of the ion transfer. The reversibility

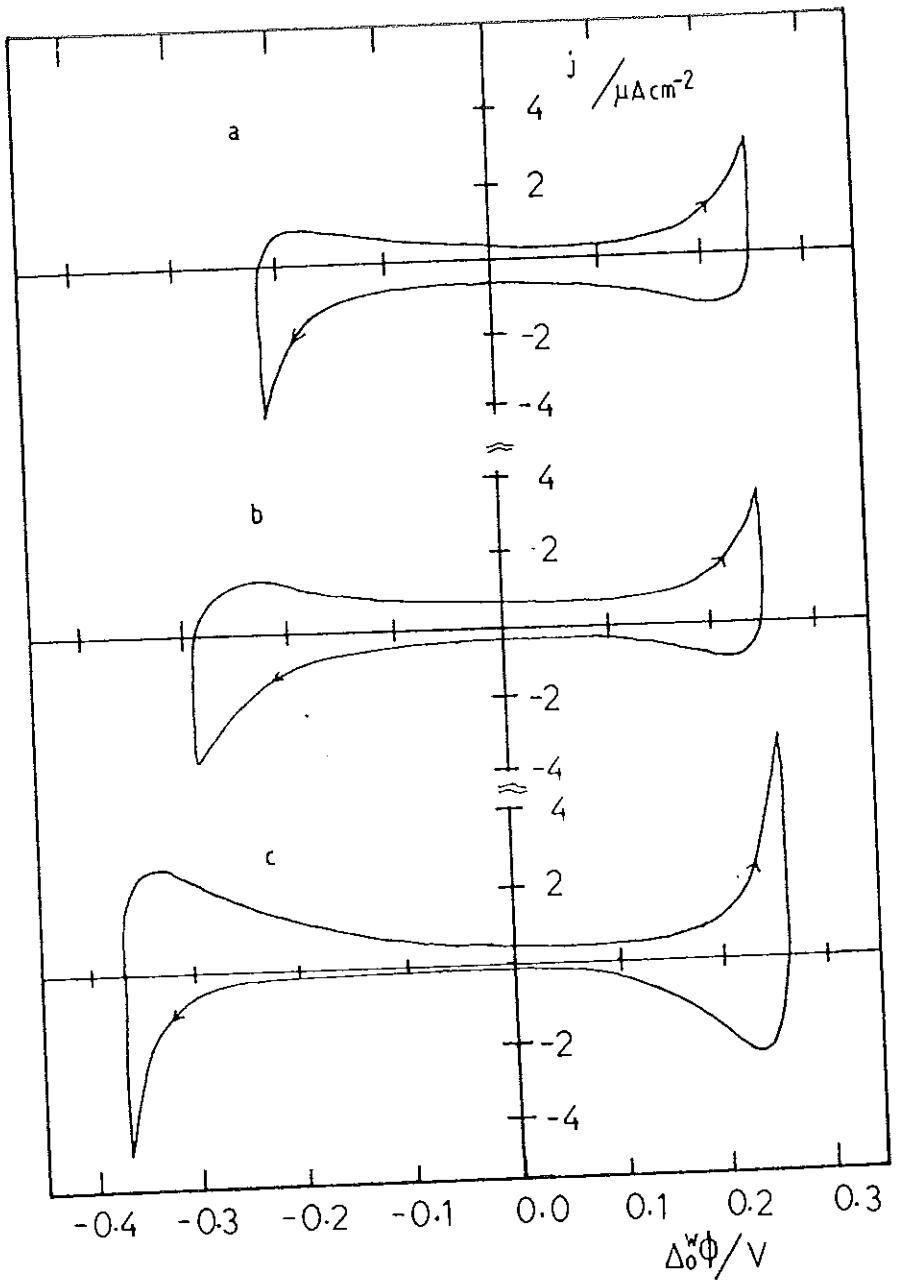

Fig. 5.1.1. Comparison of the dc voltammograms of the base electrolytes : 10 mM LiCl (a), 10 mM LiF (b); and 5 mM Li_2SO_4 (c) in the aqueous phase and 10 mM PNPDCC in o-nitrotoluene. Sweep rate = 10 mV s^{-1}.

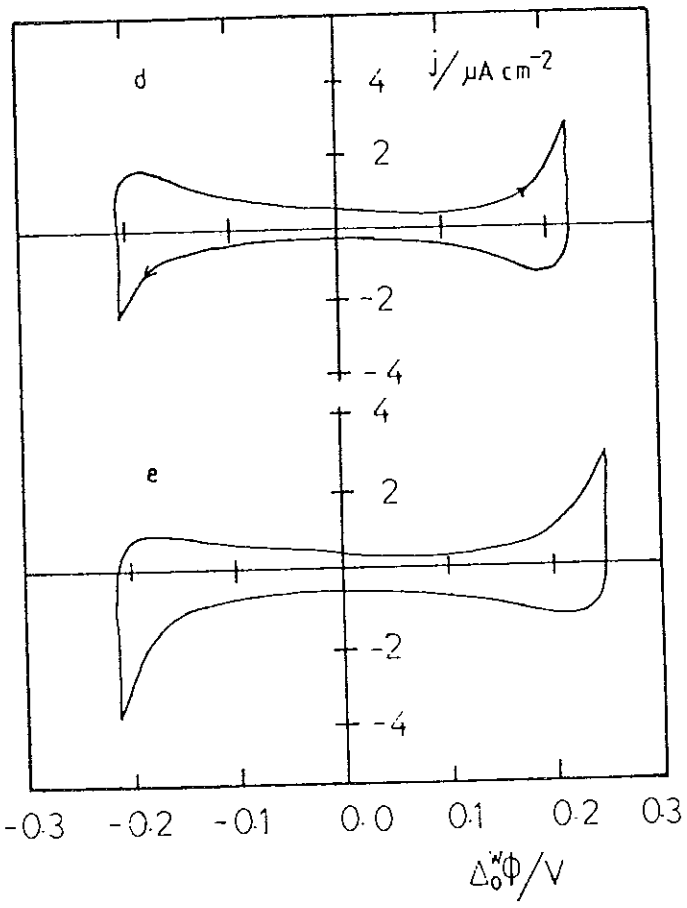

Fig. 5.1.2. Comparison of the dc voltammograms of 10 mM LiCl in the aqueous phase and 10 mM PNPTPB (d), and 10 mM PNPDCC (e) in o-nitrotoluene.

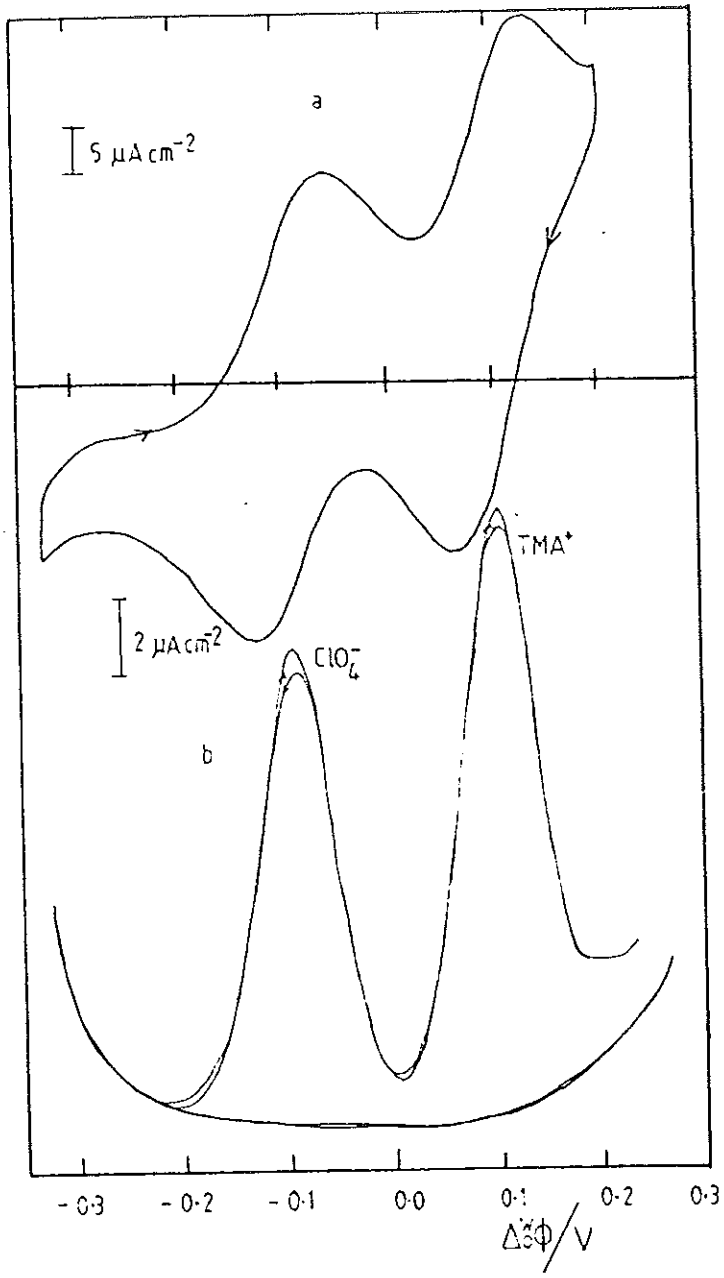

Fig. 5.1.3. Dc (a), and ac (b), voltammograms for the transfer of 0.1 mM ClO_4^- and TMA^+ across the immiscible water/o-nitrotoluene interface. Ac sweep rate = 5 mV s^{-1} dc sweep rate = 25 mV s^{-1}, and f = 70 Hz.

of the process is also apparent from the peaks of the ac voltammograms which show half-peak width of 90 mV [4,5].

The dependence of the peak current I_p on the square root of the sweep rate and concentration was checked by using the Randles-Sevcik equation [4],

$$I_p = 0.4463Z^{3/2}FAC^b(F/RT)^{1/2}\nu^{1/2}D^{1/2} \qquad (5.1.1)$$

where A is the interfacial area (cm^2), C^b is bulk electrolyte concentration (mole dm^{-3}) and is the sweep rate (V s^{-1}).

Figure 5.1.4 illustrates the plots of I_p vs $\nu^{1/2}$ for the transfer of TEA^+ at different concentrations and Fig. 5.1.5 shows the dependence of I_p on concentration at various sweep rates. In both cases linear dependence is observed. From the slopes of the plots the diffusion coefficient of TEA^+ ion in water D_w was evaluated. The calculated average value of D_w obtained from I_p vs $\nu^{1/2}$ and I_p vs C^b is 1.2×10^{-5} cm^2/s and 1.1×10^{-5} cm^2/s, respectively. This result is comparable with the value that can be calculated from the conductivity data at infinite dilution ($D_w = 8.7\times10^{-6}$ cm^2/s) [6].

The half-wave potentials $\Delta^w_o\phi_{1/2}$ of the transferred ions were determined from the peak potentials $\Delta^w_o\phi_p$ of the dc voltammograms from the relationship [2],

$$\Delta^w_o\phi_p = \Delta^w_o\phi_{1/2} \pm 0.0285/|Z| \qquad (5.1.2)$$

where (+) and (-)stand for the positive and negative current peaks, respectively. Alternatively $\Delta^w_o\phi_{1/2}$ values were directly measured from the ac peak potentials and related to the standard Galvani potential difference using the equation [3]

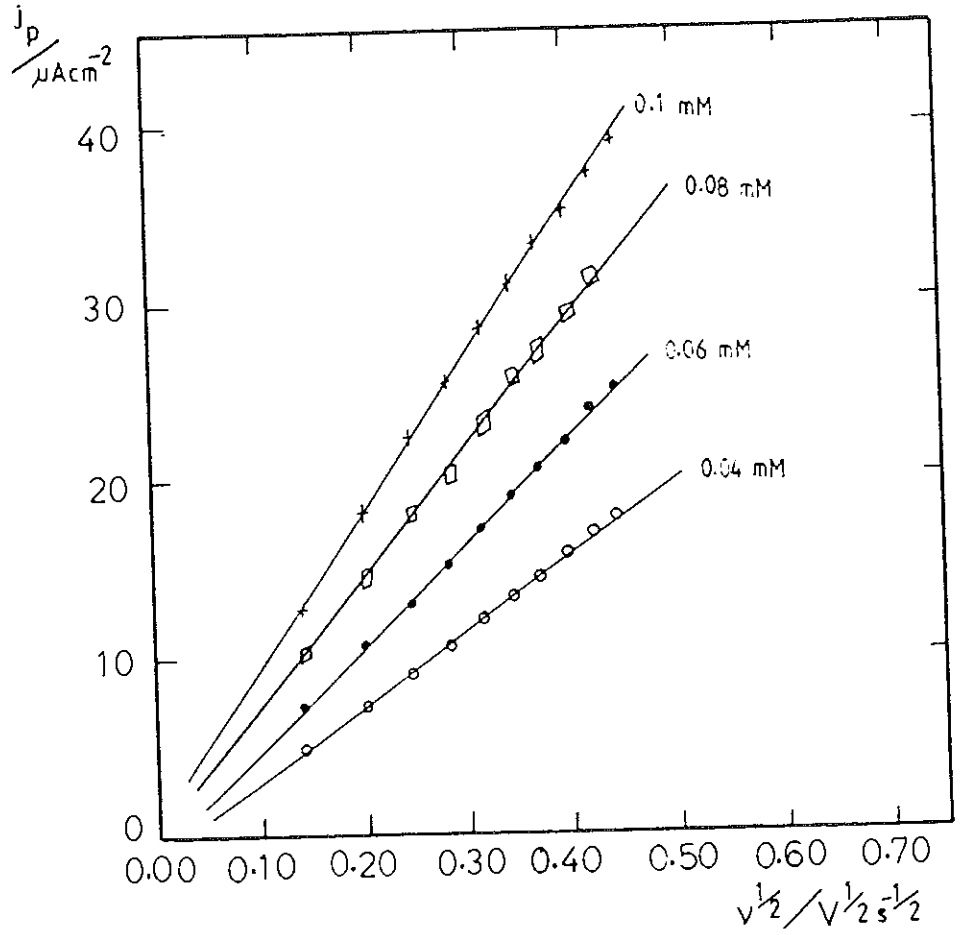

Fig. 5.1.4. Dependence of peak current j_p on the square root of the sweep rate ($v^{1/2}$) for the transfer of different concentrations of TEA^+ across the water/o-nitrotoluene interface.

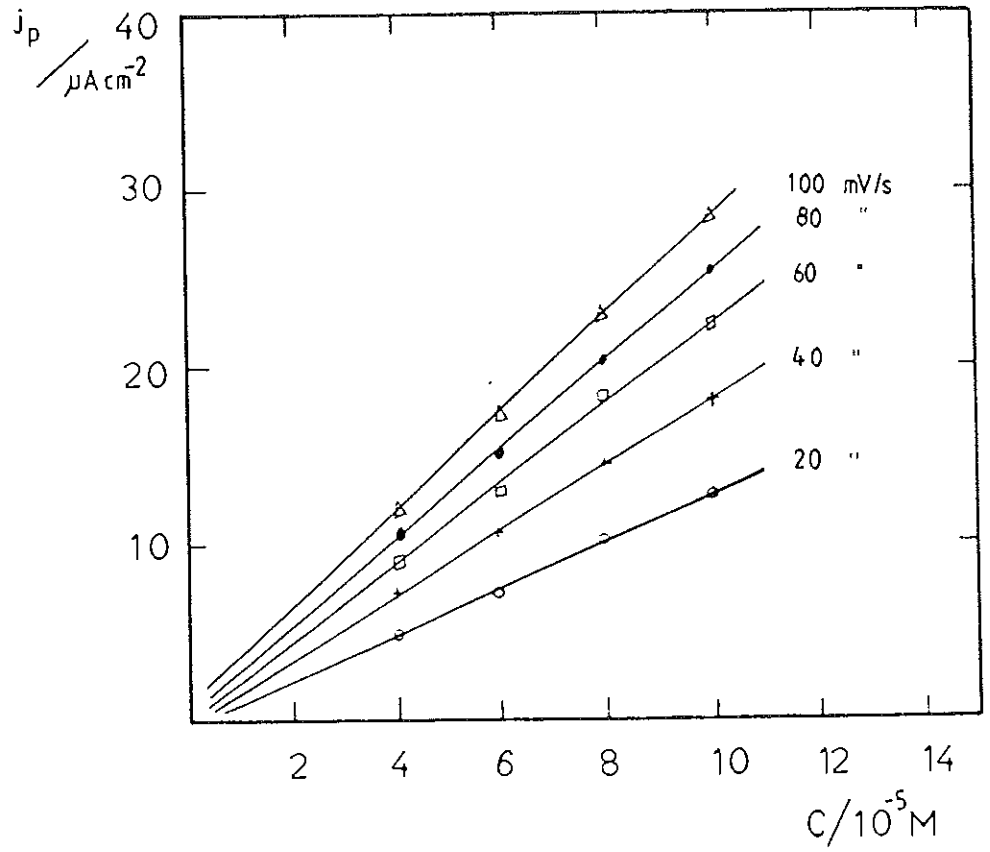

Fig. 5.1.5. Concentration dependence of the peak current j_p for the transfer of TEA^+ across the water/o-nitrotoluene interface at different sweep rates.

$$\Delta^{w}{}_{o}\phi_{1/2} = \Delta^{w}{}_{o}\phi^{0} + (RT/ZF)\ln(D_w/D_o)^{1/2}(\gamma_o/\gamma_w) - (RT/ZF)\ln[1 + K^{o}{}_{a}\alpha C^{b}(\gamma_o)^2 (D^{o}{}_{a}/D_o)]^{1/2} \quad (5.1.3)$$

where $\gamma_{w,o}$ is the single ion activity coefficient, $D^{o}{}_{a}$ and $K^{o}{}_{a}$ are the diffusion coefficient and the association constant of the ion pair, respectively, $C^{b}{}_{o}$ is the bulk concentration of the organic base electrolyte and α is the degree of dissociation in the organic phase.

The ratio of the activity coefficients of the ions was assumed to be unity for the concentrations (0.1 mM) used in these experiments. The contribution due to ion association in the organic phase was found to be very small and thus was not considered.

Table 5.1.1 lists the diffusion coefficient of the studied ions together with their radii and hydration energies. The diffusion coefficients of the ions in o-nitrotoluene were calculated from estimated values of ion conductivity λ^{o}_{i} and from the relationship [6]

$$D_i = (RT\lambda^{o}_{i})/|Z_i|F^2 \quad (5.1.4)$$

The single ion conductivities in o-nitrotoluene were calculated according to the method of Coetzee and Cunningham [8]. The method of evaluation is based indirectly on tetraisoamylammonium tetraisoamylborate as a reference electrolyte, and assuming that Walden's product holds for the reference electrolyte in the solvent.

The values of the standard Gibbs energies of transfer $\Delta G^{0}{}_{tr}{}^{w\rightarrow o\text{-}nt}$ were determined from $\Delta^{w}{}_{o}\phi^{0}$ according to equation (2.1.4). Details of the experimental results are shown in Table 5.1.2.

Table 5.1.1

Diffusion coefficients of ions in water (D_w) and in o-nitrotoluene ($D_{o\text{-}nt}$), ionic radii and hydration energies (ΔG_h^o) of ions used in the calculations.

Ion	Ionic radii (nm) [a]	ΔG_h^o (kJ mol^{-1})	$D_w \times 10^6$ (cm^2 s^{-1}) [b]	$D_{o\text{-}nt} \times 10^6$ (cm^2 s^{-1}) [c]
TMA^+	0.258	-200.8	11.9	4.0
TEA^+	0.310	-171.5	8.7	3.6
TBA^+	0.383	-135.1	5.2	2.6
$TPAs^+$	0.397 [e]		5.6	2.4
Li^+	0.094	-479.5	10.3	5.6
ClO_4^-	0.245	-196.6	17.9	4.4
IO_4^-	0.254	-190.6	14.5	4.3
SCN^-	0.195 [d]	-254.8	17.5	4.7
NO_3^-	0.195	- 253.1	19.0	5.3
TPB^-	0.386 [e]		5.6	2.4
Cl^-	0.181	-286.3	20.3	7.6
F^-	0.133 [d]		14.7	4.1

[a] From [7] unless shown otherwise.

[b] Calculated from conductivity data of [6].

[c] Calculated according to [8].

[d] From [9].

[e] Calculated from molar volumes using the Stearn-Eyring formula [10].

Table 5.1.2

Peak potentials, $\Delta^{w}{}_{o}\phi_{p}$, half-wave potentials, $\Delta^{w}{}_{o}\phi_{1/2}$, standard Galvani potential differences, $\Delta^{w}{}_{o}\phi^{o}$, and standard Gibbs energies of transfer of ions, $\Delta G^{o}{}_{tr}{}^{w\rightarrow o\text{-}nt}$ obtained experimentally for the water (w)/o-nitrotoluene (o-nt) system.

Ion	$\Delta^{w}{}_{o}\phi_{p}$ / V	$\Delta^{w}{}_{o}\phi_{1/2}$ / V	$\Delta^{w}{}_{o}\phi^{o}$ / V	$\Delta G^{o}{}_{tr}{}^{w\rightarrow o\text{-}nt}$ /kJ mol^{-1}
TMA^{+}	0.130	0.102	0.087	8.4
TEA^{+}	0.035	0.007	-0.005	-4.8
TBA^{+}	-0.160	-0.188	-0.197	-19.0
$TPAs^{+}$	-0.228	-0.257	-0.256	-24.7
Li^{+}	0.270	0.242	0.222	21.4
ClO_4^{-}	-0.115	-0.087	-0.069	6.7
IO_4^{-}	-0.110	-0.082	-0.066	6.4
SCN^{-}	-0.160	-0.132	-0.115	11.1
NO_3^{-}	-0.220	-0.190	-0.170	16.4
TPB-	0.228	0.257	0.256	-24.7
Cl^{-}	-0.250	-0.222	-0.202	19.5

For comparison theoretical $\Delta G^0_{tr}{}^{w\to o\text{-}nt}$ values were evaluated from the equations of Abraham and Liszi. The results of the calculations are given in Table 5.1.3. The computations were carried out using the values of the hydration energies (ΔG_h^0) shown in Table 5.1.1. Details of the calculations are presented in Table 5.1.3.

A comparison of the experimental and theoretical values of $\Delta G^0_{tr}{}^{w\to o\text{-}nt}$ for selected ions is given in Table 5.1.4. As can be seen from the table the experimental values of $\Delta G^0_{tr}{}^{w\to o\text{-}nt}$ lie in between the theoretically calculated values for fully hydrated and non-hydrated ions. Particular mention may be made of $\Delta G^0_{tr}{}^{w\to o\text{-}nt}$ for the ClO_4^-, IO_4^-, and TBA^+ ions, the experimental values of which are very close to those theoretically calculated assuming no hydration in the organic phase. By contrast, the experimental values of $\Delta G^0_{tr}{}^{w\to o\text{-}nt}$ for TMA^+, TEA^+, Li^+ and Cl^- are close to the theoretically calculated values assuming the ions are hydrated in the organic phase. These considerations appear to favor the retention of water of hydration in the organic solvent on transfer from the aqueous phase. Independent spectroscopic evidence might be necessary in order to understand the state of ions in water-saturated organic solvents that are immiscible with water. However, the results obtained in this study could have very important consequences for the understanding of the kinetics of ion transfer.

The results of the water/o-nitrotoluene system have in part been reported in ref. 11.

Table 5.1.3

Theoretical calculation of standard Gibbs energy of transfer of ions $\Delta G^0_{tr}{}^{w\rightarrow o\text{-}nt}$ (kJ mol^{-1}) for the water/o-nitrotoluene system based on the model of Abraham and Liszi.

	a				b			
Ion	ΔG^0_{el}	ΔG^0_n	ΔG^0_s	$\Delta G^0_{tr}{}^{w\rightarrow o\text{-}nt}$	ΔG^0_{el}	ΔG^0_n	ΔG^0_s	$\Delta G^0_{tr}{}^{w\rightarrow o\text{-}nt}$
TMA^+	-193.7	7.9	-185.8	19.6	-212.6	7.9	-204.6	0.8
TEA^+	-166.0	-1.2	-167.2	9.0	-181.2	-1.2	-182.4	-6.3
TBA^+	-138.8	-17.7	-156.5	-16.7	-150.5	-17.9	-168.2	-28.4
Li^+	-460.2	30.0	-430.2	53.9	-498.9	-30.0	-468.9	15.2
ClO_4^-	-202.3	9.7	-192.7	8.6	-222.3	9.7	-212.6	-11.4
IO_4^-	-197.9	8.5	-189.5	5.7	-215.6	8.5	-207.2	-12.0
SCN^-	-245.0	16.4	-228.6	30.9	-270.1	16.4	-253.7	3.5
NO_3^-	-245.0	16.4	-228.6	29.2	-270.1	16.4	-253.7	-4.1
Cl^-	-260.8	18.3	-242.5	48.4	-287.8	18.3	-269.5	21.4

[a] Calculated for non-hydrated ions in the organic phase. [b] Calculated for fully hydrated ions in the organic phase. ΔG^0_n Calculated using data for nitrobenzene (m=-3.217, c=10.19) [7]. ΔG^0_{el} calculated for non-hydrated ions in the organic phase using the radius of o-dichlorobenzene (r=0.286 nm) [7]. $\Delta G^0_{tr}{}^{w\rightarrow o\text{-}nt}$ obtained after adding 4.61 kJ/mol to the sum of ΔG^0_s and ΔG^0_h values (on molar scale).

Table 5.1.4

Comparison of the experimental and theoretically calculated (from the Abraham and Liszi model) values of standard Gibbs energies of transfer of selected ions from water to o-nitrotoluene.

Ion	$\Delta G^0_{tr}{}^{w\rightarrow o\text{-}nt}$ (exp.)/kJ mol^{-1}	$\Delta G^0_{tr}{}^{w\rightarrow o\text{-}nt}$ (theor.)/kJ mol^{-1}	
		(a)	(b)
TMA^+	8.4	19.6	0.8
TEA^+	-4.8	9.0	-6.3
TBA^+	-19.0	-16.7	-28.4
Li^+	21.4	53.9	15.2
ClO_4^-	6.7	8.6	-11.4
IO_4^-	6.4	5.7	-12.0
SCN^-	11.1	30.9	3.5
Cl^-	19.5	48.4	21.4

[a] Calculated for non-hydrated ions in the organic phase.

[b] Calculated for fully-hydrated ions in the organic phase.

5.1.2 *ION TRANSFER ACROSS THE IMMISCIBLE WATER/BENZONITRILE INTERFACE*

Figure 5.1.6 shows the dc cyclic voltammogram for the transfer of ClO_4^- across the water/benzonitrile interface when LiCl and TBATPB were used as base electrolytes in the water and benzonitrile phases, respectively. The ion transfer was found to be reversible, as seen from the peak separation of 60 mV. This was also found to be the case for the other ions investigated, up to sweep rates of 100 mV/s. The dependence of I_p vs the square root of the sweep rate ($\mu^{1/2}$) for a given concentration of four ions, as well as those of I_p vs. the concentration of these ions at a given sweep rate, were found to be linear. Such dependencies are shown in Fig. 5.1.7 and 5.1.8, respectively.

From the $\Delta^o_w\phi_p$ the values of $\Delta^o_w\phi_{1/2}$ and $\Delta^o_w\phi^o$ were subsequently determined. Table 5.1.5 lists the diffusion coefficient of ions in benzonitrile estimated from ref. 8.

Table 5.1.5

Estimated diffusion coefficient of ions in benzonitrile.

Ion	TMA^+	TEA^+	TBA^+	$TPAs^+$	IO_4^-	ClO_4^-	Pi^-	TPB^-
$D_i\,10^6$ (BN)	6.5	5.8	4.3	3.4	7.0	7.1	5.3	3.4

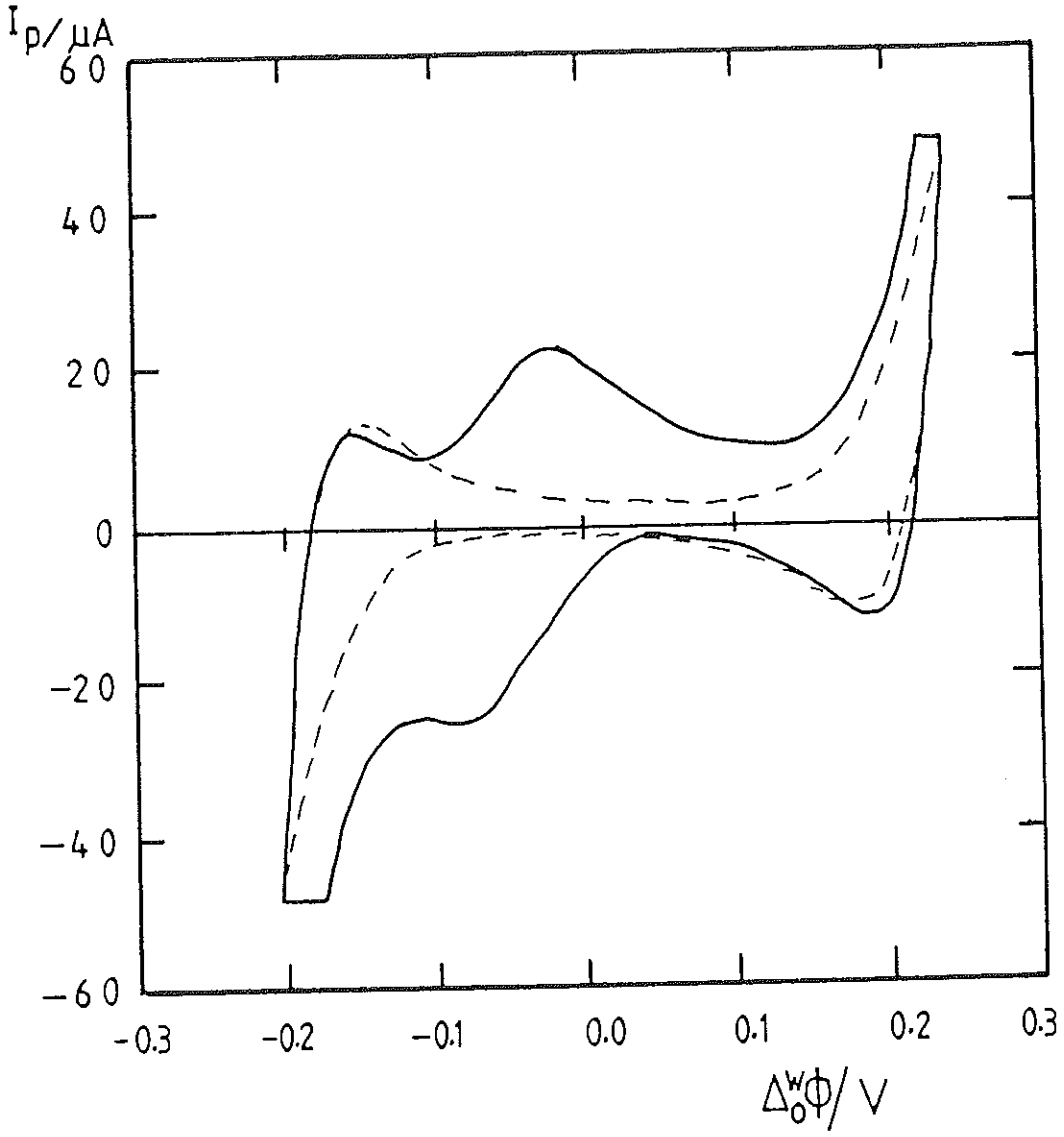

Fig. 5.1.6. Cyclic voltammogram for the transfer of 1 mM ClO_4^- across the water/benzonitrile interface (———); supporting electrolytes 10 mM TBATPB in BN and 10 mM LiCl in water (---).

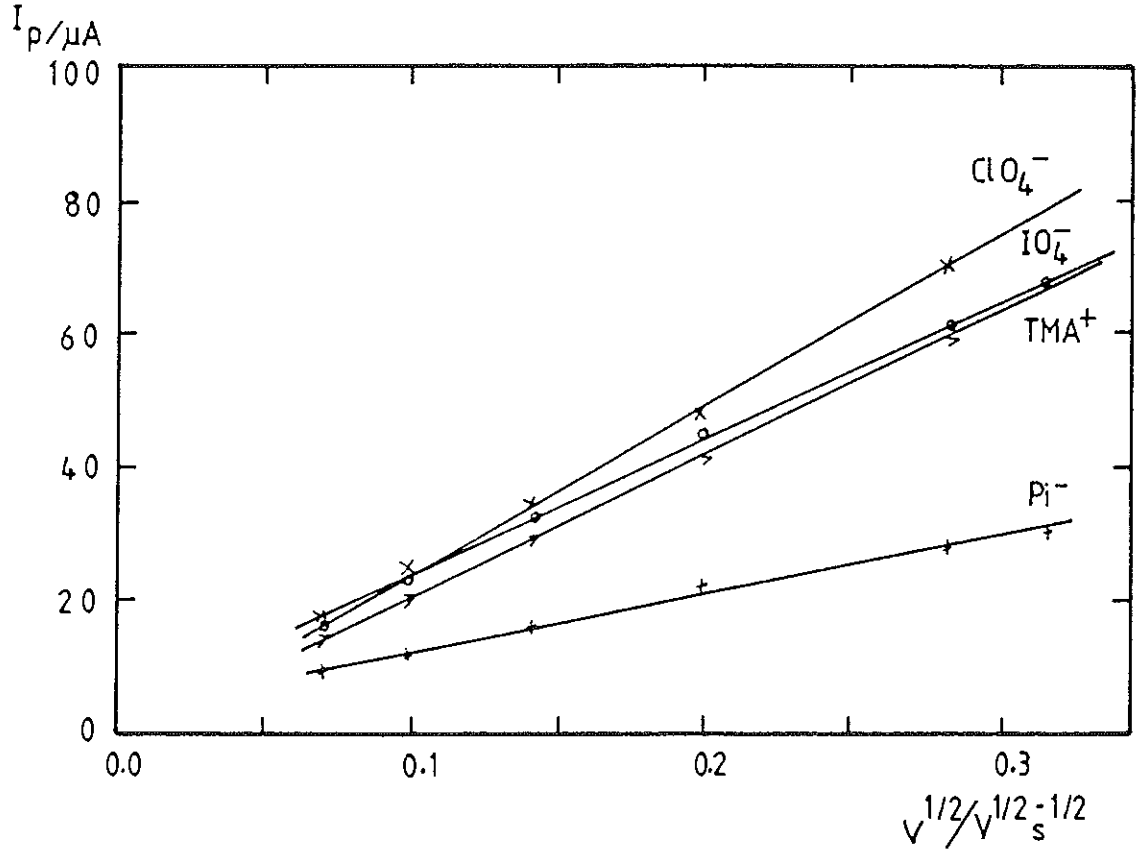

Fig. 5.1.7. Peak current I_p vs square root of the sweep rate ($v^{1/2}$) for 0.8 mM ClO_4^-, IO_4^-, TMA^+ and Pi^-

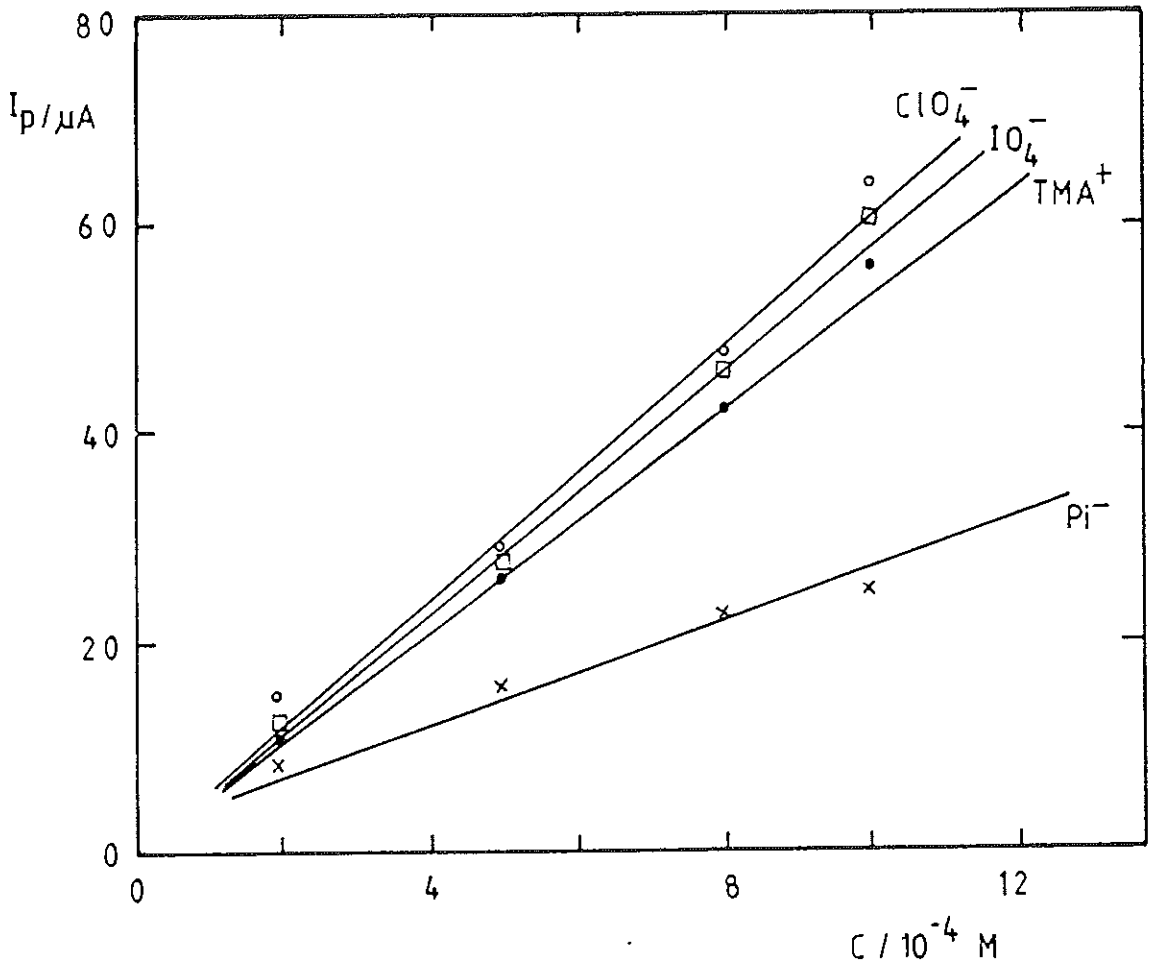

Fig. 5.1.8. Peak current I_p vs concentrations of ClO_4^-, IO_4^-, TMA^+ and Pi^- at a sweep rate of 40 mV s^{-1}.

The ratio of the activity coefficients was assumed to be unity, and ion association in the organic phase was not considered. It has been shown from the results of solubility experiments of the same system [12,13] that use of ion-pair formation constant K_a and the ion size parameter in the extended Debye-Hückel equation for the calculation of activity coefficients does not significantly affect the ΔG^0_{tr} values.

In Table 5.1.6 the details of the experimental results are given. For comparison, $\Delta G^0_{tr}{}^{w\rightarrow bn}$ values obtained from solubility experiments [13] together with theoretically calculated values are presented in Table 5.1.7.

It is seen that there are some discrepancies between the two experimental results. However, it should be noted that the voltammetric experiments were done on mutually saturated solvents, whereas the solubility measurements were carried out in the pure dry solvents. Hence the observed difference between the two experimental results is not unexpected. The discrepancies is seem to be much larger than those observed in the nitrobenzene/water and 1,2-dichloroethane/water systems [2]. This may be due to the slightly higher mutual solubility of water and benzonitrile. However, as in the previous system (water/o-nitrotoluene), the voltammetrically obtained $\Delta G^0_{tr}{}^{w\rightarrow bn}$ values lie in between the theoretically estimated values.

The above results of the water/benzonitrile system have been reported in ref. 14.

Table 5.1.6

Peak potentials, $\Delta^{w}{}_{o}\phi_{p}$, half-wave potentials, $\Delta^{w}{}_{o}\phi_{1/2}$, standard Galvani potential differences, $\Delta^{w}{}_{o}\phi^{o}$, and standard Gibbs energies of transfer of ions, $\Delta G^{o}{}_{tr}{}^{w\rightarrow bn}$ obtained experimentally for the water (w)/benzonitrile (bn) system.

Ion	$\Delta^{w}{}_{o}\phi_{p}$ / V	$\Delta^{w}{}_{o}\phi_{1/2}$ / V	$\Delta^{w}{}_{o}\phi^{o}$ / V	$\Delta G^{o}{}_{tr}{}^{w\rightarrow bn}$ /kJ mol^{-1}
TMA^{+}	0.108	0.080	0.072	6.9
TEA^{+}	-0.008	-0.037	-0.042	-4.1
TBA^{+}	-0.155	-0.184	-0.187	-18.0
$TPAs^{+}$	-0.183	-0.212	-0.216	-20.8
ClO_4^{-}	-0.090	-0.062	-0.050	4.8
IO_4^{-}	-0.069	-0.041	-0.029	2.8
Pi^{-}	0.034	0.063	0.068	-6.6
TPB-	0.183	0.212	0.216	-20.8
$TPBCl^{-}$	0.200	0.229	0.223	-22.5

Table 5.1.7

Comparison of experimental and theoretical values of standard Gibbs energies of transfer of ions for the water/benzonitrile system.

Ion	$\Delta G^0_{tr}{}^{w\rightarrow bn}$ (exp.)/kJ mol^{-1}		$\Delta G^0_{tr}{}^{w\rightarrow bn}$ (theor.)/kJ mol^{-1}	
	a	b	c	d
TMA^+	6.9	2.5	18.6	0.8
TEA^+	-4.1	-4.8	8.1	-6.4
TBA^+	-18.0		-17.4	-28.5
$TPAs^+$	-20.8	-35.3		
ClO_4^-	4.8	13.2	7.5	-11.3
IO_4^-	2.8		6.3	-11.8
Pi^-	-6.6	0.4	0.6	-14.4
TPB^-	-20.8	-35.3		

[a] From the present experimental results.

[b] From the solubility data of [14].

[c] Calculated for non-hydrated ions in the organic phase (on molar scale) using the radius of chlorobenzene, r = 0.2769 nm, and the data for nitrobenzene m =-3.2165, c = 10.1899 [7]).

[d] Calculated for fully hydrated ions in the organic phase on molar scale.

5.1.3 *ION TRANSFER ACROSS THE IMMISCIBLE WATER/o-DICHLOROBENZENE INTERFACE*

Figure 5.1.9 shows dc cyclic voltammogram obtained for the system water/o-dichlorobenzene using Li_2SO_4 and PNPDCC as base electrolytes in the water and organic phase, respectively. As can be seen from the voltammogram the available potential window is wider than those of the previous immiscible systems studied during the course of this work.

Figure 5.1.10 illustrates the ac cyclic voltammograms for the transfer ClO_4^-, Pi^-, TEA^+ TBA^+ and TPA^+ ions across the water/o-dichlorobenzene interface. At low sweep rates (5-100 mV) all the investigated ions showed reversible transfer behaviour.From the peaks of the ac voltammograms, the $\Delta^w{}_o\phi_{1/2}$ values were directly obtained and used to determine the $\Delta^w{}_o\phi^o$ values. Due to the low dielectric constant of o-dichlorobenzene ion association in the organic phase was considered and the extended Debye-Hückel theory [6] was employed for the evaluation of the activity coefficients. These latter quantities and the degree of dissociation α were calculated from the following two equations [6].

$$-\log\gamma^o = A(C^o\alpha)^{1/2} / (1+Ba(C^o\alpha)^{1/2}) \qquad (5.1.5)$$

and

$$K^o_{ab} = (1-\alpha)/C^o\alpha^2(\gamma^o)^2 \qquad (5.1.6)$$

where A and B are parameters in the Debye-Hückel theory whose values are dependent on temperature and dielectric constant of the solvent. (For o-dichlorobenzene, the values of A and B are 11.6 $mol^{-1/2}\,l^{1/2}\,(deg\,K)^{3/2}$ and 9.32 $\times\,10^7\,cm^{-1}\,mol^{-1/2}\,l^{1/2}\,(deg\,K)^{1/2}$). K^o_{ab} is the association constant of the base electrolyte in the organic phase, and a is the ion size parameter.

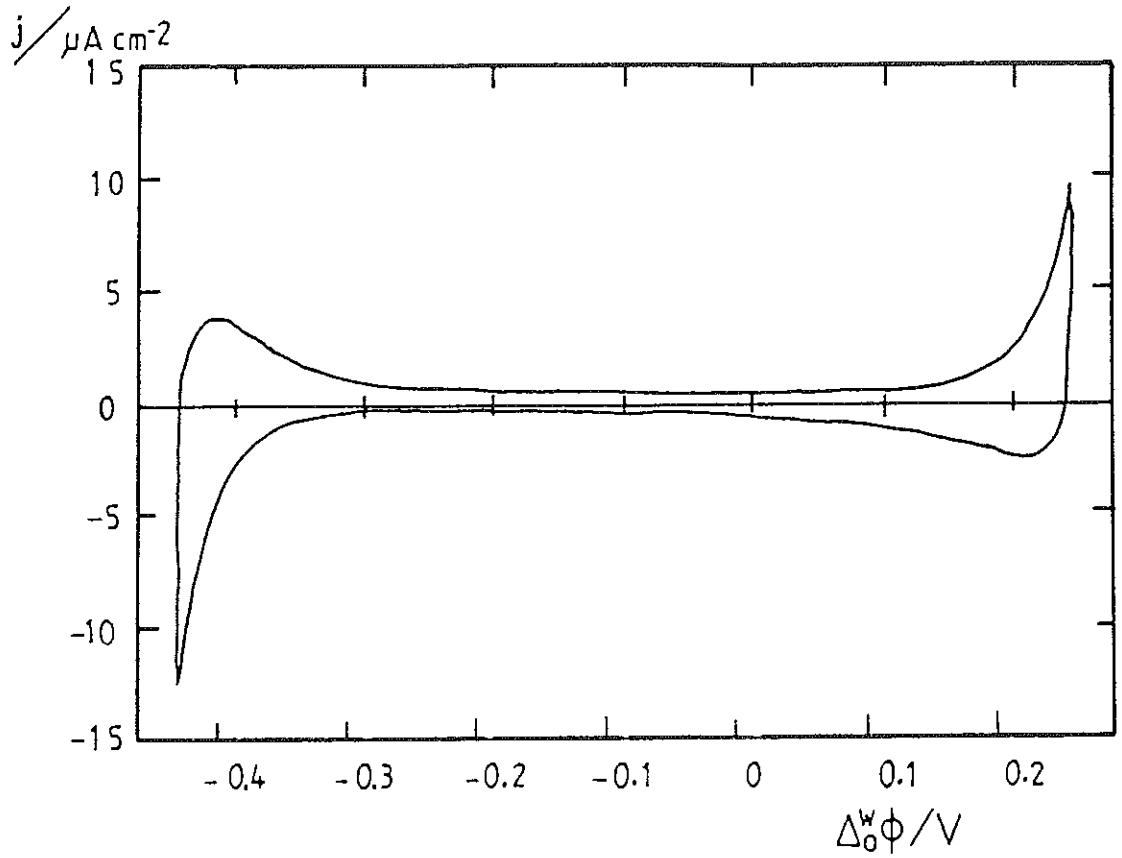

Fig. 5 1.9. Dc cyclic voltammogram of the base electrolytes at the immiscible water/o-dichlorobenzene interface. Electrolytes: 5 mM Li_2SO_4 (aq.) and 10 mM PNPDCC (organic), sweep rate = 10 mV s^{-1}.

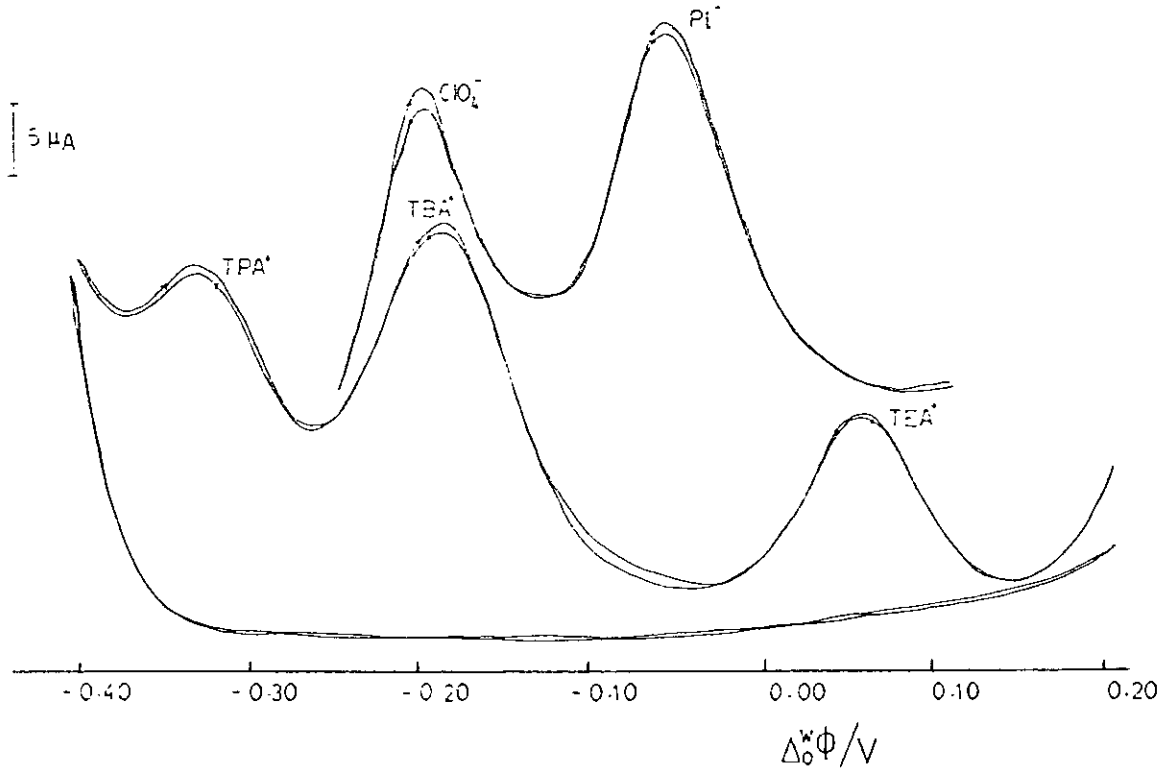

Fig. 5.1.10. Ac cyclic voltammograms for the transfer of 0.1 mM ClO_4^-, Pi^-, TEA^+, TBA^+ and TPA^+ ions across the water/o-dichlorobenzene interface. f = 35 Hz, sweep rate = 5 mV s^{-1}.

By assuming that the activity coefficients of the cation and the anion of the base electrolytes are the same [3], the values of α and γ^0 were calculated from the above two equations using an iterative technique. For the calculations, the ion size parameter a was taken from refs. 3 and 15. Due to lack of data pertaining to o-dichlorobenzene, association constants were estimated from known values in 1,2-dichloroethane and 1,1-dichloroethane [15].

Table 5.1.8 lists the values of $\Delta^{w}{}_{o}\phi_{1/2}$, $\Delta^{o}{}_{w}\phi^{o}$ and $\Delta G^{o}{}_{tr}{}^{w\rightarrow o\text{-}dcb}$. In Table 5.1.9 a comparison is made of the experimental results with theoretical values. As can be seen from the table it seems that there is a fair agreement between the experimental results and the theoretical $\Delta G^{o}{}_{tr}{}^{w\rightarrow o\text{-}dcb}$ values calculated for non-hydrated ions. The transfer of the ions across the interface without an hydration shell is thus indicated.

Table 5.1.10 shows the experimental results of the present system with those reported by Kihara et al. [17]. As shown in the table, these workers have reported two values of half-wave potential for a given ion when crystal violet tetraphenylborate and tetraphenylarsonium dipicrylaminate were used as the organic base electrolytes. Thus it is not possible to make direct comparison between their data and the present results. However there is a general agreement in the trend of the magnitude of the half-wave potentials.

In Figure 5.1.11 is depicted the dependence of $\Delta^{w}{}_{o}\phi_{1/2}$ vs 1/a as shown for the tetraalakylammonium ions investigated. It is seen that there exists a linear relationship. This linear dependence could be a tool to estimate $\Delta^{w}{}_{o}\phi_{1/2}$ values of other tetraalkylammonium ions whose transfer across the liquid/liquid interface may fall outside the workable potential window.

Table 5.1.8

Half-wave potentials, $\Delta^{w}_{o}\phi_{1/2}$, standard Galvani potential differences, $\Delta^{w}_{o}\phi^{o}$, and standard Gibbs energies of transfer of ions, $\Delta G^{o}_{tr}{}^{w\rightarrow o\text{-dcb}}$ obtained experimentally for the water (w)/o-dichlorobenzene (o-dcb) system using Li_2SO_4 and PNPDCC as base electrolytes.

Ion	$\Delta^{w}_{o}\phi_{1/2}$ / V	$\Delta^{w}_{o}\phi^{o}$ / V	$\Delta G^{o}_{tr}{}^{w\rightarrow o\text{-dcb}}$ /kJ mol^{-1}
TMA^+	0.218	0.268	26
TEA^+	0.059	0.105	10
$TPrA^+$	-0.088	-0.042	-4
TBA^+	-0.185	-0.141	-14
$TPeA^+$	-0.331	-0.291	-28
$TPAs^+$	-0.324	-0.288	-28 [a]
ClO_4^-	-0.199	-0.224	24
NO_3^-	-0.391	-0.414	40
MnO_4^-	-0.135	-0.148	14
Pi^-	-0.057	-0.088	9
TPB-	0.324	0.288	-28[a]

[a] This value was obtained from solubility experiment [16].

Table 5.1.9

Experimental and theoretical values of standard Gibbs energies of transfer of ions for the water/o-dichlorobenzene system.

Ion	$\Delta G^0_{tr}{}^{w\rightarrow bn}$ (exp.)/kJ mol^{-1}	$\Delta G^0_{tr}{}^{w\rightarrow bn}$ (theor.)/kJ mol^{-1}	
	a	b	c
TMA^+	26	26	7
TEA^+	10	13	-3
$TPrA^+$	-4	-1	-15
TBA^+	-14	-15	-27
$TPeA^+$	-28	-28	-39
ClO_4^-	24	15	-5
NO_3^-	40	37	11
Pi^-	9	7	-9

[a] From the present experimental results.

[b] Calculated for non-hydrated ions in the organic phase (on mol l^{-1} scale).

[c] Calculated fo fully hydrated ions in the organic phase (on mol l^{-1} scale)

The radius of o-dichlorobenzene, r=0.2769 nm, and data for chlorobenzene, m = -3.307, c = 9.9616 were used for the calculations [7]

Table 5.1.10

Comparison of half-wave potentials ($\Delta^{w}_{o}\phi_{1/2}$) for the transfer ions across the water/o-dichlorobenzene interface obtained from voltammetric experiments.

Ion	$\Delta^{w}_{o}\phi_{1/2}$ / V		
	a	b	c
TMA^+	0.218	0.120	0.060
TEA^+	0.059	0.000	0.010
$TPrA^+$	-0.088	-0.160	-0.140
TBA^+	-0.185	-0.270	-0.250
ClO_4^-	-0.199	-0.220	-0.230

[a] From the present experimental results.

[b] From ref. 17 using crystal violet tetraphenylborate as the organic base electrolyte.

[c] From ref. 17 using tetraphenylarsonium dipicrylaminate as the organic base electrolyte.

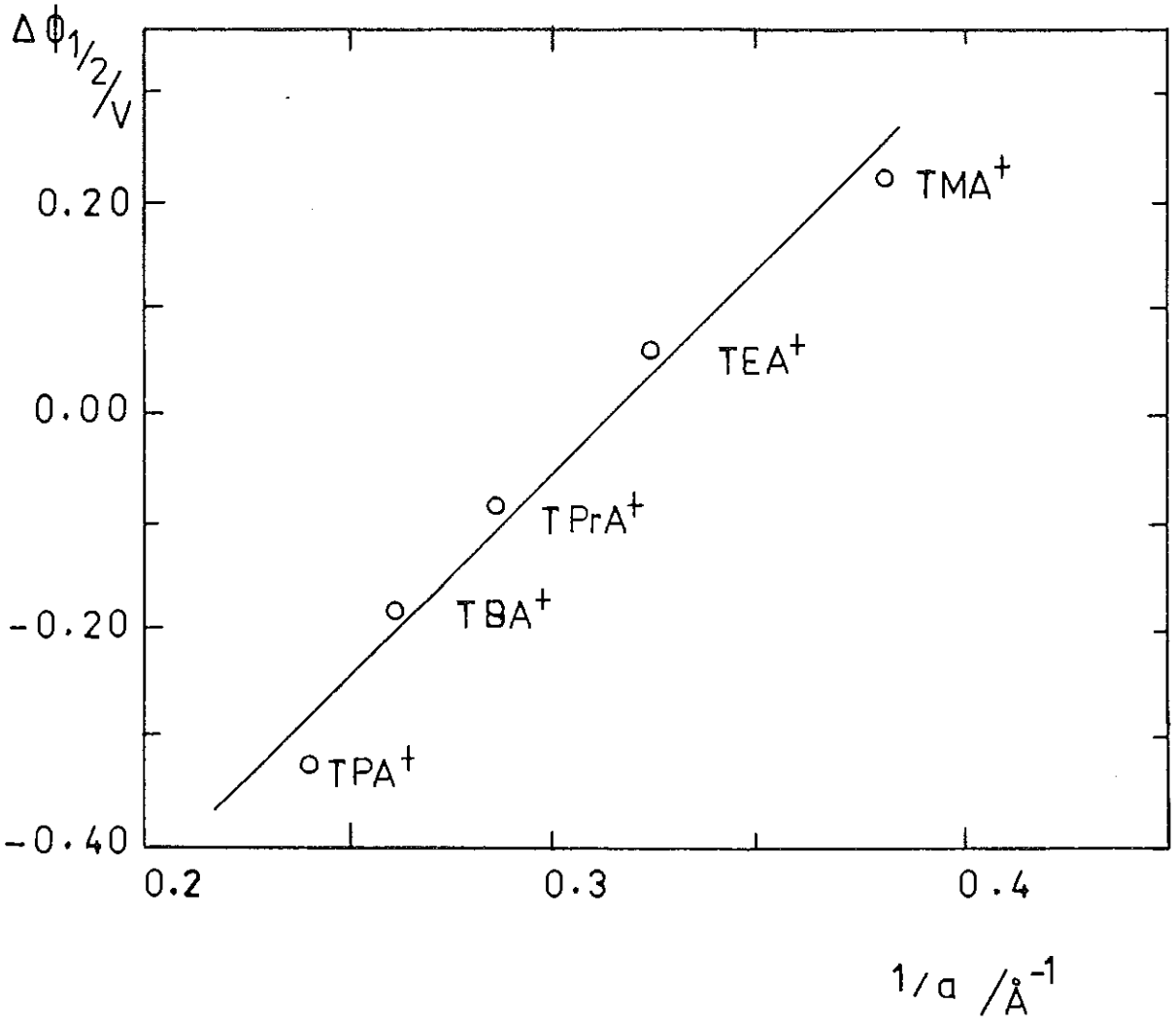

Fig. 5.1.11. Dependence of the half-wave potential $\Delta\Phi_{1/2}$ on the inverse of the ionic radius 1/a of tetraalkylammonium ions.

5.2 COMPLEX-ION TRANSFER AND FACILITATED ION TRANSFER STUDIES

5.2.1 *TRANSFER OF TRANSITION METAL-TERPYRIDINE COMPLEXES ACROSS THE WATER / NITROBENZENE INTERFACE*

Cobalt-Terpyridine

Figure 5.2.1 shows the ac and dc voltammograms of the supporting electrolyte and of an air-saturated solution of Co-terpyridine in a 5:1 metal to ligand concentration ratio across the water/nitrobenzene interface. In the absence of the ligand no transfer of the metal cation was observed across the interface. From the above voltammograms three distinct peaks can be seen which correspond to the transfer of different species. All the peaks show reversible transfer behaviour. It is seen from the ac voltammogram that the peak at more negative potentials (peak I) and the peak at more positive potentials (peak III) show half-peak widths of 45 mV corresponding to the transfer of a +2 charged species, whereas the peak at the centre (peak II) has a half-peak width of 30 mV indicating the transfer of a +3 charged complex. This is also apparent from the dc voltammogram`s forward and reverse peak separations.

Figure 5.2.2 shows the transfer behaviour of complexes which were prepared from 1:1 and 1:2 (Co-ligand) ratios of an air saturated aqueous solution. When the ligand concentration in the solution was increased from a ratio of 5:1 to 1:1, the ac current of peak III decreased, whereas that of peak I was highly enhanced. As shown in the figure, for a 1:2 metal:ligand concentration ratio, peak III disappeared completely followed by a considerable decrease in the height of peak II and an increase in the height of peak I.

The transfer behaviour of the complexes which were prepared under a nitrogen atmosphere in 1:1 and 1:5 ratios are compared in Figure 5.2.3. For the

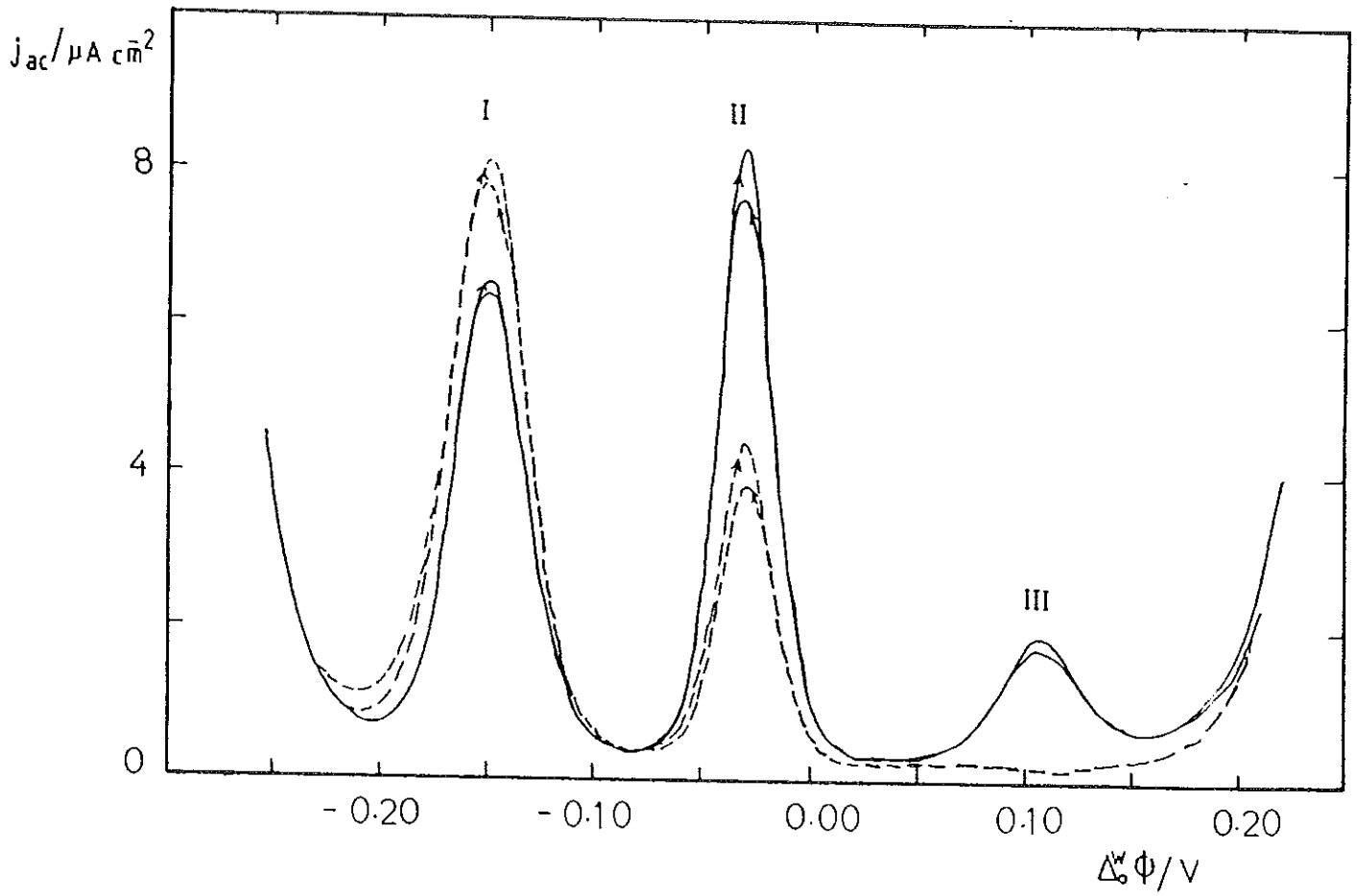

Fig. 5.2.2. Comparison of the ac voltammograms (f = 20 Hz) of (——) 0.1 mM Co^{2+}, 0.1 mM terpyridine, and (---) 0.1 mM Co^{2+}, 0.2 mM terpyridine, + 5 mM Li_2SO_4 in the aqueous phase, and 10 mM PNPDCC in nitrobenzene. Sweep rate = 5 mV s^{-1}, pH 6.5.

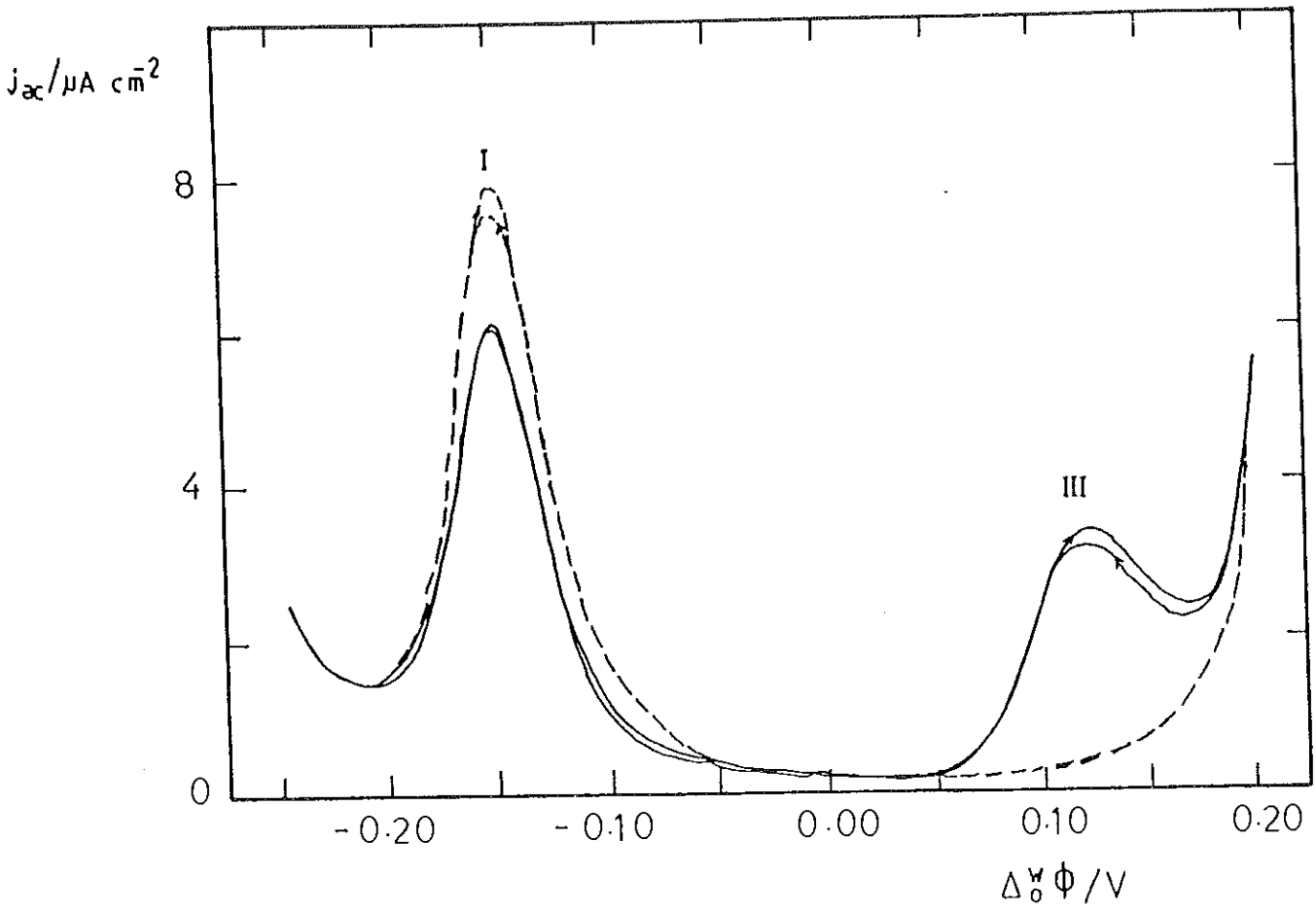

Fig. 5.2.3. Comparison of the ac voltammograms (f = 20 Hz) of (——) 0.1 mM Co^{2+}, 0.1 mM terpyridine, and (---) 0.1 mM Co^{2+}, 0.5 mM terpyridine,+ 5 mM Li_2SO_4 in the aqueous phase; organic phase as in Fig. 5.2.2. Solutions prepared under nitrogen almosphere. Sweep rate = 5 mV s^{-1}.

1:1 ratio.it is seen that peak II, which is due to the transfer of a +3 charged species, has vanished completely from the voltammogram. Under this condition, peak III appears or disappears, depending on the metal to ligand concentration ratio. For a 1:1 ratio, peak III was noticeable, but when the concentration of the ligand became high, this peak disappeared.

For further identification of the transferred species absorption experiments were carried out. Figure 5.2.4 shows the absorption spectrum of a fresh solution of the complex (0.1 mM Co^{2+} and 0.5 mM terpyridine) which was prepared under nitrogen atmosphere. The free terpyridine absorbs in the region of 290 nm which is sufficiently far from the absorption maxima of the complex (Fig. 5.2.5). The spectrum of the complex of Fig. 5.2.4 has bands in the visible region at 553, 505 and 445 nm, which correspond to those reported in the literature [18] for the complex $[Co(terpy)_2]^{2+}$.

Figure 5.2.6 illustrates the ac voltammogram for the transfer of Co-terpyridine complex prepared in a 1:5 (metal:ligand) concentration ratio in the presence of 10% H_2O_2. It can be seen that the current due to peak II (of the +3 charged complex) is much larger than that of peak I indicating the oxidation of the +2 complex to a +3 state. Addition of a few drops of 0.1 mM Co^{2+} solution to the electrochemical cell resulted in an increase of peak I and a decrease of peak II. As shown in Fig. 5.2.7, the absorption spectrum of the H_2O_2-oxidized solution of the complex displays peaks at 338 and 278 nm, which correspond to the characteristic absorption of $[Co(terpy)_2]^{3+}$ [19].

Based on the above results the observed peaks, namely peak I, and III were assigned to the transfer of the $[Co(terpy)_2]^{2+}$, and $[Co(terpy)]^{2+}$ complexes, respectively. This is also ascertained from thermodynamic considerations. The $[Co(terpy)]^{2+}$ complex, which was detected only in the presence of excess metal ion or in 1:1 ratio, is believed to be more strongly solvated in water than the $[Co(terpy)_2]^{2+}$ complex. Therefore its transfer peak should be expected to appear at more positive potentials than that of its di - ligand

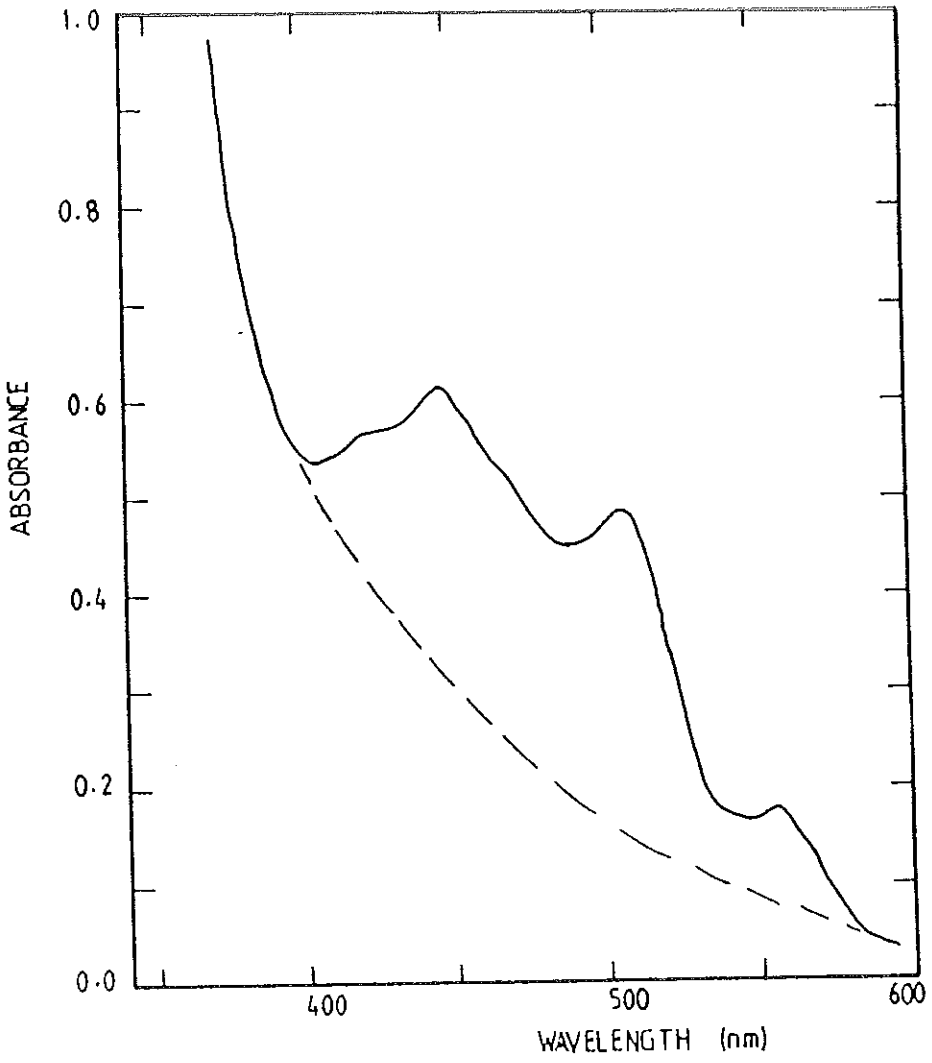

Fig. 5.2.4. Absorption spectrum of an aqueous solution of the complex containing 0.1 mM Co^{2+} + 0.5 mM terpyridine prepared under N_2 atmosphere.

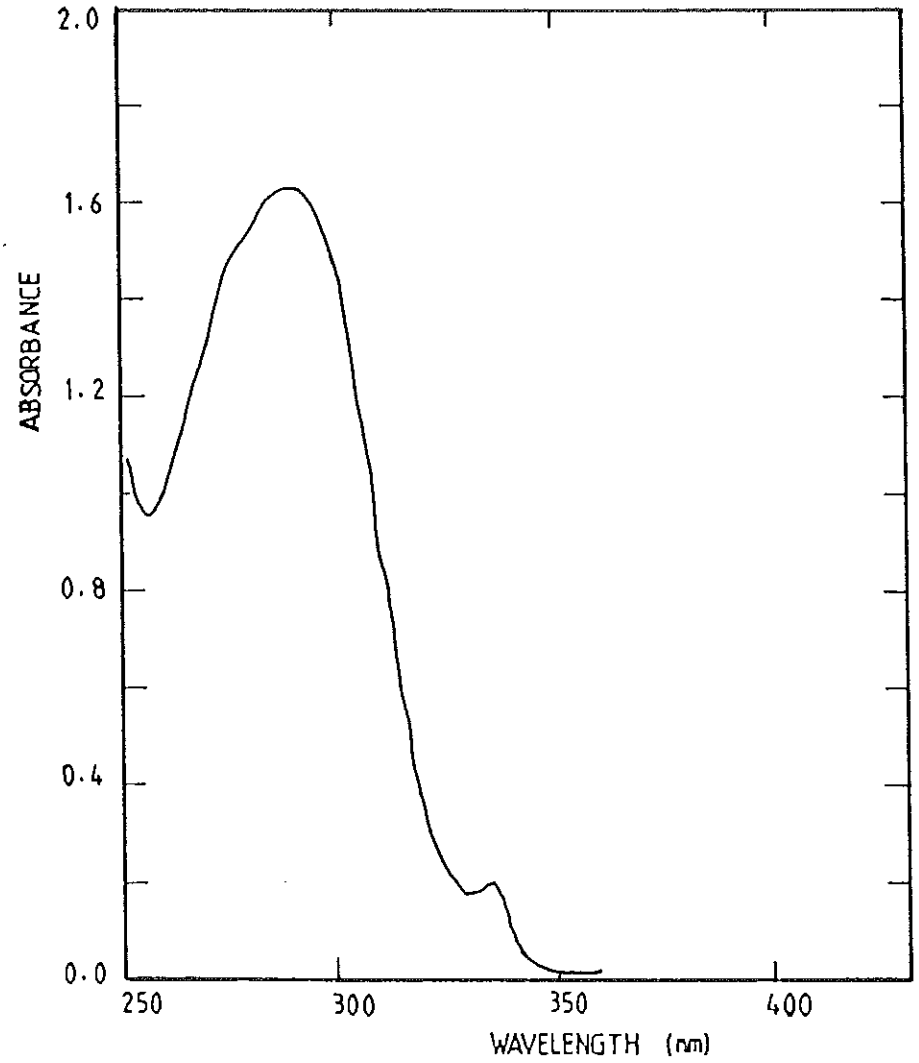

Fig. 5.2.5. Absorption spectrum of an aqueous solution 0.5 mM terpyridine.

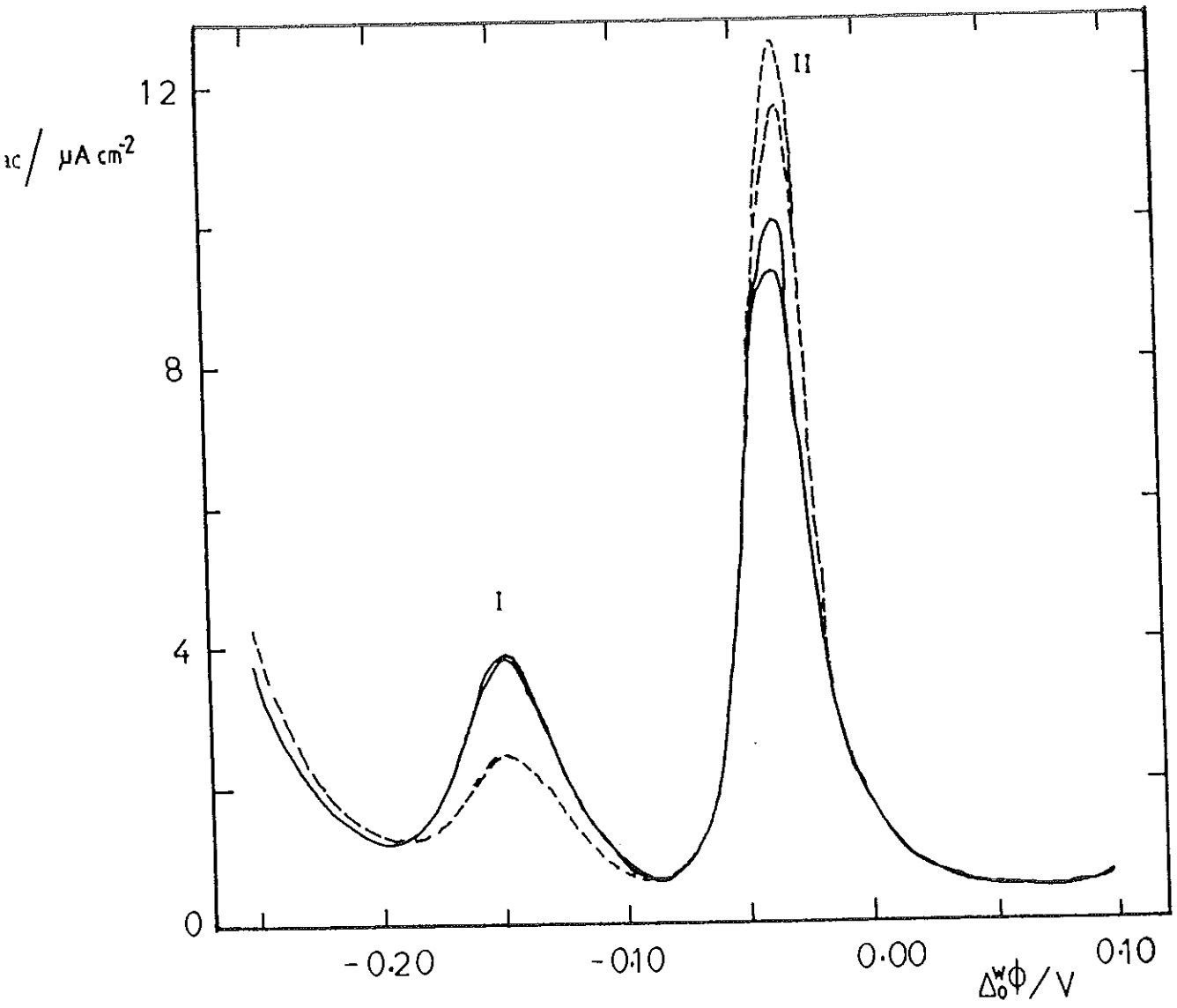

Fig. 5.2.6. Ac Voltammogram of 0.1 mM Co^{2+} and 0.5 mM terpyridine after oxidation of the solution by 10% H_2O_2 (---), and after addition of a few drops of 0.1 mM Co^{2+} to the aqueous phase in the electrochemical cell (———) . Supporting electrolyte: 5 mM Li_2SO_4 (aqueous), and 10 mM PNPDCC (nitrobenzene). Sweep rate = 5 mV s^{-1}, f = 20 Hz.

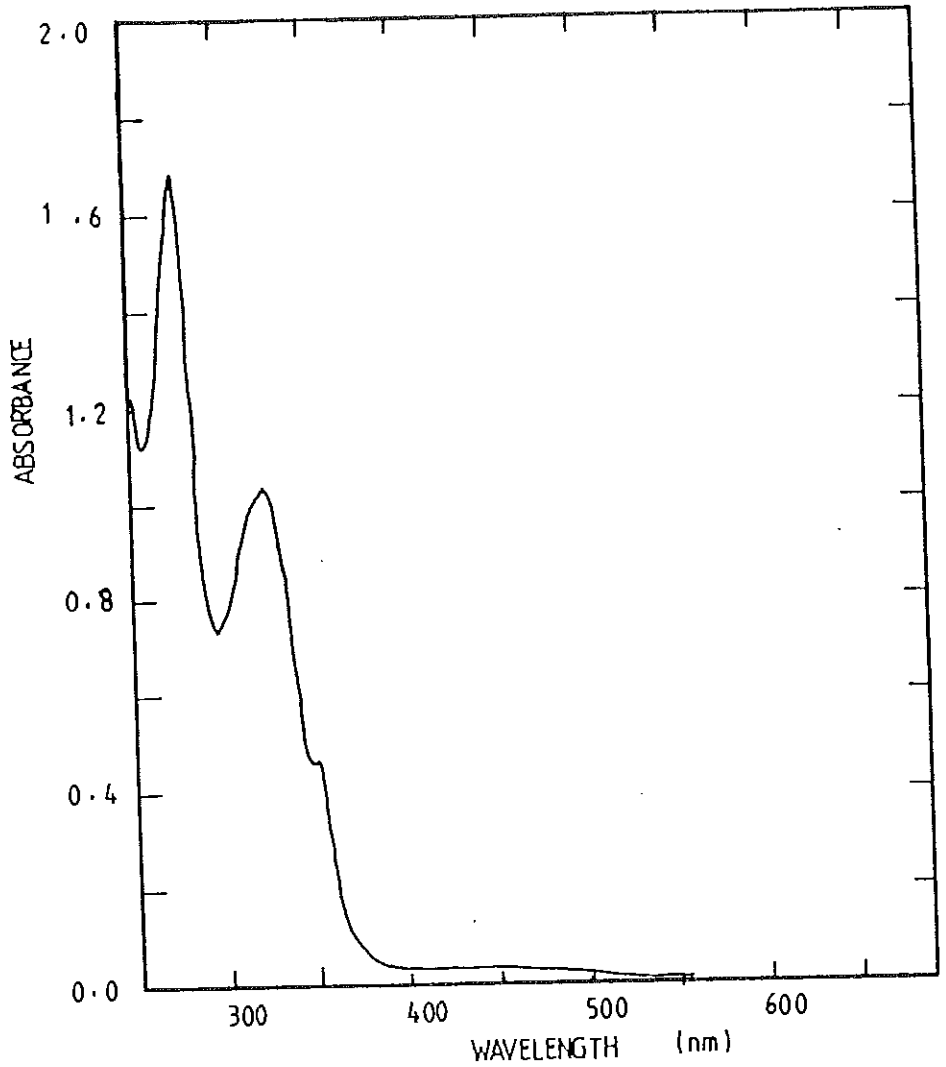

Fig. 5.2.7. Absorption spectrum of an aqueous solution of the complex containing 0.1 mM Co^{2+} + 0.5 mM terpyridine + 10 % H_2O_2.

analogue. Peak II corresponds to the transfer of the +3 charged complex ($[Co(terpy)_2]^{3+}$). Its appearance can be attributed to the oxidation of either Co^{2+} to Co^{3+} or $[Co(terpy)_2]^{2+}$ to $[Co(terpy)_2]^{3+}$ according to the following scheme:

$$Co^{2+}(aq) - e^- = Co^{3+}(aq)$$

$$+ 2\ \text{Terpyridine} \rightleftharpoons \qquad \rightleftharpoons + 2\ \text{Terpyridine}$$

$$[Co(terpy)_2]^{2+} - e^- = [Co(terpy)_2]^{3+}$$

The variation of the peak current due to the transfer of the Co-terpyridine complexes as a function of pH was studied for an air saturated solution of a 1:1 (metal:ligand) concentration ratio (Fig. 5.2.8). In the pH region between 5 to 8, all three peak heights remain unaffected (as compared to Fig 5.2.2), and the intensity of the ac current peaks is in the order: peak II > I > III. The observed large current of $[Co(terpy)_2]^{3+}$ is probably due to its charge. As shown in the figure, an increase in the pH to a value of 11.4 results in the disappearance of peak III, and a decrease in the peak intensities of I and II. At this pH, the relative decrease of peak II is much greater than that of peak I. The elimination of peak III, and the decrease in the peak intensities is probably associated with the dissociation of the complexes due to attack by OH^- ions. This dissociation is much more pronounced for $[Co(terpy)]^{2+}$ (peak III), since the OH^- can easily attack the central metal from the vacated position, and a rupture of the nitrogen-metal bond may take place [20]. At such high pH, the stability of the complexes is in the order $[Co(terpy)_2]^{2+} > [Co(terpy)_2]^{3+} > [Co(terpy)]^{2+}$. At low pH (pH = 2.7), the intensity of the peak currents is in the order of I > II > III. The current density of peak II (of the trivalent complex) decreases, whereas peak III does not show appreciable changes. On the other hand, peak I

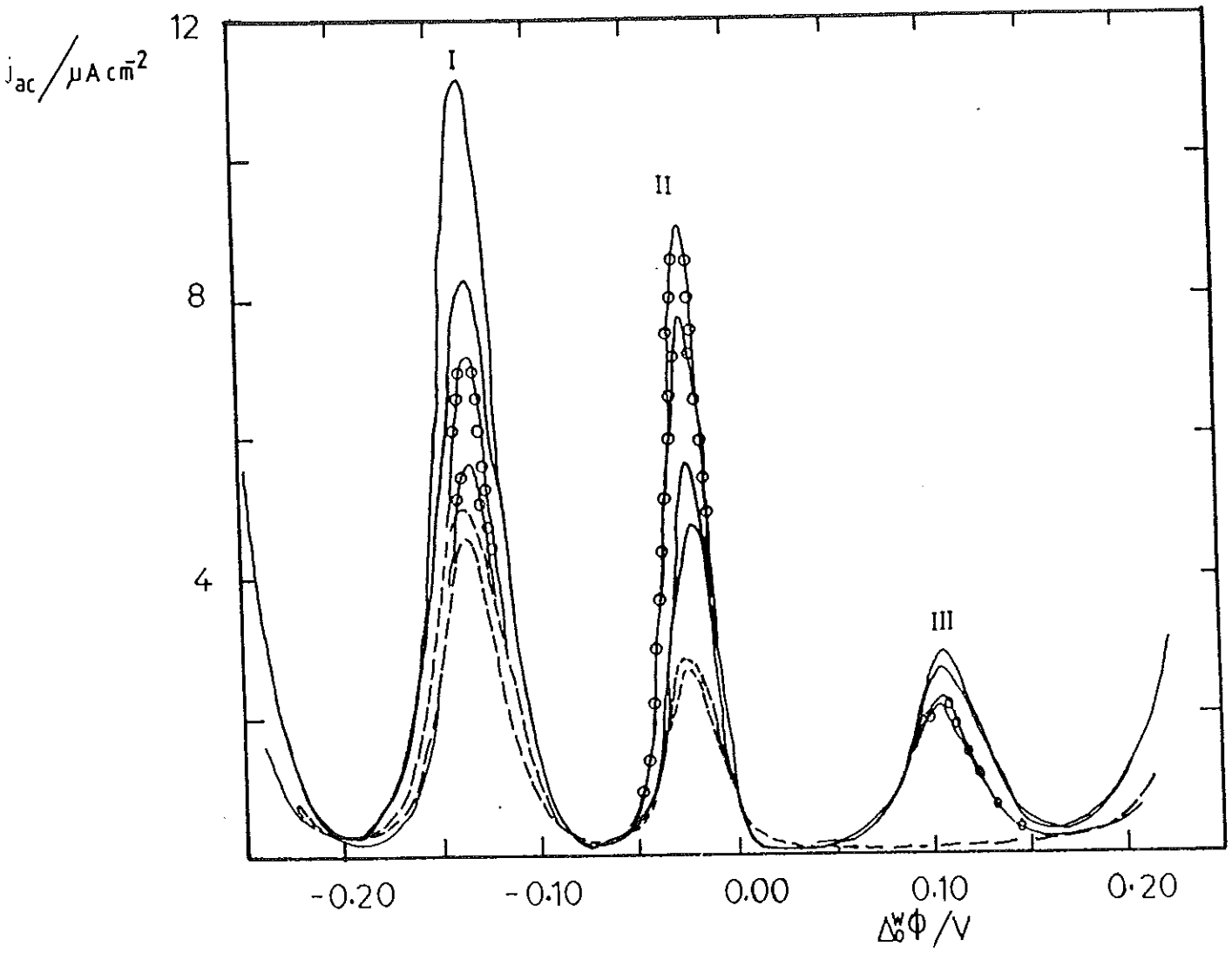

Fig. 5.2.8. Ac cyclic voltammograms for the transfer of Co-terpyridine complexes across the water/nitrobenzene interface at different pHs. Air-saturated solutions containing 0.5 mM Co^{2+} and 0.5 mM terpyridine. (——) pH 2.7; (-o-) pH 5-8; (---), pH 11.4. All other conditions an in Fig.5.2.6.

exhibits enhancement in the current density. This may be caused by the reduction of the Co^{3+} complex which is favorable at low pH [21].

The pH dependence of the dissociation of metal-terpyridine complexes has been well studied [20], and it is believed that both OH^- and H^+ can facilitate the dissociation by attaching themselves to the metal ion and to the basic nitrogen of the ligand, respectively. The observed voltammetric results show clearly the effect of pH on these complexes, and their stability. In all the studies, shifts in peak potentials due to pH variations were not detected, nor was proton-assisted transfer of the ligands.

Iron-Terpyridine

The transfer of Fe^{2+}-terpyridine complex across the water/nitrobenzene interface showed a single peak which corresponds to the transfer of $[Fe(terpy)_2]^{2+}$ species, irrespective of the metal:ligand concentration ratio (i.e. either excess ligand or excess metal). As shown in Fig. 5.2.9, the absorption spectrum of an aqueous solution of the complex revealed bands at 552 (maximum peak) and 610 nm, with a broad shoulder in the range 475-500 nm, which are characteristic of $[Fe(terpy)_2]^{2+}$ [22]. It has been reported [22] that the complex $[Fe(terpy)]^{2+}$ can be detected spectroscopically, but that it disproportionates rather rapidly. Its presence (during the time scale of the voltammetric experiments) was not detected in this investigation.

Figure 5.2.10 illustrates the ac and dc voltammograms for the transfer of the complex $[Fe(terpy)_2]^{2+}$ as recorded during the initial stages of the cycles. The transfer of $[Fe(terpy)_2]^{2+}$ yields well defined voltammograms; however, interfacial instability was visually observed during the initial sweeps. This effect was reflected in the dc voltammograms by the appearance of a shoulder near the peak for the transfer of the complex. This shoulder decreased gradually upon repeated cycling, and disappeared completely after about twenty cycles, at which point the interfacial instability also disappeared. This behaviour was

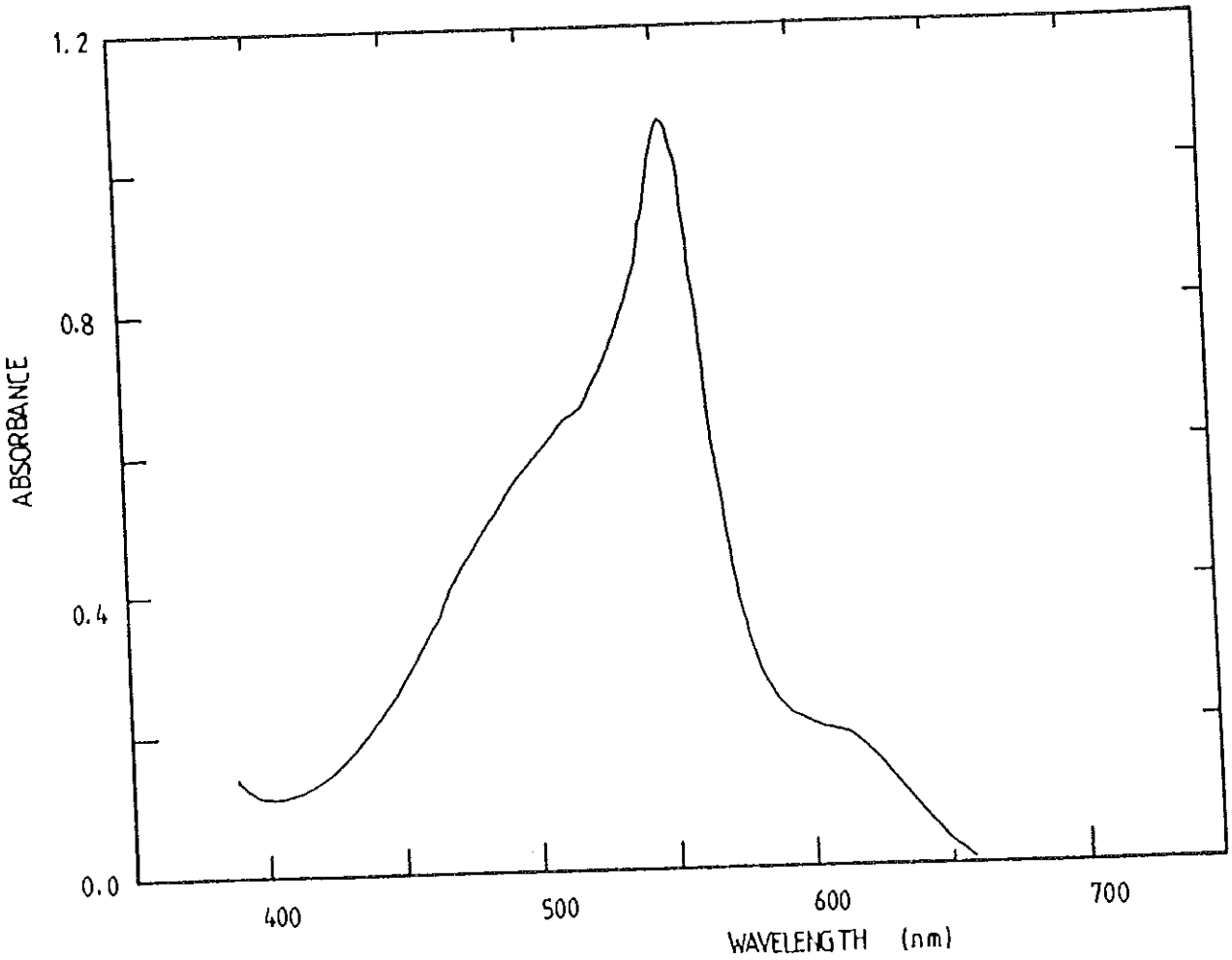

Fig. 5.2.9. Absorption spectrum of an aqueous solution of the complex containing 0.1 mM Fe^{2+} + 0.1 mM terpyridine

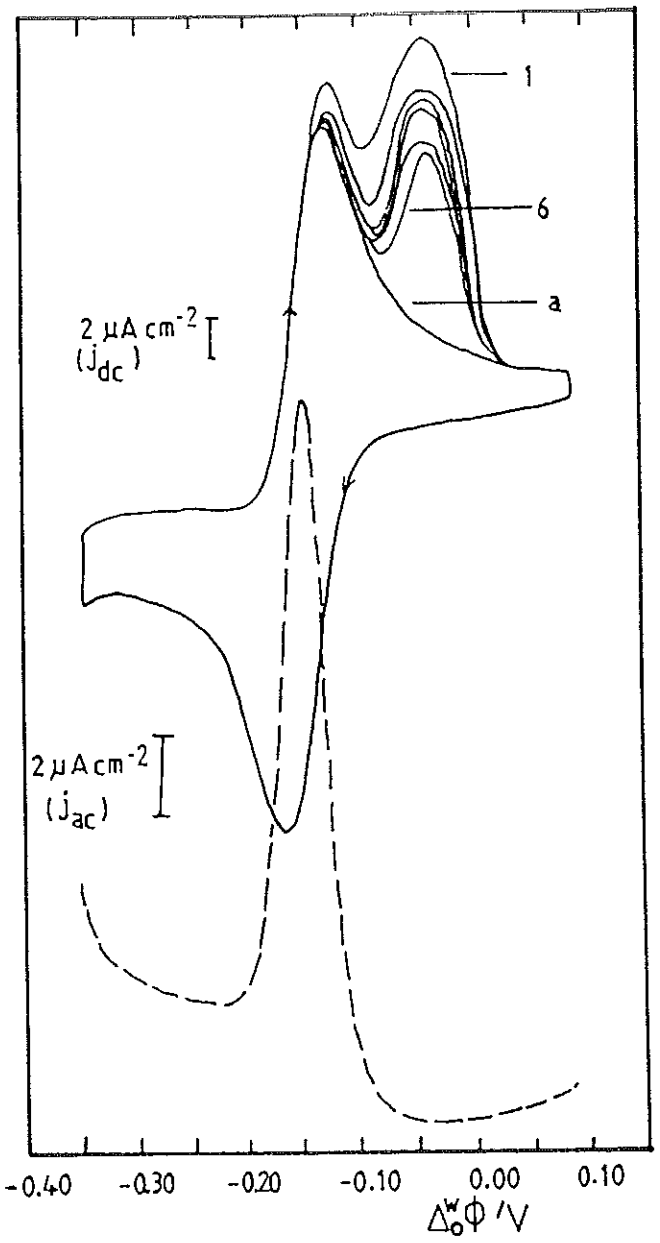

Fig. 5.2.10. Ac and dc cyclic voltammograms for the transfer of $[Fe(terpy)_2]^{2+}$ across the water/nitrobenzene interface. Aqueous phase: 0.1 mM Fe^{2+} and 0.1 mM terpyridine in 5 mM Li_2SO_4; organic phase :10 mM PNPDCC; 1 to 6 show the first stage of the experimental cycles and (a) is after 20 cycles. Ac sweep rate = 5 mV s^{-1} and dc sweep rate = 10 mV s^{-1}

found to be very reproducible. As can be seen from the above figure the ac voltammogram is insensitive to such behaviour. The observation of interfacial instability at the water/nitrobenzene interface has previously been reported by Nakache et al.[23]. There are two known effects which cause hydrodynamic instabilities of interfaces [24]. The first one is the existence of a non-uniform interfacial surface tension (Marangoni effect) which causes a macroscopic movement in at least one of the phases, and as a result a friction occurs on the interface. The second one is due to the existence of free electric charges (e.g. ions or electrons) adsorbed at the interface which is common in liquid/liquid systems with a flat charged interface. In the present system, not much can be said about the observed phenomena since little is understood about the changes in the interfacial tension and the physical mechanisms controlling interfacial instability. [24].

The peak due to the transfer of the $[Fe(terpy)_2]^{3+}$ complex was found to be very weak and appeared at the same potential as that of $[Co(terpy)_2]^{3+}$. Apart from this peak, another peak, corresponding to the transfer of a +2 charged species appeared at a peak potential which matched that of the transfer of $[Fe(terpy)_2]^{2+}$. It has been reported that direct addition of terpyridine to a solution of Fe^{3+} results in a rapid reduction and the formation of $[Fe(terpy)_2]^{2+}$ [25]. The second wave could therefore be attributed to the transfer of $[Fe(terpy)_2]^{2+}$.

Nickel, Copper, and Zinc-Terpyridine

Figure 5.2.11 compares the ac voltammograms for the transfer of the terpyridine complexes of Ni^{2+}, Zn^{2+}, and Cu^{2+} for a metal:ligand concentration ratio of 5:1. The peaks which are seen in the positive potential region are due to the transfer of the mono-ligand complexes, whereas the peaks in the negative region correspond to the di-ligand complexes. All the transfer processes exhibit diffusion-controlled reversible behaviour. It is seen that the Ni^{2+} complexes

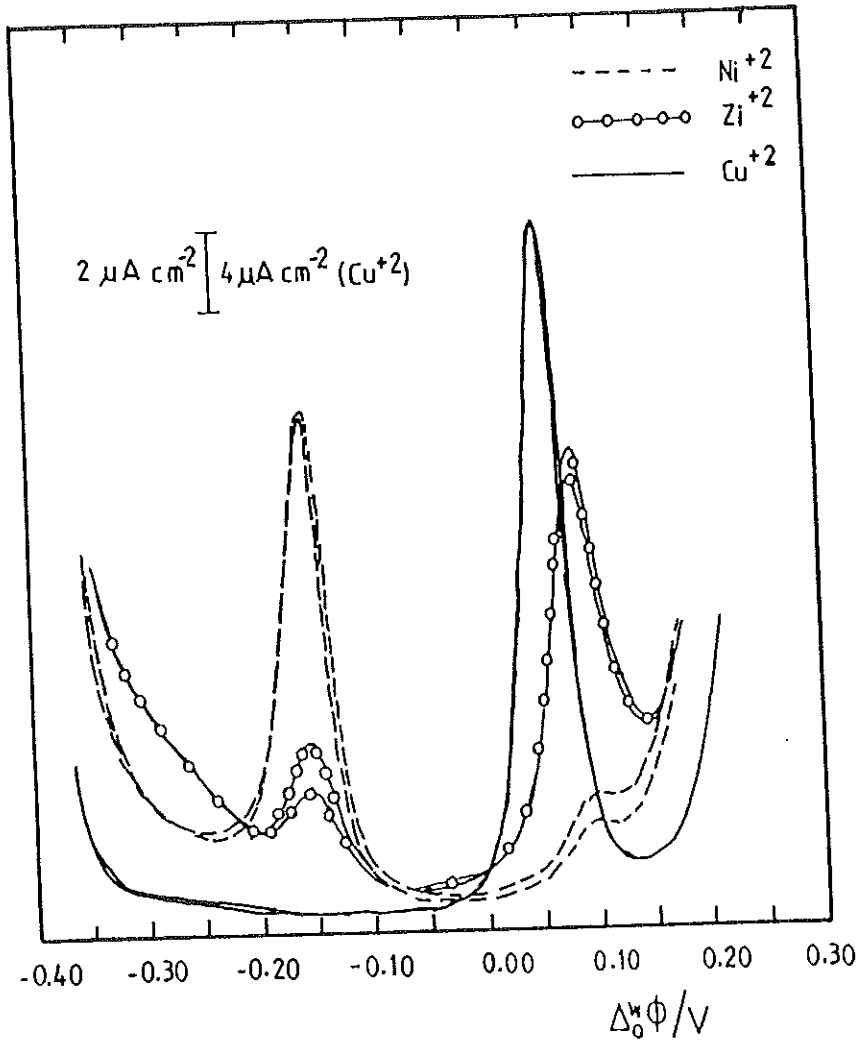

Fig. 5.2.11. Ac cyclic voltammograms for the transfer of Cu (——), Ni (---), and Zn (-o-)-terpyridine complexes across the water/nitrobenzene interface. Aqueous solution containing 0.5 mM M^{2+} (M^{2+} = Cu^{2+}, Ni^{2+} or Zn^{2+}) and 0.1 mM terpyridine + 5 mM Li_2SO_4; organic phase :10 mM PNPDCC. Sweep rate = 5 mV s^{-1}, f = 20 Hz.

show predominantly the transfer of the $[Ni(terpy)_2]^{2+}$ complex, while the $[Ni(terpy)]^{2+}$ peak appears as a shoulder even though the complexes were prepared from an excess amount of Ni^{2+} ions. On the other hand, the transfer of Zn^{2+} complexes shows the opposite behaviour, with a relatively larger transfer peak of $[Zn(terpy)]^{2+}$ than that of $[Zn(terpy)_2]^{2+}$. The transfer peak of the Cu^{2+} complex is completely dominated by $[Cu(terpy)]^{2+}$, with a peak current density which is three times larger than that of $[Zn(terpy)]^{2+}$. For complex solutions which were prepared from excess ligand concentration, transfer peaks which are exclusive to the di-ligand complexes were observed for all three metal complexes. The relative stabilities of the complexes may be inferred from the corresponding peak current densities; accordingly, for the mono-ligand complexes, the following order is observed :

$$[Cu(terpy)]^{2+} > [Zn(terpy)]^{2+} > [Ni(terpy)]^{2+}$$

For the di-ligand complexes, the order is :

$$[Ni(terpy)_2]^{2+} > [Zn(terpy)_2]^{2+} > [Cu(terpy)_2]^{2+}.$$

Table 5.2.1 presents the stability constants of the mono and di-ligand terpyridine complexes of some transition metals as reported in ref. 22. In general, the values are in fair agreement with the order given above, with the exception of the reversed order of the mono-ligand complexes of Ni^{2+} and Zn^{2+}.

The half-wave potentials of the transferring complexes were read from the peak positions of the ac voltammograms and the standard Galvani potential differences were then evaluated. In calculating the $\Delta^{w}_{o}\phi^{o}$ values, it was assumed that the activity coefficients of the complexes were the same in both phases and ion pair formation in the organic phase was neglected. The diffusion coefficients of the complexes in the aqueous phase were calculated using

Table 5.2.1.

Stability constants of metal-terpyridine complexes [22].

Metal ion	log K_{ML}	log K_{ML2}
Cu^{2+}	13.0	
Ni^{2+}	10.7	21.8 (β_2)
Zn^{2+}	6.0	

convolution potential sweep voltammetry (CPSV). CPSV has been employed for the data processing of linear sweep voltammograms of charge transfer processes [26-28]. According to this technique, diffusion-controlled reversible current potential curves are analysed using the equation :

$$\{(m_d - m)/m\}_w = (D_w/D_o)^{1/2} \exp[-ZF(\Delta^w_o\phi - \Delta^w_o\phi^0)/RT] \qquad (5.2.1)$$

where m represents the convoluted current and m_d is the limiting convoluted current which is expressed by

$$(m_d)_w = ZFAD_w^{1/2} C^o_w \qquad (5.2.2)$$

Figures 5.2.12 and 5.2.13 illustrate plots of the convolution current (m), and of the logarithmic value ($Y = \log[(m_d - m)/m]$ as a function of the potential for the transfer of $[Cu(terpy)]^{2+}$ and $[Cu(terpy)_2]^{2+}$ complexes from water to nitrobenzene, respectively. The analysis of the convolution curves were made from the linear sweep voltammograms of Fig. 5.2.14. In the presence of large excess of terpyridine the initial concentration of Cu^{2+} was taken as the bulk concentration of $[Cu(terpy)_2]^{2+}$, assuming that all of the Cu^{2+} ions were complexed. Similarly, for the concentration of the $[Cu(terpy)]^{2+}$ complex, the concentration of the ligand was used assuming that all the ligand molecules were consumed in the complex formation in the presence of five fold concentration of Cu^{2+}.

The reversibility of the transfer process can be further checked from the plots of Y vs $\Delta^w_o\phi$ which give straight lines with reciprocal slopes of 30 mV. The limiting values of the convoluted current for $[Cu(terpy)]^{2+}$ and $[Cu(terpy)_2]^{2+}$ were determined from the convolution integral curves as m_d = 37.8 μA $s^{1/2}$ and 13 μA $s^{1/2}$, respectively. From these values the diffusion coefficients of the complexes in water were evaluated as $D_w = 8.1 \times 10^{-6}$ $cm^2 s^{-1}$

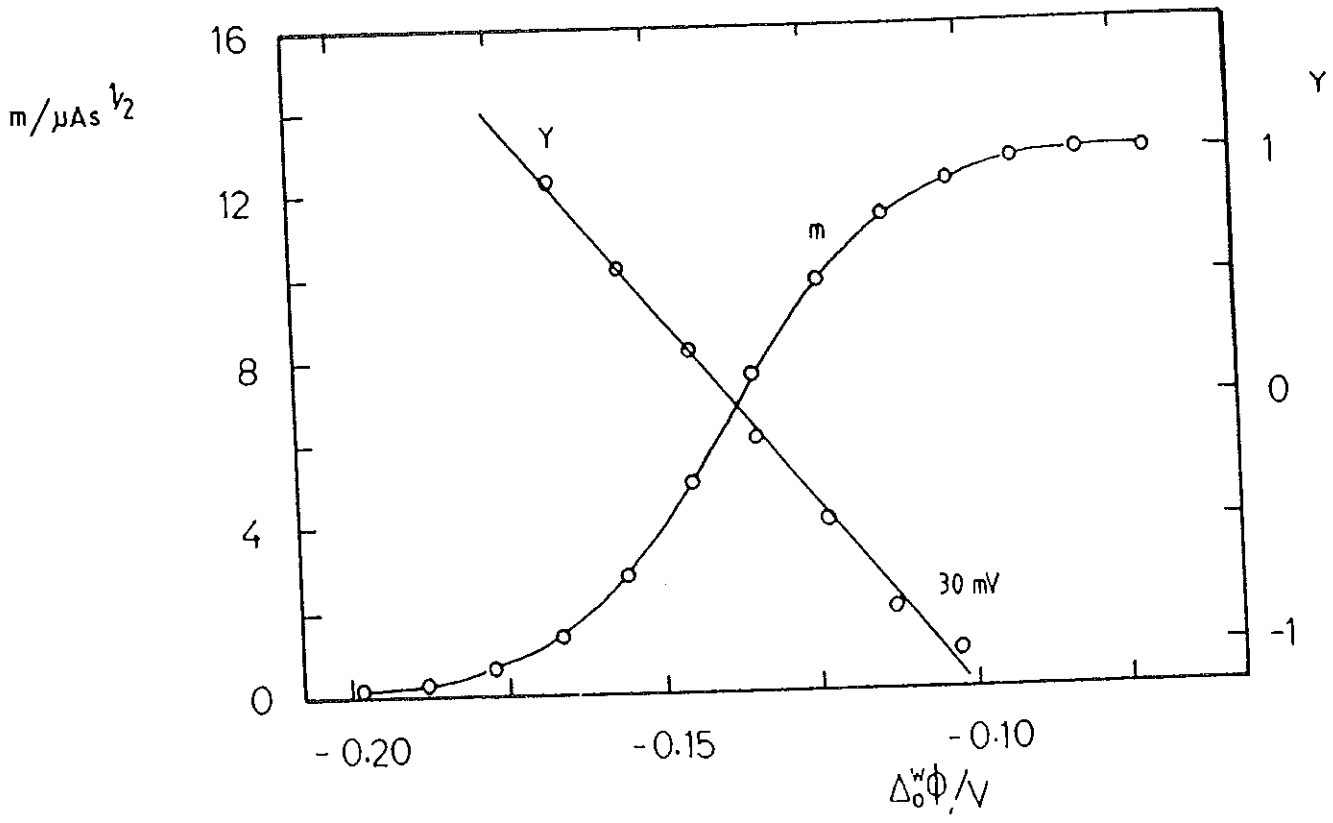

Fig 5.2.12. Plot of the convoluted current, m, and of Y vs. the potential for the transfer of $[Cu(terpy)_2]^{2+}$ across the water/nitrobenzene interface. Aqueous phase: 0.1 mM Cu^{2+}, 0.5 mM terpyridine, 5 mM Li_2SO_4; organic phase: as in Fig. 5.2.11. Sweep rate = 10 mV s^{-1}.

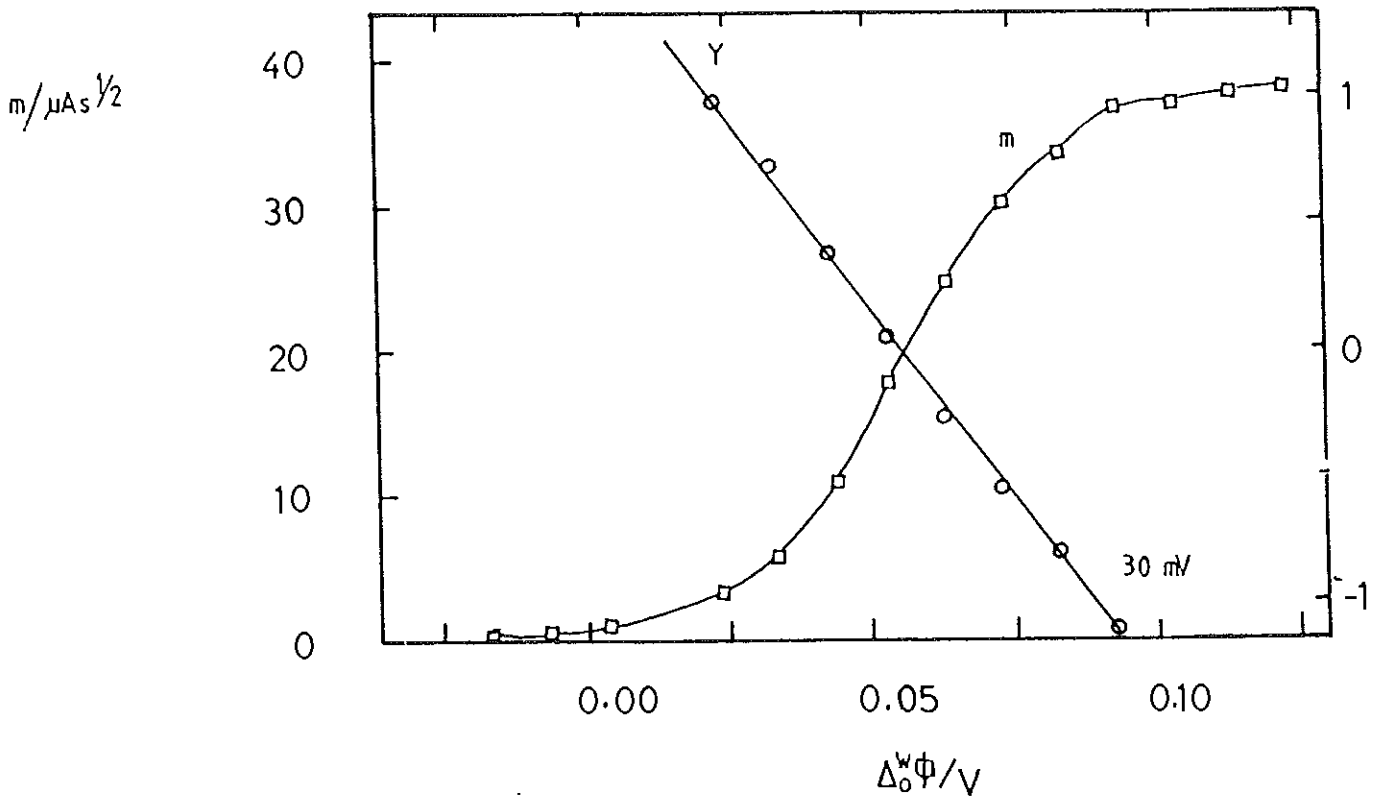

Fig. 5.2.13. Plot of the convoluted current, m, and of Y vs. the potential for the transfer of [Cu terpy]$^{2+}$ across the water/nitrobenzene interface. Aqueous phase: 0.5 mM Cu^{2+}, 0.1 mM terpyridine, 5 mM Li_2SO_4; organic phase: as in Fig. 5.2.11. Sweep rate = 10 mV s^{-1}.

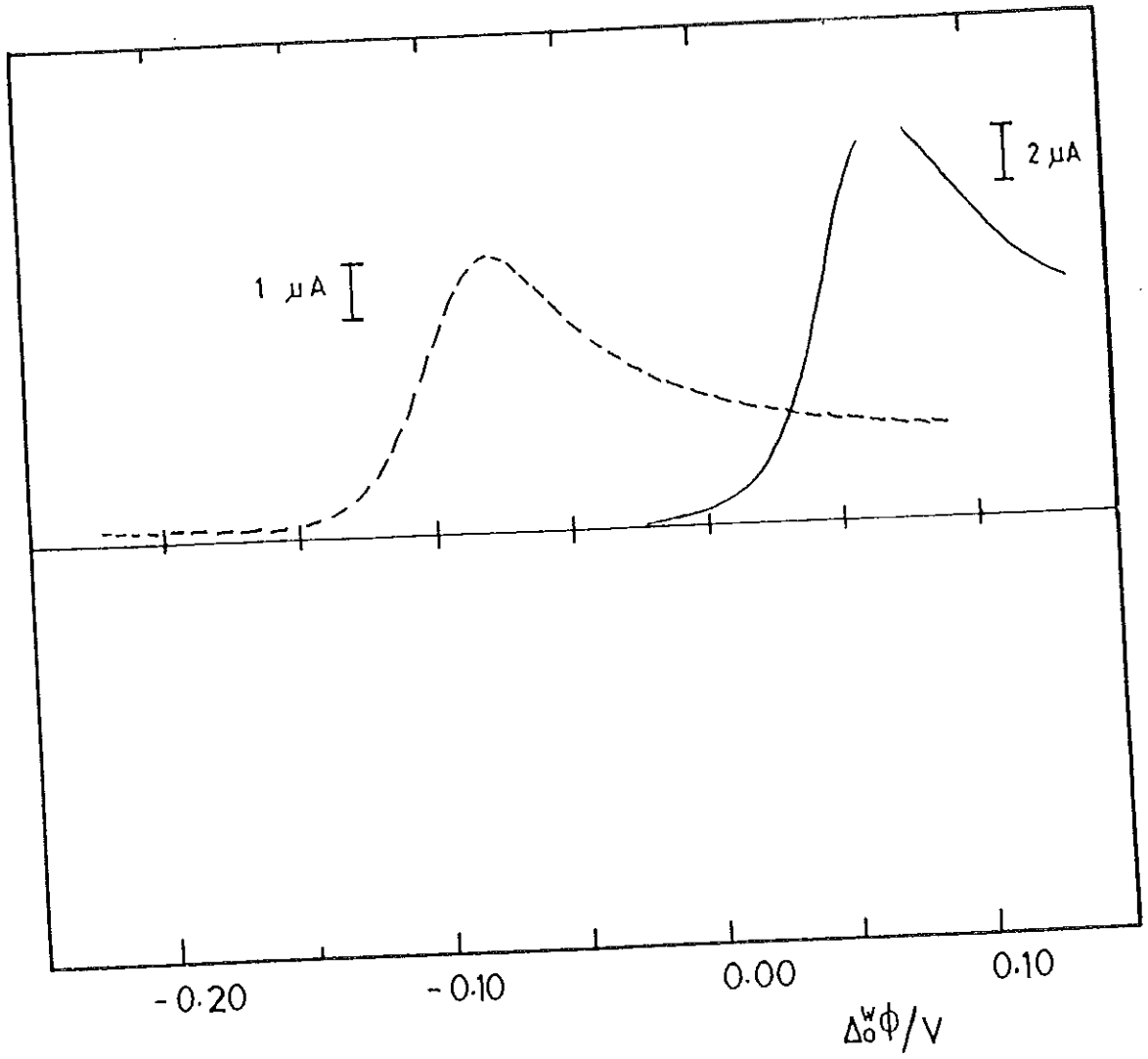

Fig. 5.2.14. Single sweep voltammograms for the transfer of $[Cu\ terpy]^{2+}$ (——), and $[Cu(terpy)_2]^{2+}$ (---) from water to nitrobenzene. All other conditions as in Fig.5.2.12 or 5.2.13, respectively.

and $D_w = 3.8 \times 10^{-6}$ cm^2 s^{-1} for the mono and the di-ligand species, respectively. Similarly, the diffusion coefficients of the other complexes were calculated from the values of the limiting convoluted current. The diffusion coefficients of the complexes in the organic phase were computed by employing Walden's rule [6].

$$D_o = (D_w \eta_w)/\eta_o \qquad (5.2.3)$$

where η_w and η_o are the viscosities of water and nitrobenzene, respectively.

Table 5.2.2 lists the diffusion coefficients of the complex ions in water, the half-wave potentials, the standard Galvani potential differences and the standard Gibbs energy of transfer from water to nitrobenzene. In Table 5.2.3 the $\Delta G^o{}_{tr}{}^{w\rightarrow nb}$ values of the mono and di-ligand complexes are tabulated and their absolute differences, $\Delta|\Delta G^o{}_{tr}{}^{w\rightarrow nb}|$ are compared.

It is interesting to note that the $\Delta G^o{}_{tr}{}^{w\rightarrow nb}$ values of the di-ligand complexes of Co^{2+}, Ni^{2+}, Zn^{2+}, and Fe^{2+} are, within experimental error, equal to each other (-29 to -31 kJ mol^{-1}), and hence independent of the nature of the central metal ion. The same holds for the di-ligand complexes of Co^{3+} and Fe^{3+} (-11 kJ mol^{-1}). Comparison of the $\Delta G^o{}_{tr}{}^{w\rightarrow nb}$ values for the mono and di-ligand complexes of Ni^{2+} and Co^{2+}, respectively, indicates clearly that the exchange of three water molecules in the inner coordination sphere by one molecule of terpyridine alters the Gibbs energy of transfer by about 49 kJ/mol. The configuration of the mono and di-complexes of these metal cations are well known in that their inner coordination spheres have octahedral structures [29]. This implies that each ligand molecule has been substituted by three water molecules. In a similar work Homolka and Wendt [30] obtained the $\Delta|\Delta G^o{}_{tr}|$ value for Ni^{2+} complexes to be 33 kJ mol^{-1} for the exchange of two water molecules by a molecule of bipyridine. Based on these observations and from the view point of structural similarity between bipyridine and terpyridine, it is

Table 5.2.2.

Diffusion coefficients D_w, half-wave potentials, $\Delta^w{}_o\phi_{1/2}$, standard Galvani potential differences, $\Delta^w{}_o\phi^o$, and standard Gibbs energies of transfer of the complex ions from water to nitrobenzene, $\Delta G^o{}_{tr}{}^{w\rightarrow nb}$.

Complex ion	$D_w \times 10^6$ ($cm^2\ s^{-1}$)	$\Delta^w{}_o\phi_{1/2}$ (V)	$\Delta^w{}_o\phi^o$ / V (V)	$\Delta G^o{}_{tr}{}^{w\rightarrow nb}$ ($kJ\ mol^{-1}$)
$[Co(terpy)]^{2+}$	7.8	0.108	0.103	19.9
$[Co(terpy)_2]^{2+}$	4.0	-0.150	-0.155	-29.9
$[Co(terpy)_2]^{3+}$	5.0	-0.033	-0.037	-10.7
$[Ni(terpy)]^{2+}$	8.1	0.100	0.094	18.1
$[Ni(terpy)_2]^{2+}$	5.3	-0.154	-0.160	-30.9
$[Zn(terpy)]^{2+}$	7.6	0.084	0.078	15.1
$[Zn(terpy)_2]^{2+}$	5.3	-0.156	-0.162	-31.3
$[Cu(terpy)]^{2+}$	7.8	0.056	0.051	9.8
$[Cu(terpy)_2]^{2+}$	3.8	-0.144	-0.149	-28.8
$[Fe(terpy)_2]^{2+}$	4.0	-0.148	-0.152	-29.3
$[Fe(terpy)_2]^{3+}$	5.1	-0.032	-0.038	-10.9

Table 5.2.3

Standard Gibbs energies of transfer of metal cations, complex ions and changes in the Gibbs energy of transfer, $\Delta|\Delta G^0_{tr}{}^{w\to nb}|$ across the water/nitrobenzene interface.

Metal ion	$\Delta G^0_{tr}{}^{w\to nb}$ (kJ mol^{-1})	Complex ion	$\Delta G^0_{tr}{}^{w\to nb}$ (kJ mol^{-1})	$\Delta|\Delta G^0_{tr}{}^{w\to nb}|$ (kJ mol^{-1})
Co^{2+}	69.3	$[Co(terpy)]^{2+}$	19.9	
		$[Co(terpy)_2]^{2+}$	-29.9	49.8
Ni^{2+}	70.0	$[Ni(terpy)]^{2+}$	18.1	
		$[Ni(terpy)_2]^{2+}$	-30.9	49.0
Zn^{2+}	64.5	$[Zn(terpy)]^{2+}$	15.1	
		$[Zn(terpy)_2]^{2+}$	-31.3	46.4
Cu^{2+}	59.2	$[Cu(terpy)]^{2+}$	9.8	
		$[Cu(terpy)_2]^{2+}$	-28.8	38.6
		$[Co(terpy)_2]^{2+}$	-29.9	
		$[Co(terpy)_2]^{3+}$	-10.7	19.2
		$[Fe(terpy)_2]^{2+}$	-29.3	
		$[Fe(terpy)_2]^{3+}$	-10.9	18.4

possible to conclude that every pyridine moiety contributes to the change in the Gibbs energy of transfer by about 16 kJ mol^{-1}.

Figure 5.2.15 shows a linear relationship between the standard Gibbs energy of transfer values and the number of pyridyl units in the complex, for the Ni-bipyridine and Ni-terpyridine complexes. For the former, the values reported in ref. 30 were taken. Extrapolation of the linear plot to zero ligand (i.e. for the uncomplexed Ni^{2+} ion) leads to a value of approximately 70 kJ/mol for the standard Gibbs energy of transfer of Ni^{2+} across the water-nitrobenzene interface. This agrees well with the similarly extrapolated value for Ni^{2+} reported in ref. 29. For Co^{2+}, Zn^{2+}, and Cu^{2+}, sufficient data are not available to warrant an extrapolation; however, tentative estimates give values in the range between 70 and 50 kJ mol^{-1} (see Table 5.2.3). These values are not unreasonable when one compares them with the values of other divalent cations reported in the literature. For example, the $\Delta G^0_{tr}{}^{w\rightarrow nb}$ of Mg^{2+}, Ca^{2+}, Sr^{2+}, and Ba^{2+} are reported to be 71.4, 68.3,67.2, and 63.3, respectively [31]. The present method of extrapolation may thus provide an estimate of ΔG^0_{tr} values for ions that transfer across an interface at potentials that fall well beyond the available potential window for given solvent systems.

The observed anomaly in the ΔG^0_{tr} value of $[Cu(terpy)]^{2+}$ as compared to the value of the analogous mono-ligand complexes of $[Zn(terpy)]^{2+}$ and $[Ni(terpy)]^{2+}$ might be explained in terms of structural differences and number of water molecules involved in the inner coordination sphere. It has been indicated that the $[Cu(terpy)]^{2+}$ complex possesses a distorted trigonal bipyramidal geometry of five coordination of the type $[Cu(terpy)(H_2O)_2]^{2+}$ [29]. Such type of coordination has also been reported for the mono-ligand complex of Zn^{2+} which is believed to have a distorted square based pyramidal structure [29]. However the observed difference in the ΔG^0_{tr} value of this complex from the rest is not that much pronounced. In general variations in the ΔG^0_{tr} values of the complexes reflect differences in the number of water

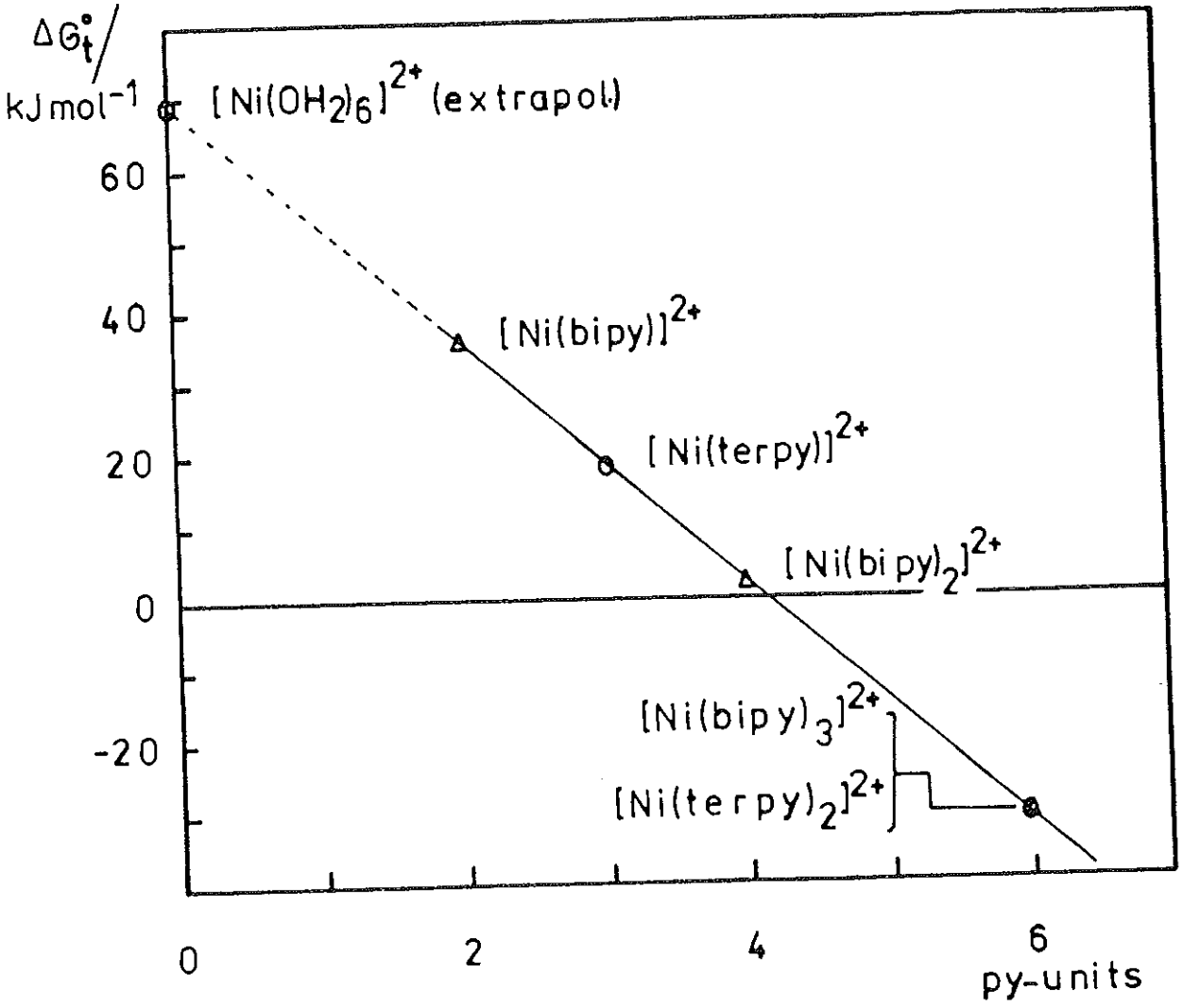

Fig. 5.2.15. $\Delta G^{o}_{tr}{}^{(w\rightarrow o)}$ of Ni-bipyridine and Ni-terpyidine complexes vs. the number of pyridyl units. (Δ) From ref. 30; (0) this work.

molecules of the inner sphere as well as the geometrical structure of the complexes.

Part of this work has been reported in ref. 32.

5.2.2 *TRANSFER OF CUPROUS ION ACROSS THE WATER/1,2-DICHLOROETHANE INTERFACE FACILITATED BY 2,2'-BIQUINOLINE*

Figure 5.2.16 shows the dc voltammogram obtained in the presence of 1 mM Cu^+ in the aqueous phase and 0.1 mM 2,2'-biquinoline (biq) in the organic phase using 10 mM LiCl and TPAsTPBCl as base electrolytes. In the absence of the ligand or the metal ion no transfer of charged species was detected. Thus the observed peaks of the voltammogram correspond to the transfer of Cu^+ facilitated by biquinoline. As can be seen from the voltammogram the separation between the forward and reverse peaks is 60 mV and the peak potential was found to be independent of scan rate in the range 5-100 mV/s. A 60 mV shift in the half-wave potential was also observed for ten fold change in the concentration of Cu^+. As shown by Fig. 5.2.17 both the positive and negative peak currents are linearly dependent on the square root of the scan rate. The peak currents were also found to be proportional to the concentration of biquinoline in the organic phase. This implies that the observed behaviour fulfils the criteria for a reversible transfer of a monovalent cation present in excess in the aqueous phase and facilitated by a ligand present at low concentration in the organic phase and forming a 1:1 complex [33]. The mechanism of the transfer process from the aqueous to the organic phase is:

1) diffusion of the ligand to the interface.
2) complex formation between a ligand molecule and Cu^+ ion at the interface in a 1:1 ratio.
3) transfer and diffusion of the complex into the bulk of the organic phase.
4) reaction of the complex with more ligands, if thermodynamically possible.

The reverse of this sequence occurs during the return sweep. Since the size of the ligand is very similar to that of the complex, it is possible to assume

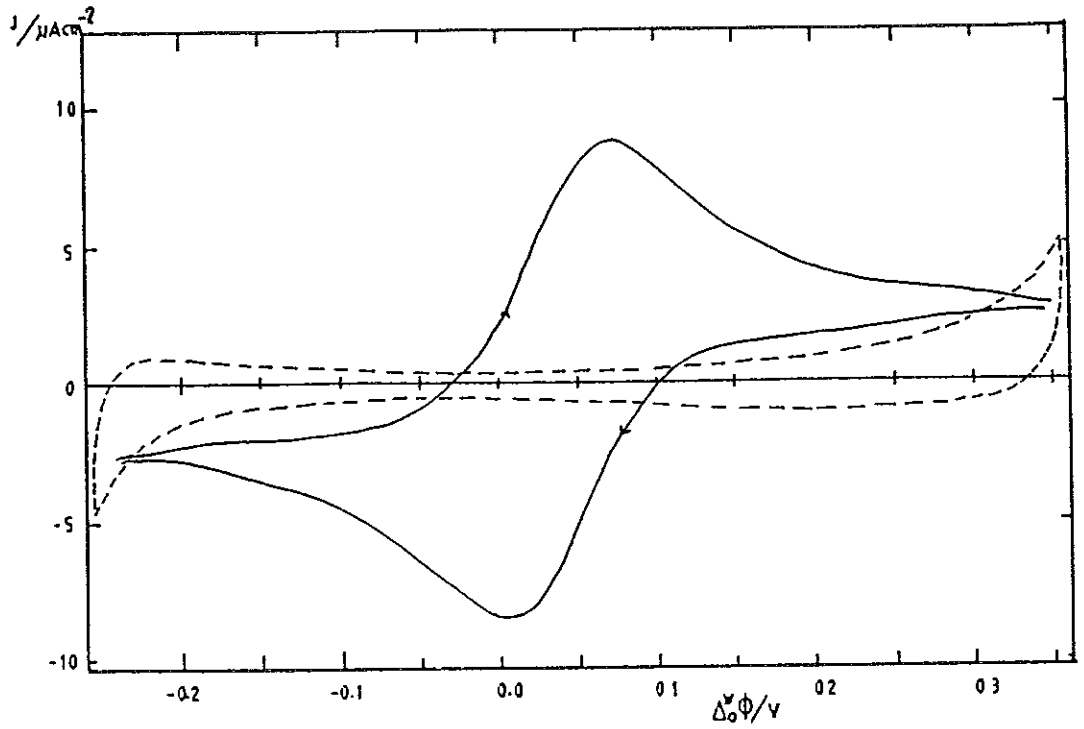

Fig. 5.2.16. Cyclic voltammogram of 1 mM Cu^{+} transfer across the water/1,2-DCE interface facilitated by 0.1 mM 2,2'-biquinoline in the organic phase. Base electrolytes: 10 mM LiCl (aq. pH 4.5) and 10 mM TPAsTPBCl (organic). Sweep rate = 20 mV s^{-1}. (---) voltammogram of the base electrolyte in the presence of Cu^{+}.

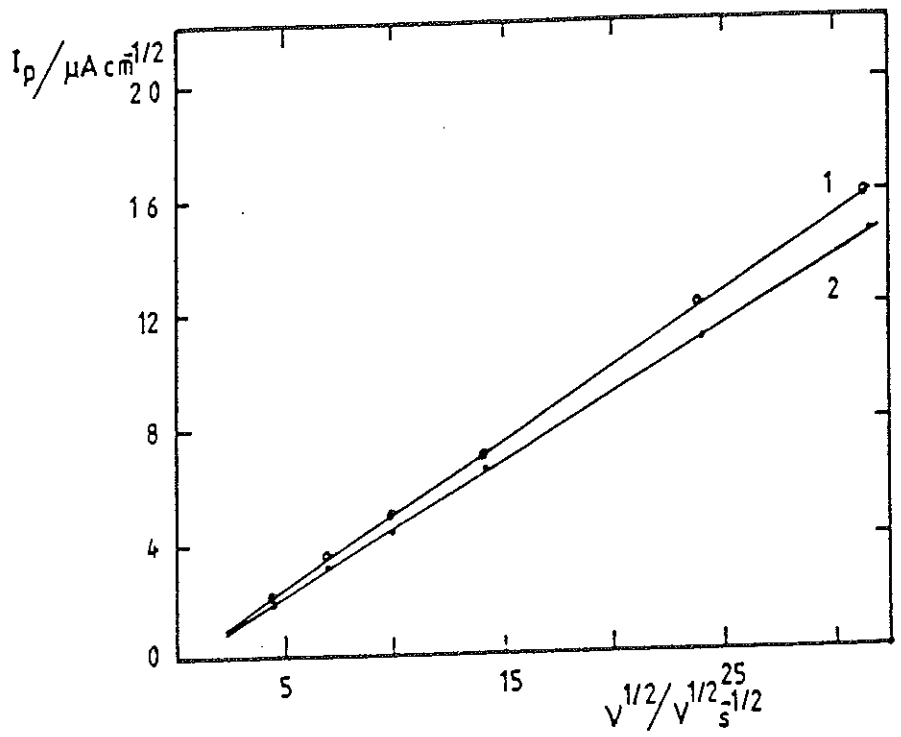

Fig. 5.2.17. Dependence of the peak currents on the square root of the sweep rate. (1) positive peak current, (2) negative peak current. Concentration of electrolytes: 1 mM Cu^{+} (aq.) and 0.1 mM 2,2'-biquinoline (organic).

that the diffusion coefficients of the ligand and the complex are the same in the organic phase. Thus the half wave potential due to the facilitated ion transfer is expressed as [33],

$$\Delta^{w}{}_{o}\phi_{1/2} = \Delta^{w}{}_{o}\phi^{o}{}_{M^+} - (RT/ZF)\ln K^{(o)}{}_{ML^+} - (RT/ZF)\ln a^{(w)}{}_{M^+} \qquad (5.2.4)$$

where $\Delta^{w}{}_{o}\phi^{o}{}_{M^+}$ is the standard galvani transfer potential of the metal ion, $K^{(o)}{}_{ML^+}$ is the stability constant of the complex in the organic phase and $a^{(w)}{}_{M^+}$ is the activity of the metal ion in the aqueous phase. Equation 5.2.4 can be used for calculating the stability constant of the complexation reaction. This requires the knowledge of the standard galvani potential difference of the Cu^+ ion which is not easily accessible from experimental measurement . Therefore the value of $\Delta^{w}{}_{o}\phi^{o}$ was determined from standard Gibbs energy of transfer which was calculated theoretically using the model of Abraham and Liszi [7,34] considering a "naked" Cu(I) species in the organic phase. For the Cu^+ ion, $\Delta^{w}{}_{o}\phi^{o}$ = 0.57 V and the value of log $K^{(o)}{}_{ML^+}$ was calculated to be 12.2.

The effect of excess ligand concentration on the behaviour of the facilitated ion transfer was also investigated. Figure 5.2.18 shows a voltammogram recorded after several experimental cycles in the presence of 0.1 mM Cu^+ in the aqueous phase and 2 mM biquinoline in the organic phase, respectively. At the beginning of the experimental cycles a very high positive current was observed which decreased gradually with time and reached a limiting value. Development of a pink colour in the organic phase was also apparent with an increase in contact time. As shown in the figure a positive current peak corresponding to the facilitated transfer of Cu^+ is observed, whereas in the reverse scan, no negative peak current is seen. However, at faster sweep rates (> 100 mV s^{-1}), a negative peak current was detected. This indicates that the transfer process can be followed by further complexation reactions to give higher complexes in the organic phase. The voltammetric response observed in Fig. 5.2.18 is

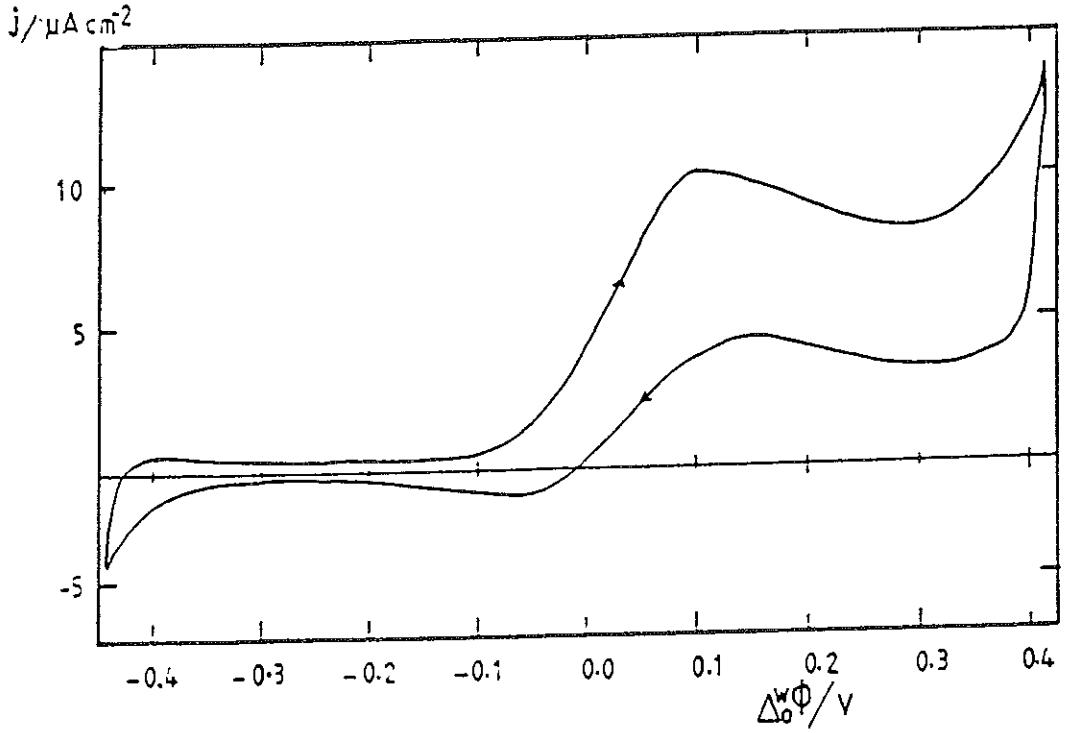

Fig. 5.2.18. Voltammogram of 0.1 mM Cu^{+} transfer facilitated by 2 mM 2,2'-biquinoline in the organic phase. Sweep rate = 10 mV s^{-1}.

characteristic of an CEC mechanism, i.e, the ion transfer is preceded by a preequilibrium and followed by further complexation [35,36]. The proposed reaction sequence is:

$$CuCl_2^-(w) \longrightarrow Cu^+(w) + 2Cl^-(w) \qquad (5.2.5)$$

$$Cu^+(w) + L(o) \rightleftharpoons [CuL]^+(o) \qquad (5.2.6)$$

$$[CuL]^+(o) + L(o) \longrightarrow [CuL_2]^+(o) \qquad (5.2.7)$$

The reaction of Eq. (5.2.7) is irreversible and this explains the changes with sweep rate observed in the reverse scan. However further work is required to elucidate the details of the mechanism.

In summary, the transfer of Cu^+ facilitated by biquinoline strongly depends on the metal ion and ligand concentrations. At low ligand and high metal ion concentrations the transfer shows a reversible behaviour with the formation of $[CuL]^+$ complex. On the other hand in the presence of excess ligand and low metal ion concentrations the transfer becomes irreversible due to the relatively fast formation of $[CuL_2]^+$ complex.

5.3 ELECTRICAL DOUBLE LAYER STUDIES

The structure of the electrical double layer at the water/nitrobenzene and water/1,2-dichloroethane interfaces has been studied by impedance measurements [37-44]. In the present work experiments were first performed for the above systems using LiCl and TBATPB as base electrolytes in order to check the proper functioning of the instrumentation and method of measurements adopted. The results of the impedance measurements (capacitance data) are shown in Table 5.3.1. It can be seen that the values of the capacitance minimums of water/nitrobenzene and water/1,2-dichloroethane are approximately 9.6 and 7.1 $\mu F\ cm^{-2}$,respectively. These values are in very good agreement with the results of same systems reported in the literature as 9.5 and 7.5 $\mu F\ cm^{-2}$ respectively [38,39,44]. The potentials of the capacitance minimums for water/nitrobenzene and water/1,2-dichloroethane are in the range 0.04 to 0.06 V and -0.01 to 0.01 V respectively. These are also within the range of the values reported as 0.030 to 0.060 V [37,40,45] and 0.00 to 0.01 V [39,44] for water/nitrobenzene and water/1,2-dichloroethane interfaces, respectively. As it is mentioned in chapter three, impedance measurements were carried out at the water/o-nitrotoluene and water/o-dichlorobenzene interfaces and the results of the investigations are described as follows.

5.3.1 *The Water/o-Nitrotoluene Interface*

Figure 5.3.1 shows ac voltammograms of the in-phase and quadrature components for the system 10 mM LiCl(w) and 10 mM TBATPB(o-nt). Impedance measurements were carried out within a potential range where charge transfer can be neglected. The in-phase and quadrature components of the ac current were

Table 5.3.1 Capacitance values measured at the water/nitrobenzene and water/1,2-dichloroethane interfaces using 10 mM LiCl in the aqueous phase and 10 mM TBATPB in the organic phase.

$\Delta^{w}_{o}\phi$ / V	C/μF cm^{-2} (w/nb)	C/μF cm^{-2} (w/1,2-dce)
0.170	15.42	
0.160	14.40	
0.150	13.50	
0.140	12.79	
0.130	12.10	
0.120	11.64	10.28
0.110	11.05	9.92
0.100	10.36	9.25
0.090	10.08	9.12
0.080	10.08	8.64
0.070	9.75	8.14
0.060	9.75	8.15
0.050	9.60	8.00
0.040	10.20	7.71
0.030	10.80	7.46
0.020	11.00	7.10
0.010	11.24	7.14
0.000	11.50	7.10
-0.010	11.70	7.02
-0.020	11.93	7.19
-0.030	12.30	7.25

Table 5.3.1 (cont.)

$\Delta^{w}_{o}\phi$ / V	C/μF cm^{-2} (w/nb)	C/μF cm^{-2} (w/1,2-dce)
-0.040	12.52	7.25
-0.050	12.92	7.57
-0.060	13.30	7.95
-0.070	13.72	8.50
-0.080	14.40	8.79
-0.090	15.12	9.73
-0.100	16.23	10.34

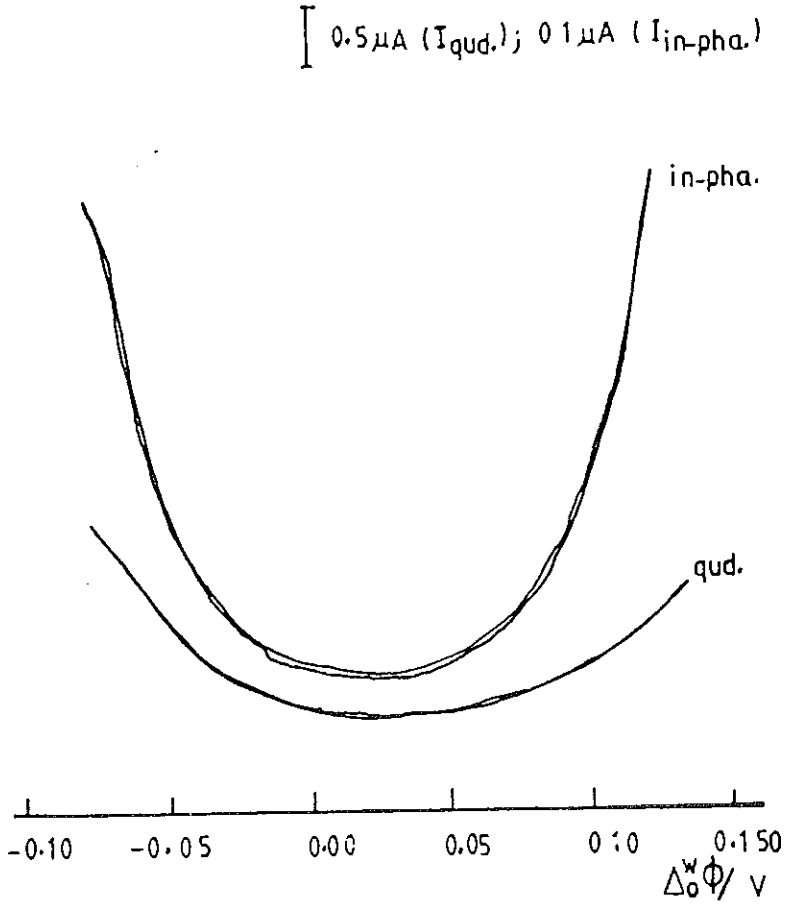

Fig. 5.3.1. Quadrature and in-phase components of ac impedance measurements at the water/o-nitrotoluene interface. Electrolyte concentration: 10 mM LiCl (aq.) and 10 mM TBATPB (o-nt). Sweep rate = 5 mV s^{-1}; f = 20 Hz; ΔE = 5 mV.

recorded as a function of potential at a given frequency. This was repeated for different frequencies. The results were transformed into real Z' and imaginary Z'' parts of the complex impedance Z as described in Chapter 2.

Figure 5.3.2 (a) and (b) show typical impedance plots in the frequency range 20 up to 200 Hz at different potentials for each set of base electrolyte concentration. The ohmic potential drops between the two reference electrodes were completely compensated. The impedance diagrams indicate the absence of a semicircle or semi-ellipse which is characteristic of a slow faradaic or electrochemical adsorption step, respectively [39]. Artifacts caused by phase shifts due to the electronic circuitry or to the impedance of the reference electrodes were not detected within the frequency range investigated [46]. In Fig. 5.3.2 (a) at $\Delta^{w}{}_{0}\phi$ =0.04 V (when the current is mainly a charging current) the plots approach the characteristic vertical line of a series RC network. At $\Delta^{w}{}_{0}\phi$ = -0.05 and -0.07 V the impedance plots approach the classical Warburg behaviour which is characterised by a line of slope one [4,47]. Using the same assumptions as those used by Samec et al. [37], namely (a) the faradaic impedance of the ion transfer can be approximated by a Warburg impedance, and (b) in the polarisation potential region, the Warburg impedance is much greater than the interfacial differential capacity, linear dependence of Z'' on ω or Z_C on ω should be expected.

From the values of Z' and Z'' the capacitive reactance Z_C was calculated as outlined in Chapter 2. Figure 5.3.3 shows the plots of Z_C vs the reciprocal of the frequency $1/\omega$ at three different potentials. In all cases a linear relationship was obtained. From the slopes of the plots the values of the interfacial capacity C were evaluated at various potentials. The results of the analysis for different electrolyte concentrations are presented in Table 5.3.2 together with the values of the surface charge density. The surface charge density data were obtained by integrating the measured double layer capacitance C [37].

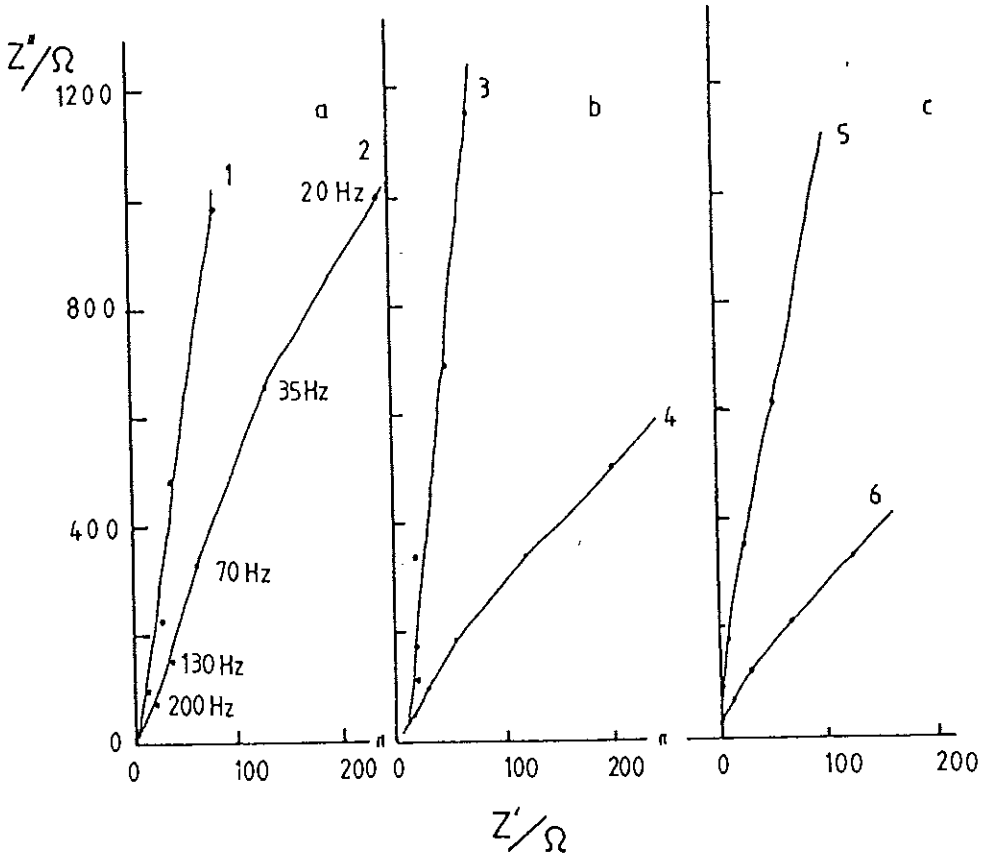

Fig. 5.3.2.(a) Complex plane impedance plots of the water/o-nitrotoluene interface. Electrolyte concentration: LiCl (aq.)/TBATPB(o-nt) 5 mM (a), 10 mM (b) and 50 mM (c); $\Delta^{w}_{o}\phi$ (V): 0.04 (1), -0.04 (2), 0.04 (3), -0.05 (4), 0.04 (5) and 0.07 (6).

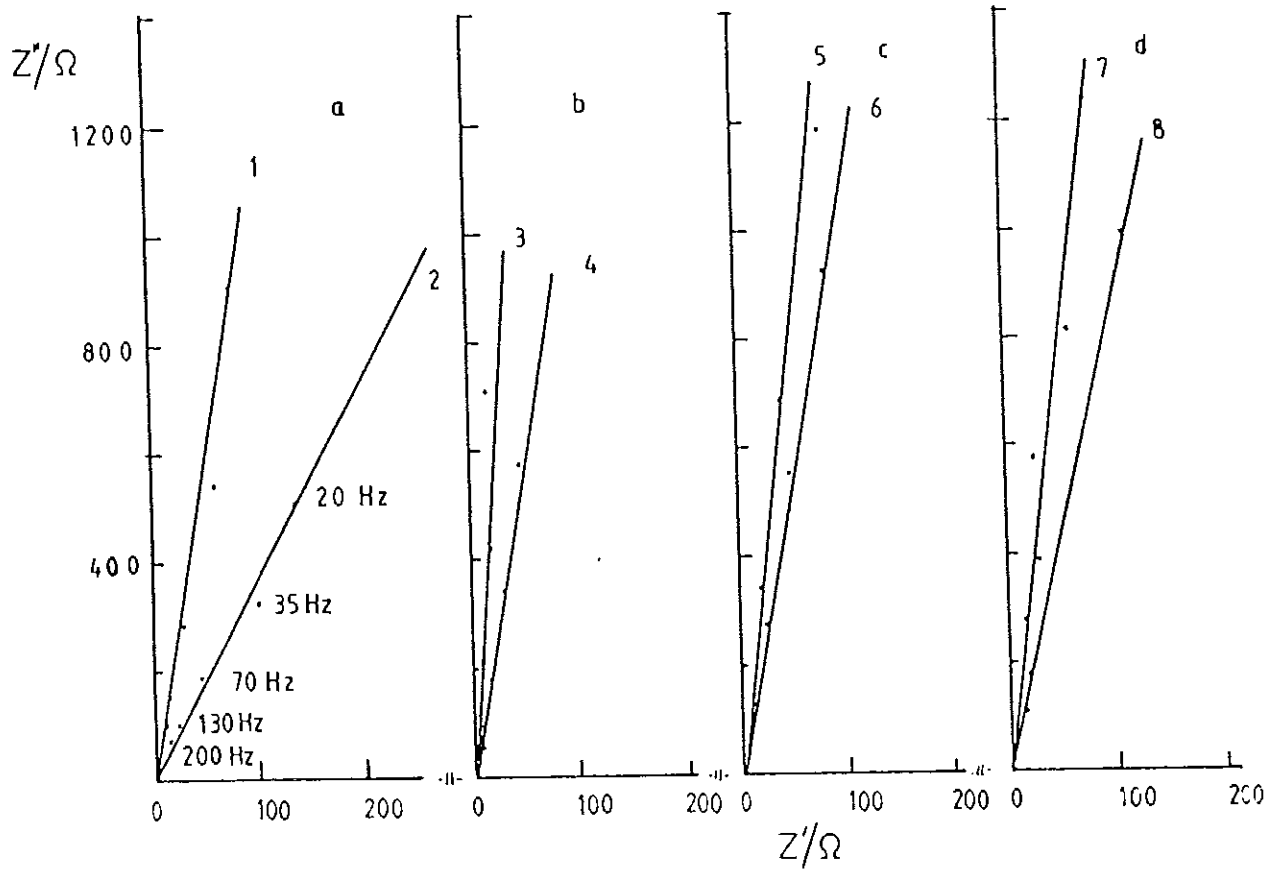

Fig. 5.3.2 (b) Electrolyte concentration: LiCl (aq.)/PNPDCC(o-nt) 50 mM (a), 100 mM (b), 10 mM (c) and 5 mM (d); $\Delta^{w}_{o}\phi$ (V): -0.01 (1), -0.17 (2), -0.02 (3), -0.13 (4), -0.20 (5), -0.08 (6), -0.02 (7), and -0.14 (8).

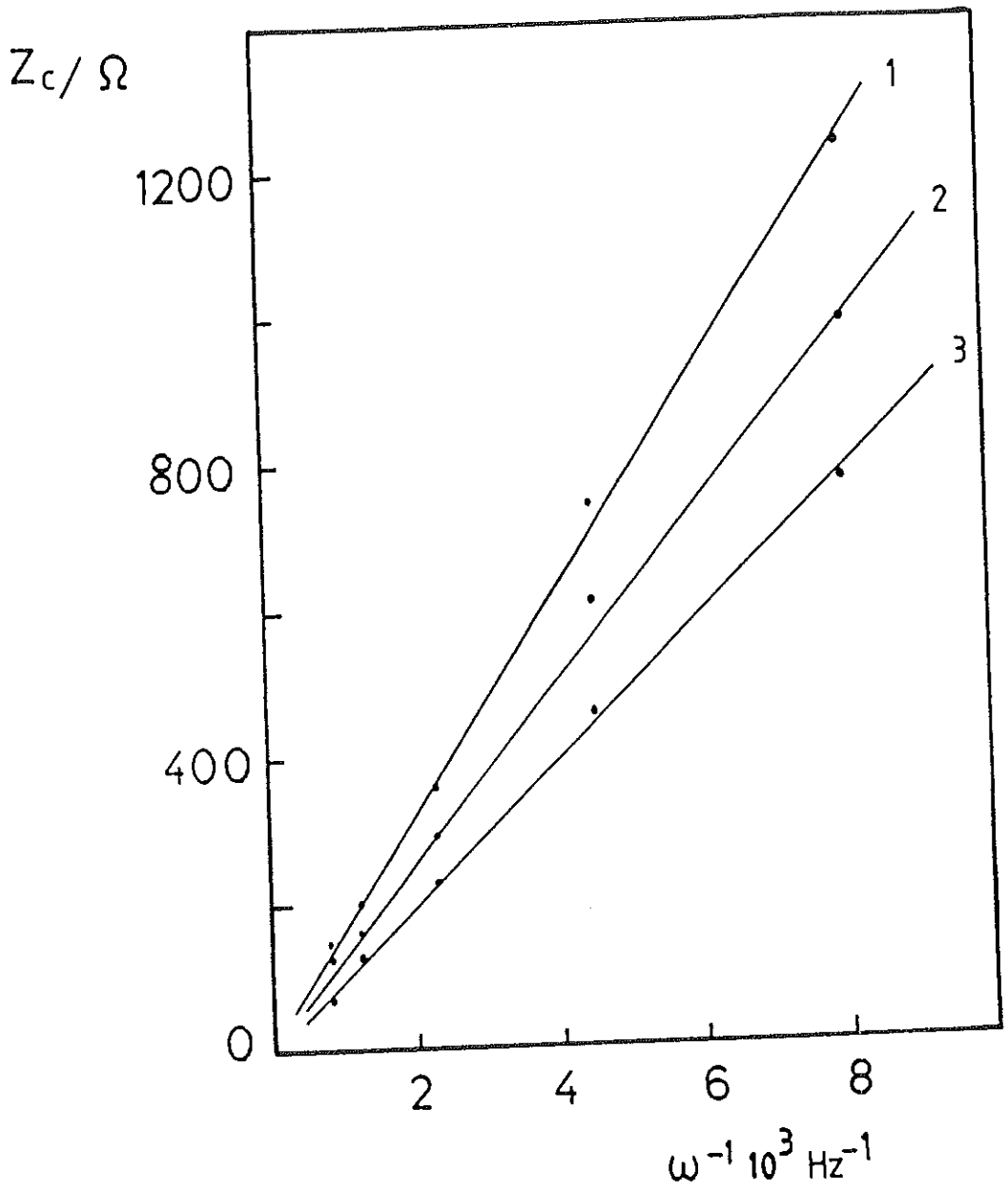

Fig. 5.3.3 Plots of the capacitance impedance Z_C vs $1/\omega$ at $\Delta^w_o\phi$ (V): 0.04 (1),-0.03 (2), and 0.14 (3). Electrolytes: 10 mM LiCl(w)/10 mM TBATPB(o-nt).

Table 5.3.2 Capacitance and charge density data at the water/o-nitrotoluene interface for the systems LiCl(w)/TBATPB(o-nt) and LiCl(w)/PNPDCC(o-nt) of various electrolyte concentrations.

5 mM LiCl (w) / 5 mM TBATPB(o-nt)				
$\Delta^{w}_{o}\phi$ / V	q^{w}/μC cm^{-2}	C/μF cm^{-2} (exp)	C_d/μF cm^{-2} (charge density)	C_d/μF cm^{-2} (theoretical)
0.130	0.60	9.71	8.58	11.98
0.120	0.50	9.08	7.91	10.99
0.110	0.42	8.47	7.41	10.15
0.100	0.33	7.93	6.92	9.40
0.090	0.26	7.36	6.59	8.74
0.080	0.19	6.67	6.33	8.16
0.060	0.06	6.00	6.03	7.21
0.050	0.00	6.00	6.00	6.84
0.030	-0.12	6.17	6.13	6.30
0.020	-0.20	6.72	6.33	6.13
0.000	-0.33	7.40	6.92	6.00
-0.010	-0.40	7.60	7.30	6.03
-0.020	-0.48	8.56	7.78	6.13
-0.040				6.54
-0.060				7.21
-0.080				8.16
-0.100				9.40

Table 5.3.2 (cont.)

10 mM LiCl (w) / 10 mM TBATPB(o-nt)				
$\Delta^{w}_{o}\phi$ / V	q^{w}/μC cm^{-2}	C/μF cm^{-2} (exp)	C_d/μF cm^{-2} (charge density)	C_d/μF cm^{-2} (theoretical)
0.140	1.17	15.46	14.52	18.35
0.130	1.02	14.43	13.37	
0.120	0.88	13.92	12.35	15.54
0.110	0.75	12.62	11.46	14.35
0.100	0.62	12.00	10.63	13.30
0.090	0.51	11.46	10.01	12.36
0.080	0.40	10.83	9.46	11.54
0.070	0.29	10.17	9.02	10.82
0.060	0.19	9.81	8.72	10.20
0.050	0.09	9.45	8.54	9.68
0.040	0.00	9.31	8.48	9.25
0.030	-0.09	9.44	8.54	8.92
0.020	-0.19	9.62	8.72	8.68
0.010	-0.29	9.80	9.02	8.53
0.000	-0.39	10.18	9.42	8.48
-0.010	-0.49	10.35	9.90	8.53
-0.020	-0.60	11.20	10.52	8.68
-0.030	-0.71	11.95	11.20	8.92
-0.040	-0.84	13.00	12.07	9.25
-0.050		14.16		9.68
-0.060				10.20
-0.070				10.82

Table 5.3.2 (cont.)

50 mM LiCl (w) / 50 mM TBATPB (o-nt)

$\Delta^{w}_{o}\phi$ / V	q^{w}/μC cm^{-2}	C/μF cm^{-2} (exp)	C_d/μF cm^{-2} (charge density)	C_d/μF cm^{-2} (theoretical)
0.110		23.60		32.09
0.100		22.47		29.73
0.090	1.41	20.89	23.93	27.64
0.080	1.20	20.20	22.71	25.80
0.070	1.01	18.63	21.71	24.19
0.060	0.82	17.71	20.83	22.81
0.050	0.65	17.31	20.17	21.64
0.040	0.47	16.85	19.61	20.68
0.030	0.31	16.16	19.25	19.93
0.020	0.15	15.50	19.04	19.40
0.010	0.00	15.49	18.97	19.08
0.000	-0.15	15.50	19.04	18.97
-0.010	-0.31	15.99	19.25	19.08
-0.020	-0.47	16.20	19.61	19.40
-0.030	-0.64	17.03	20.14	19.93
-0.040	-0.81	17.50	20.79	20.68
-0.050	-0.99	18.38	21.61	21.64
-0.060	-1.18	19.97	22.60	22.81
-0.070	-1.39	21.63	23.80	24.19

Table 5.3.2 (cont.)

5 mM LiCl (w)/ 5 mM PNPDCC (o-nt)				
$\Delta^{w}_{o}\phi$ / V	q^{w}/μC cm^{-2}	C/μF cm^{-2} (exp)	C_d/μF cm^{-2} (charge density)	C_d/μF cm^{-2} (theoretical)
0.170	0.90	9.08	10.85	
0.160	0.81	8.55	10.16	
0.150	0.73	8.00	9.52	
0.140	0.65	7.68	8.95	12.98
0.130	0.58	7.44	8.41	
0.120	0.50	7.19	7.92	10.99
0.110	0.43	6.57	7.50	10.15
0.100	0.37	6.00	7.13	9.40
0.090	0.31	5.71	6.83	8.74
0.080	0.26	5.38	6.58	8.16
0.070	0.21	5.10	6.38	7.65
0.060	0.16	4.83	6.22	7.21
0.050	0.11	4.57	6.11	6.84
0.040	0.06	4.26	6.04	6.54
0.030	0.02	4.25	6.00	6.30
0.020	0.00	4.25	6.00	6.13
0.010	-0.04	4.26	6.02	6.03
0.000	-0.09	4.43	6.07	6.00
-0.010	-0.13	4.62	6.16	6.03
-0.020	-0.18	4.69	6.29	6.13
-0.030	-0.23	5.00	6.45	6.30
-0.040	-0.28	5.31	6.67	6.54

Table 5.3.2 (cont.)

$\Delta^{w}_{o}\phi$ / V	q^{w}/μC cm^{-2}	C/μF cm^{-2} (exp)	C_d/μF cm^{-2} (charge density)	C_d/μF cm^{-2} (theoretical)
5 mM LiCl (w)/ 5 mM PNPDCC (o-nt)				
-0.050	-0.33	5.62	6.93	6.84
-0.060	-0.39	5.67	7.23	7.21
-0.070	-0.45	5.87	7.57	7.65
-0.080	-0.51	6.16	7.95	8.16
-0.090	-0.57	6.45	8.37	8.74
-0.100	-0.64	6.56	8.82	9.40
-0.110	-0.70	6.60	9.30	10.15
-0.120	-0.77	6.67	9.80	10.99
-0.130	-0.84	7.00	10.33	
10 mM LiCl (w)/ 10 mM PNPDCC (o-nt)				
0.150	1.19	12.31	14.64	
0.140	1.07	11.79	13.67	18.35
0.130	0.95	11.17	12.85	
0.120	0.84	10.58	12.08	15.54
0.110	0.74	9.99	11.38	14.35
0.100	0.64	9.43	10.76	14.00
0.090	0.55	9.07	10.22	13.30
0.080	0.46	8.45	9.76	12.36
0.070	0.38	8.13	9.34	11.54
0.060	0.30	7.84	9.05	10.82
0.050	0.22	7.59	8.80	10.20

Table 5.3.2 (cont.)

10 mM LiCl (w)/ 10 mM PNPDCC (o-nt)				
$\Delta^{w}_{o}\phi$ / V	q^{w}/μC cm^{-2}	C/μF cm^{-2} (exp)	C_d/μF cm^{-2} (charge density)	C_d/μF cm^{-2} (theoretical)
0.040	0.15	7.50	8.62	9.68
0.030	0.07	7.22	8.52	9.25
0.020	0.00	7.23	8.48	8.92
0.010	-0.07	7.16	8.52	8.68
0.000	-0.15	7.51	8.62	8.53
-0.010	-0.22	7.65	8.80	8.48
-0.020	-0.30	7.70	9.05	8.53
-0.030	-0.38	7.72	9.35	8.68
-0.040	-0.45	7.96	9.72	8.92
-0.050	-0.54	8.56	10.15	9.25
-0.060	-0.62	8.83	10.66	9.68
-0.070	-0.71	9.12	11.21	10.20
-0.080	-0.81	9.68	11.84	10.82
-0.090	-0.91	9.96	12.53	11.54
-0.100	-1.00	10.57	13.28	12.36
-0.110	-1.12	10.88	14.09	13.30
-0.120	-1.23	11.14	14.95	14.35

Table 5.3.2 (cont.)

50 mM LiCl (w)/ 50 mM PNPDCC (o-nt)				
$\Delta^{w}_{o}\phi$ / V	q^{w}/μC cm^{-2}	C/μF cm^{-2} (exp)	C_d/μF cm^{-2} (charge density)	C_d/μF cm^{-2} (theoretical)
0.120	1.77	16.37	26.23	34.75
0.110	1.61	15.78	25.16	32.09
0.100	1.45	15.35	24.18	29.73
0.090	1.30	14.70	23.28	27.64
0.080	1.16	14.40	22.46	25.80
0.070	1.01	13.79	21.73	24.19
0.060	0.88	13.51	21.09	22.81
0.050	0.75	13.05	20.53	21.64
0.040	0.62	12.82	20.05	20.68
0.030	0.49	12.58	19.66	19.93
0.020	0.36	12.50	19.36	19.40
0.010	0.24	12.30	19.14	19.08
0.000	0.12	11.85	19.01	18.97
-0.010	0.00	11.80	18.97	19.08
-0.020	-0.12	11.80	19.01	19.40
-0.030	-0.24	11.80	19.13	19.93
-0.040	-0.36	12.30	19.34	20.68
-0.050	-0.48	12.50	19.64	21.64
-0.060	-0.61	12.61	20.02	22.81
-0.070	-0.73	12.86	20.48	24.19
-0.080	-0.86	13.12	21.02	25.80
-0.090	-1.00	13.41	21.02	27.64

Table 5.3.2 (cont.)

$\Delta^{w}_{o}\phi$ / V	q^{w}/μC cm^{-2}	C/μF cm^{-2} (exp)	C_d/μF cm^{-2} (charge density)	C_d/μF cm^{-2} (theoretical)
50 mM LiCl (w)/ 50 mM PNPDCC (o-nt)				
-0.100	-1.13	14.03	22.34	29.73
-0.110	-1.28	14.61	23.13	32.09
-0.120	-1.42	14.77	24.04	34.75
-0.130	-1.57	15.46	24.09	
-0.140	-1.73	15.84	25.98	41.03
-0.150	-1.89	16.02	27.07	
100 mM LiCl (w)/ 100 mM PNPDCC (o-nt)				
0.110	2.48	20.81	36.99	45.39
0.100	2.28	20.30	35.62	42.05
0.090	2.08	19.65	34.36	39.09
0.080	1.89	19.09	33.18	36.49
0.060	1.51	18.12	31.13	32.25
0.050	1.33	17.80	30.34	30.60
0.040	1.16	16.40	29.45	29.25
0.030	0.98	17.16	28.76	28.19
0.020	0.81	16.83	28.17	27.47
0.010	0.65	16.45	27.69	26.98
0.000	0.48	16.38	27.31	26.83
-0.010	0.32	16.33	27.04	26.98
-0.020	0.16	15.92	26.88	27.47
-0.030	0.00	15.86	26.82	28.19

Table 5.3.2 (cont.)

100 mM LiCl (w)/ 100 mM PNPDCC (o-nt)				
$\Delta^{w}_{o}\phi$ / V	q^{w}/μC cm^{-2}	C/μF cm^{-2} (exp)	C_d/μF cm^{-2} (charge density)	C_d/μF cm^{-2} (theoretical)
-0.040	-0.16	15.79	26.88	29.25
-0.050	-0.32	15.85	27.04	30.60
-0.060	-0.48	15.89	27.30	32.25
-0.070	-0.64	16.13	27.66	34.21
-0.080	-0.80	16.43	28.12	36.49
-0.090	-0.96	16.63	28.68	39.09
-0.100	-1.13	16.91	29.34	42.05
-0.110	-1.30	17.12	30.09	45.39
-0.120	-1.48	18.08	30.95	49.14
-0.130	-1.66	18.51	31.91	

$$q^w = - q^o = \int_{\Delta\phi_{pzc}}^{\Delta\phi} C \, d\Delta\phi \qquad (5.3.1)$$

The calculations from Eq. (5.3.1) were carried out by assuming that the values of $\Delta\phi_{pzc}$ correspond to the potentials of the capacitance minimums. The q^w values were then used in the Gouy-Chapman theory to calculate the potentials of the aqueous and the organic sides, respectively. From these results the capacity of the diffuse double layer C_d was evaluated using Eqs.(2.2.21)-(2.2.25) of Chapter 2. For comparison C_d values were also computed from the Gouy-Chapman theory assuming that the inner potential difference $\Delta^w{}_o\phi_i$ = constant = 0 V [37-41].

Figure 5.3.4 shows the plots of the interfacial capacity C as a function of potential at various electrolyte concentrations. In the figure the plots of the diffuse double layer C_d *vs* potential calculated from the Gouy-Chapman theory by assuming $\Delta^w{}_o\phi_i$ = 0 V (dashed lines) and from the surface charge density data (circles) are included. As can be seen from this figure there is good agreement between the experimental and the calculated capacitance values at low electrolyte concentrations (5 and 10 mM). However, at high concentration the experimental capacity is lower than C_d predicted from theory. It is known that the Gouy-Chapman treatment of the diffuse double-layer is adequate at low ionic concentrations but may become progressively more imprecise as the concentration increases to the 0.1-1 M level [48]. The lack of accurate predictions for concentrated electrolyte solutions is accounted for by the fact that the theory neglects the contributions arising from the finite ion size and the image forces [44,48].

Comparison of Fig. 5.3.4 with Fig 5.3.5 illustrates the decrease in the interfacial capacitance when PNPDCC was used as the organic base electrolyte. Comparison of the capacitance minimums for the two organic base electrolytes at

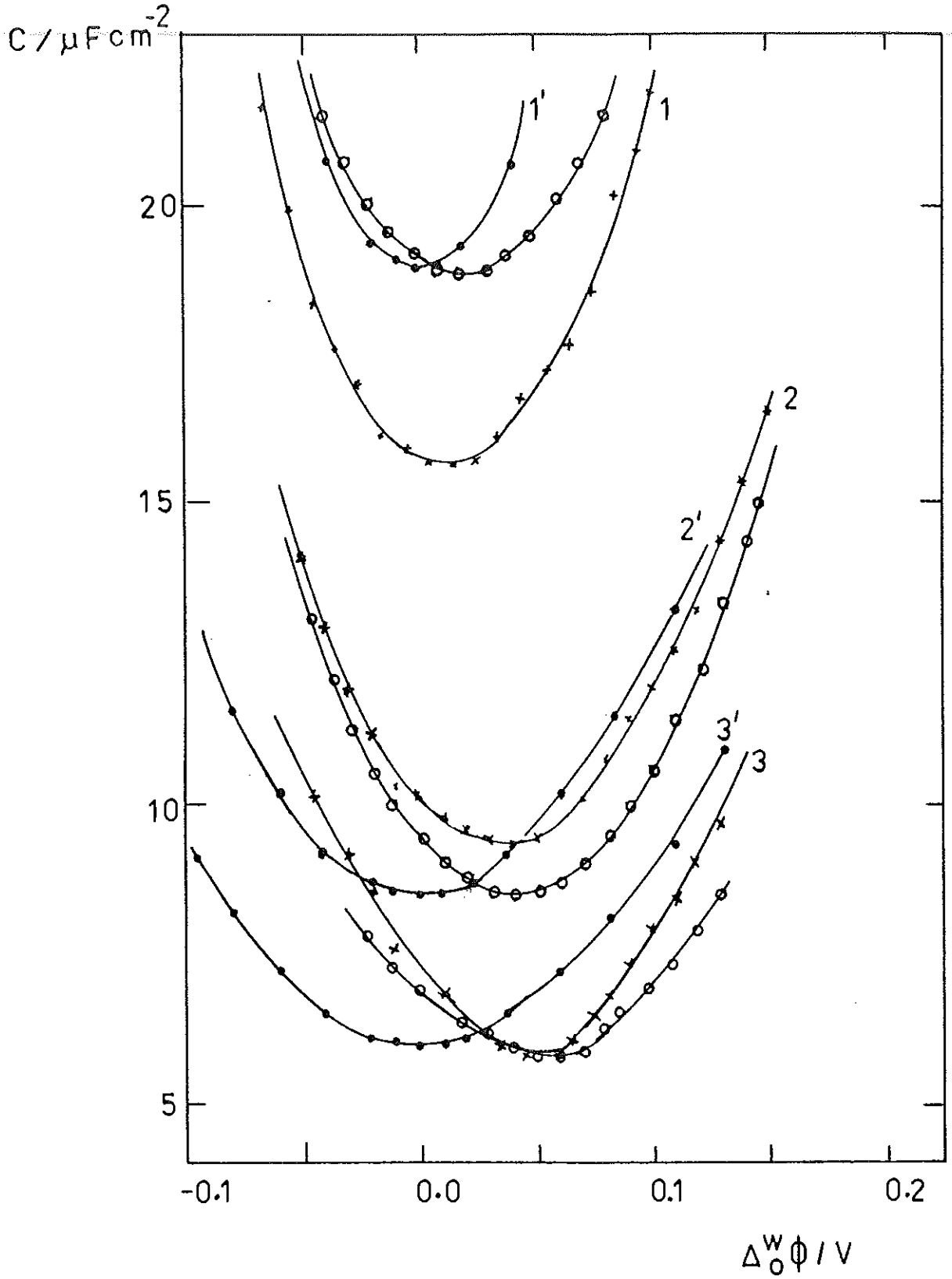

Fig. 5.3.4. Plots of the interfacial capacitance C vs $\Delta^{w}_{o}\phi$ for the system LiCl(w)/TBATPB(o-nt). Electrolyte concentration: 50 mM (1), 10 mM (2),and 5 mM (3). The curves represented by (●●●●) and (oooo) were calculated using the Gouy-Chapman theory, and the surface charge densities.

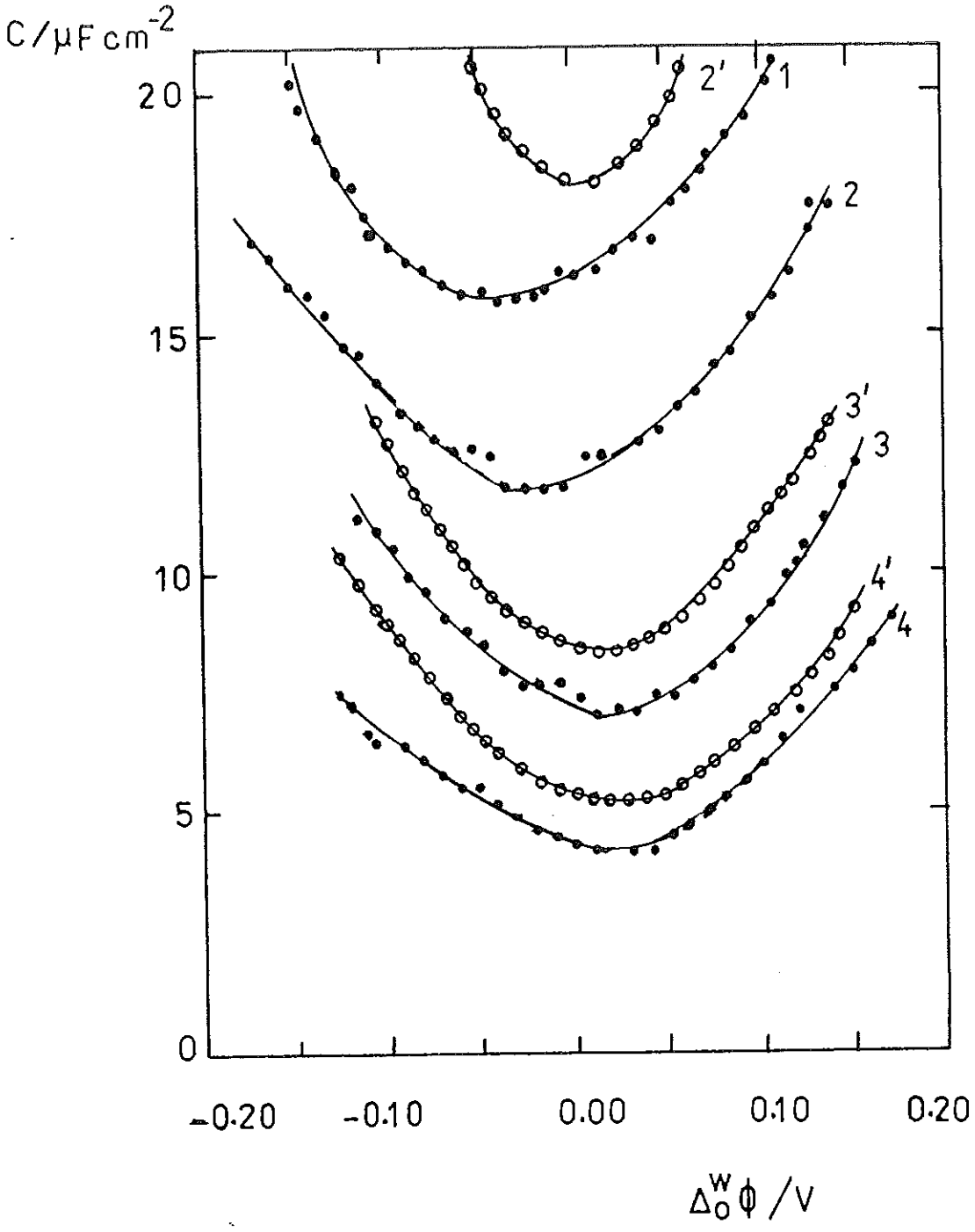

Fig. 5.3.5. Plots of the interfacial capacitance C vs $\Delta^{w}_{o}\phi$ for the system LiCl (w) /PNPDCC (o-nl). Electrolyte concentration: 100 mM (1), 50 mM (2), 10 mM (3), and 5 mM (4). The curves represented by (oooo) were obtained from surface charge density data.

different concentrations shows that their difference in the magnitude of the capacitance increases with increasing electrolyte concentrations (1.75, 2.08,3.69 μF cm^{-2} for 5, 10, 50 mM, respectively). This difference in the capacitance seems to be due to the slight contribution of the faradaic current (due to the minute ion transfer) by TBATPB, and which increases with increasing concentration. As shown by the figures, the application of PNPDCC has enabled the capacitance measurements to be carried out over a wider potential range.

It can be seen from Fig.5.3.4 that the potential of the capacitance minimum for low electrolyte concentrations (C^o=5 and 10 mM) occurs at about $\Delta^w_0\phi$=0.05 V. The minimum shifts towards negative potentials with the increase of electrolyte concentration. The same kind of shift is observed when TBATPB is substituted by PNPDCC. A similar behaviour was reported by Senda et al.[24,45] for the system LiCl in water and TBATPB in nitrobenzene. These authors tested for the existence of specific ionic adsorption, and their results indicated the absence of specific adsorption. In the classical treatment of the double layer at the mercury/electrolyte solution interface, a shift in the potential of zero charge with increase in electrolyte concentration (Esin-Markov effect) is a characteristic feature of the existence of specific ionic adsorption [48,49]. Thus, in order to detect the existence of specific adsorption at the water/o-nitrotoluene interface, the Esin-Markov coefficient (see Eq. 5.3.2) was used as a criterion by plotting the potential as a function of the logarithm of the electrolyte activity at constant charge density.

Assuming no specific adsorption, one obtains for the Esin-Markov coefficient [45,48,49],

$$\left(\partial\Delta^w_0\phi/\partial\ln a^{\pm}_{TBATPB}\right)^{o\text{-}NT}_{q^w,\,\mu_j\neq TBATPB} = -RT/F\left(1+q^w/2\right)/\left[\left(q^w/2\right)^2+\left(A^{o\text{-}NT}\right)2\right]^{1/2} \qquad (5.3.2)$$

where $A^{o\text{-}NT} = (2RT\epsilon^{o\text{-}NT}C_{TBA^+})$

Accordingly, the coefficient of the above equation should reduce to -2RT/F, -RT/F, and 0 when $q^w >> 0$, $q^w = 0$, and $q^w << 0$, respectively. The Esin-Markov plots at several constant q^w values for TBATPB and PNPDCC in o-nitrotoluene are shown in Figures 5.3.6 and 5.3.7, respectively. It can be noted from these figures that the slopes of $\Delta^w_o\phi$ vs $\ln a^{\pm}$ are closer to zero with increasing negative charges (for TBATPB slope=-0.006,-0.001 V for q^w=-0.3 , -0.5 $\mu C\,cm^{-2}$ respectively, and for PNPDCC slope=-0.003,-0.001 V for q^w=-0.5 , -1.0 $\mu C\,cm^{-2}$ respectively).This is in very good agreement with the above equation. It can also be seen from Fig. 5.3.7 that the slopes for positive charges increase negatively and approach the limiting value -0.050 V (slope=0.046 V for q^w=0.9 $\mu C\,cm^{-2}$) which is consistent with the prediction of Eq. (5.3.2). A similar increase is also apparent in Fig. 5.3.6, however, the experimental values of q^w for TBATPB were not large enough to reach the limiting value. At the potential of zero charge, Fig. 5.3.6 and 5.3.7 have slopes of -0.017 and -0.016 V, respectively. These values are very close to the expected theoretical value (RT/F=-0.025 V).

The above results indicate the apparent absence of specific adsorption for the aqueous salt LiCl and the organic salt TBATPB or PNPDCC in the concentration range and the potential range studied. Thus, the observed shift in the potential of the capacitance minimum with concentration was not due to specific adsorption.

Figures 5.3.8 and 5.3.9 show the plot of the inverse capacitance C^{-1} of the interface as a function of the inverse capacitance C_d^{-1} of the diffuse double layer at different constant charge densities (q^w). The values of C and C_d (where C_d calculated from the surface charge density data) were taken from Table 5.3.2. The solid line in each figure is the plot at $q^w = 0$. The plots seem to satisfy the equation,

$$C^{-1} = C_d^{-1} + C_i^{-1} \qquad (5.3.3)$$

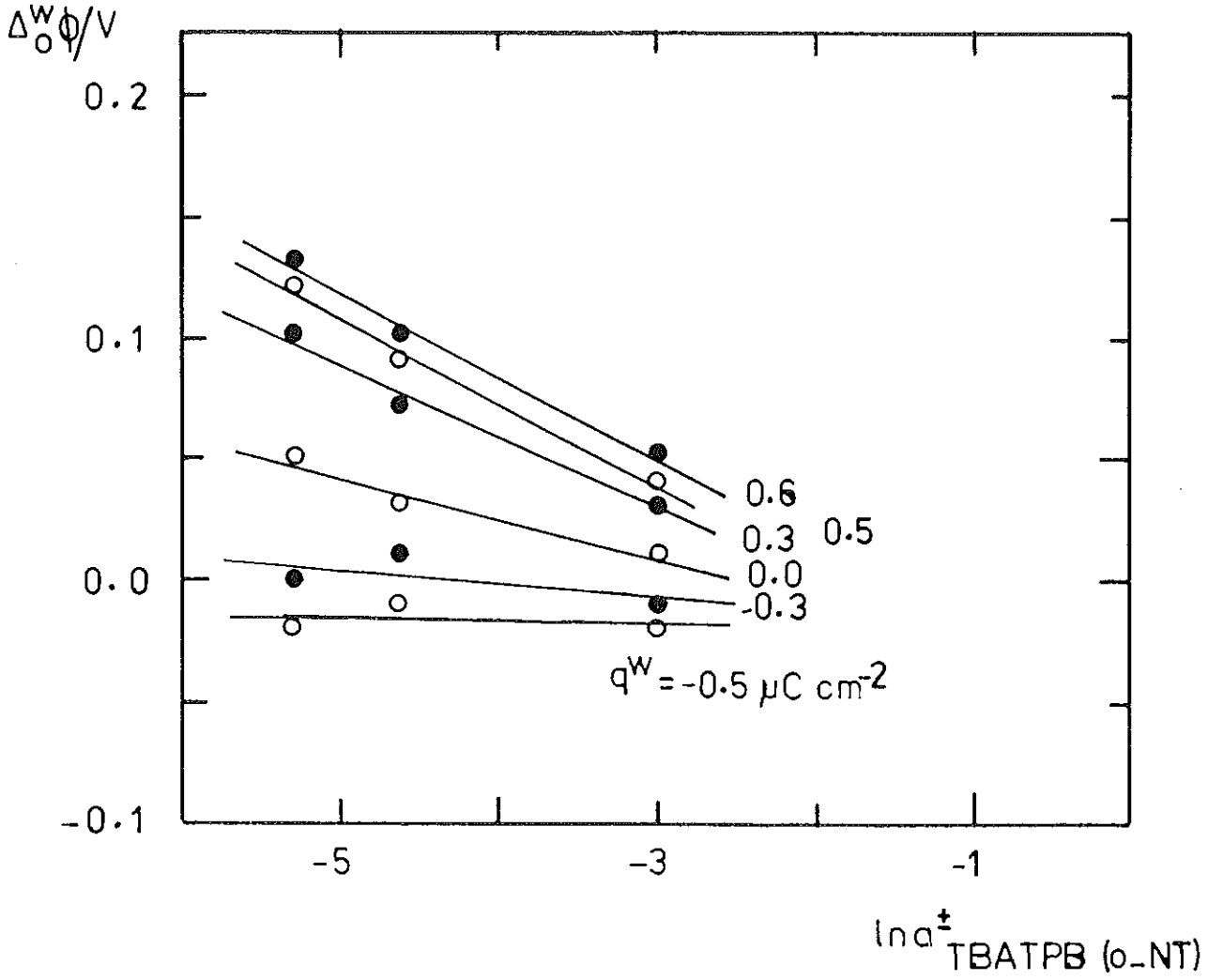

Fig. 5.3.6. Esin-Markov plots for the solutions of TBATPB in o-nitrotoluene in contact with aqueous solution of LiCl.

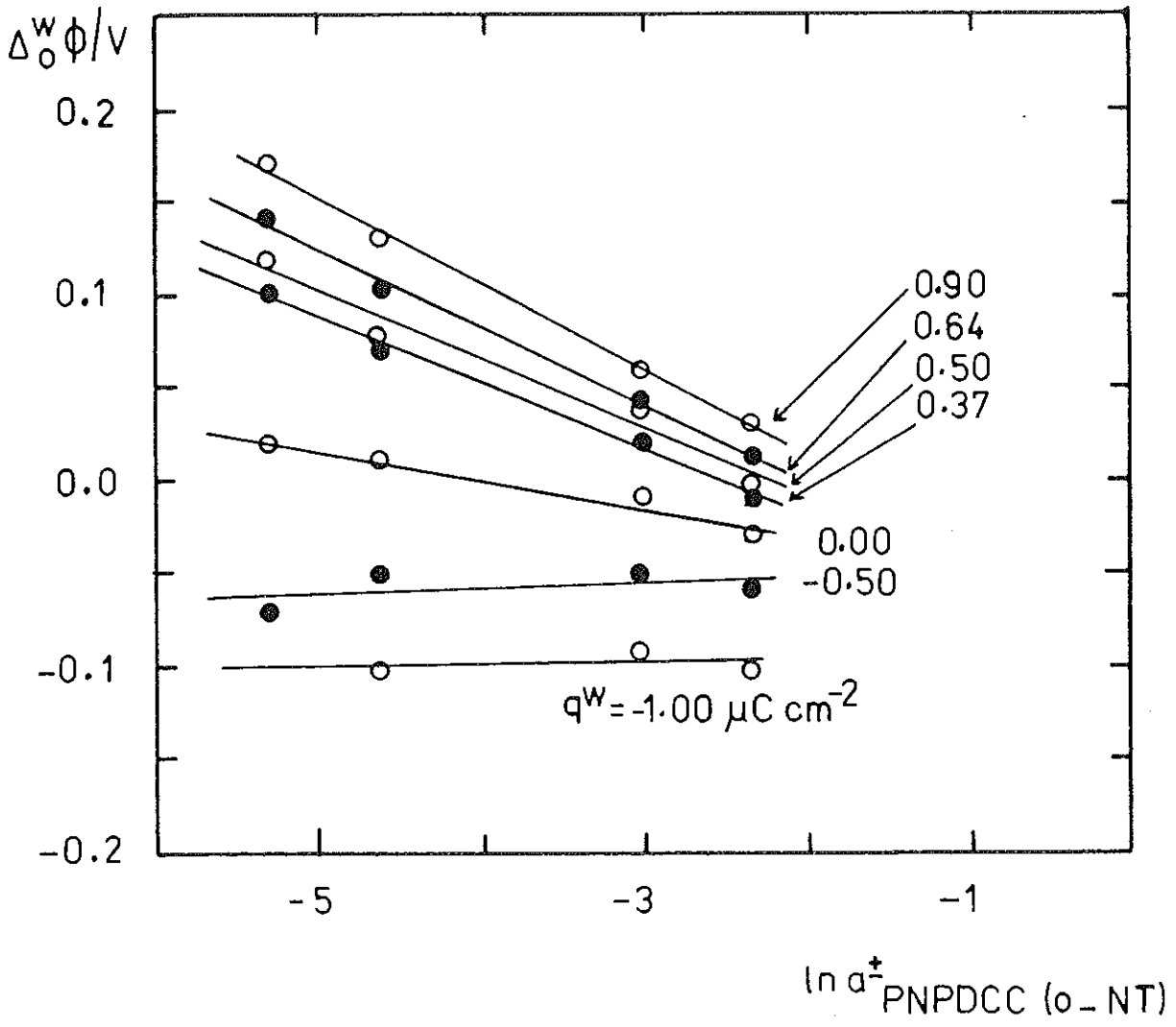

Fig. 5.3.7. Esin-Markov plots for the solutions of PNPDCC in o-nitrotoluene in contact with aqueous solution of LiCl.

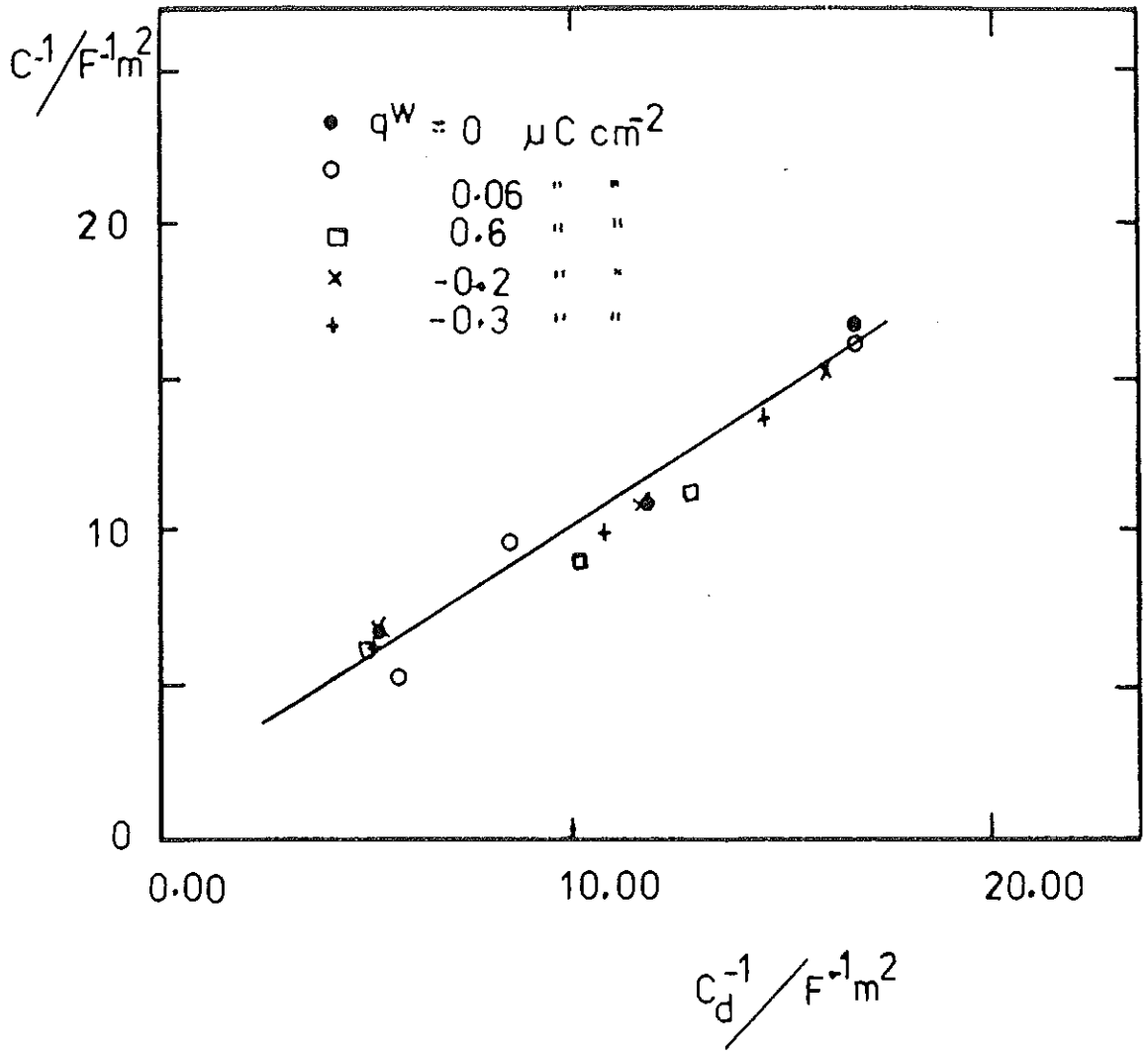

Fig. 5.3.8. Inverse capacitance C^{-1} vs C_d^{-1} for the system LiCl(w)/TBATPB at different electrolyte concentrations (C^0 = 5,10 and 50 mM) and at constant charge densities, the line is at $q^w = 0$ μC cm^{-2}.

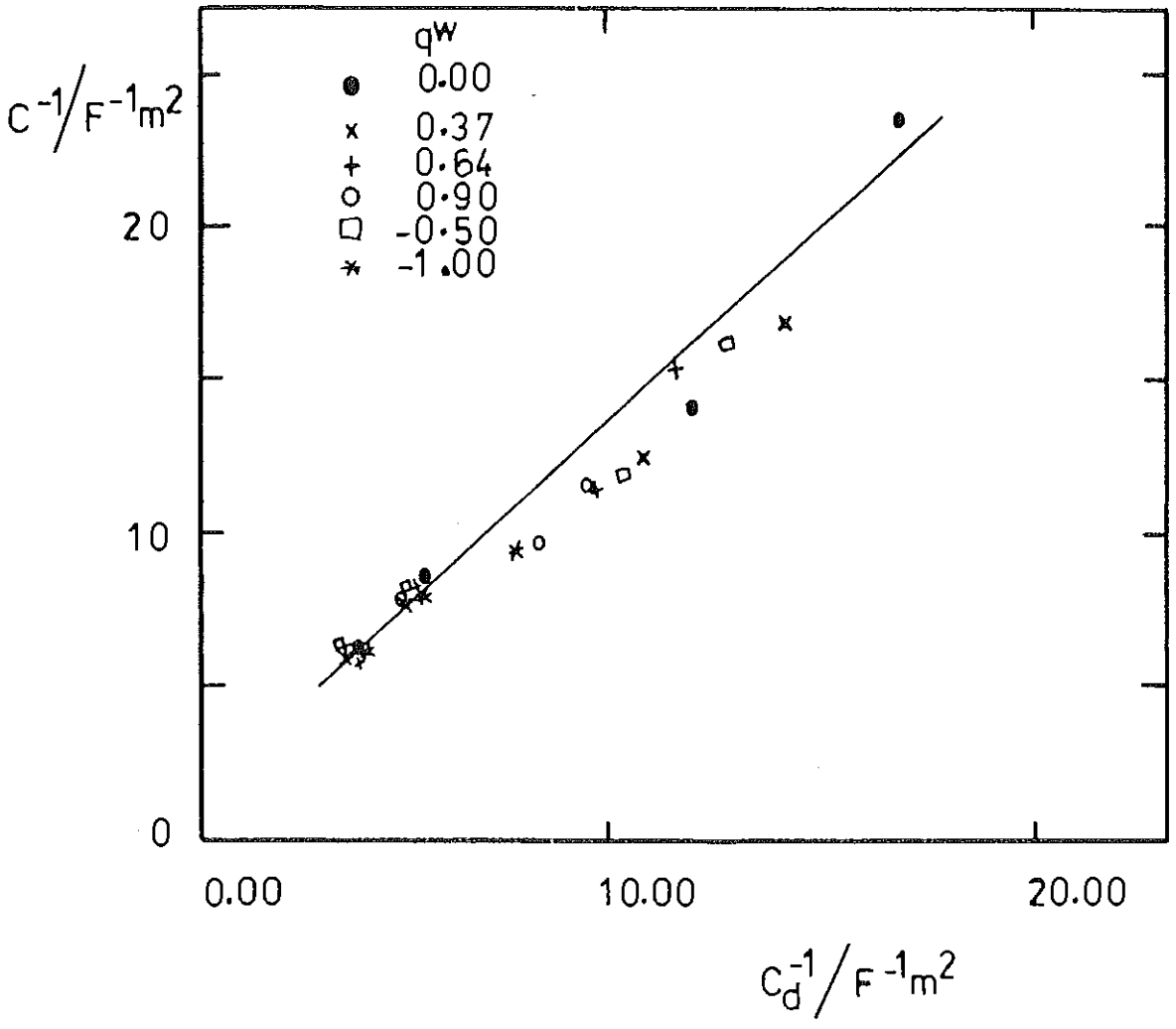

Fig. 5.3.9. Inverse capacitance C^{-1} vs C_d^{-1} for the system LiCl(w)/PNPDCC at different electrolyte concentrations (C^0 = 5, 10, 50 and 100 mM) and at constant charge densities, the line is at q^W = 0 μC cm^{-2}.

The plot of C^{-1} vs C_d^{-1} at constant q is used as an alternative criterion for checking the existence of specific adsorption in the classical treatment of the double layer [48]. At $q^w = 0$ the values of C_i^{-1} as determined from the intercepts are 1.35 and 1.32 F^{-1} m^2 for LiCl(w)/TBATPB(o-NT) and LiCl(w)/PNPDCC(o-NT), respectively. These correspond to C_i values of 74 and 76 μF cm^{-2}, respectively. The similarity in the C_i values indicate that the structure of the inner layer of the interface remains unaffected when TBATPB is replaced by PNPDCC. Furthermore, these values are comparable with the one obtained for the water/nitrobenzene, C_i = 80 μF cm^{-2} as estimated from the differential capacity of the interface using LiCl and TBATPB as base electrolytes [43]. These values are much higher than the inner layer capacitance at the interface between mercury and aqueous solutions [48].

Capacitance vs potential curves for the systems containing LiCl, LiF and Li_2SO_4 in water, TBATPB and PNPDCC in the organic phase are shown in Figures 5.3.10 and 5.3.11, respectively. The capacitance values for these systems are also tabulated in Tables 5.3.3 and 5.3.4. Comparison of the capacity curves in Fig.5.3.10 illustrates that the capacitance minimums have comparable magnitudes. This implies that there is no significant effect of the inorganic anions on the value of the capacitance when TBATPB is employed in the organic side. A similar comparison of the curves in Fig. 5.3.11 shows that the value of the capacitance minimum for SO_4^{-2} is lower than those of Cl^- and F^- by about 1.2 μF cm^{-2}. It is also apparent from both figures that the potential of the capacitance minimums for SO_4^{-2} corresponds to $\Delta^w{}_o\phi$ = 0 V.

It is well known that the streaming method is one of the simplest and fastest experimental methods for the determination of the potentials of zero charge of ideally polarisable mercury electrodes [50]. The method has been applied to liquid/liquid interfaces by assuming that the potential of a streaming jet electrode corresponds to the potential of zero charge.[51,52]. In this work, in order to compare the potential of the capacitance minimum $\Delta^w{}_o\phi_{(cap.min)}$

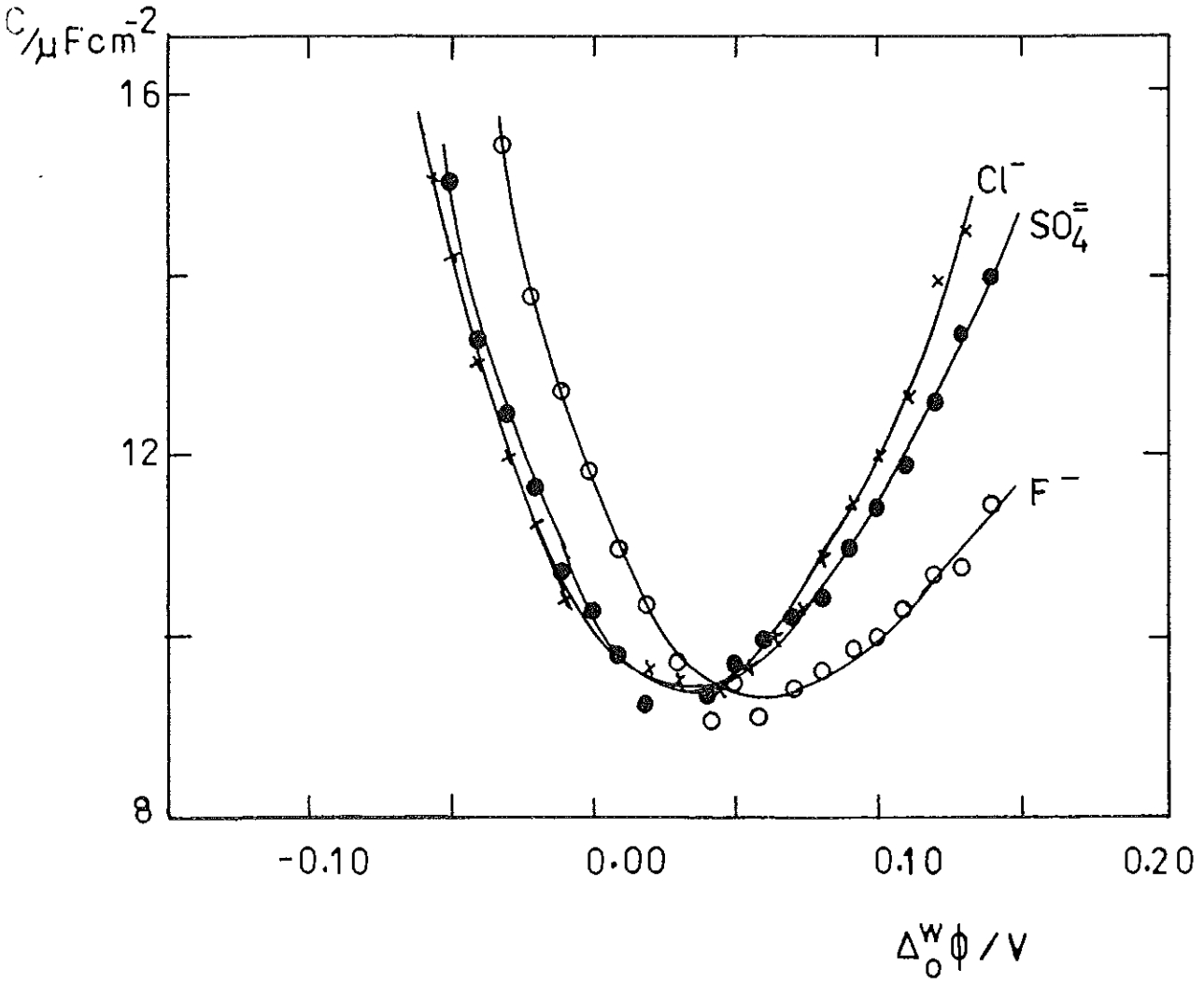

Fig. 5.3.10. Plots of the interfacial capacitance C vs $\Delta^{w}_{o}\phi$ for the water/o-nitrotoluene interface containing 10 mM LiCl, LiF and Li_2SO_4 in the aqueous phase and 10 mM TBATPB in the organic phase.

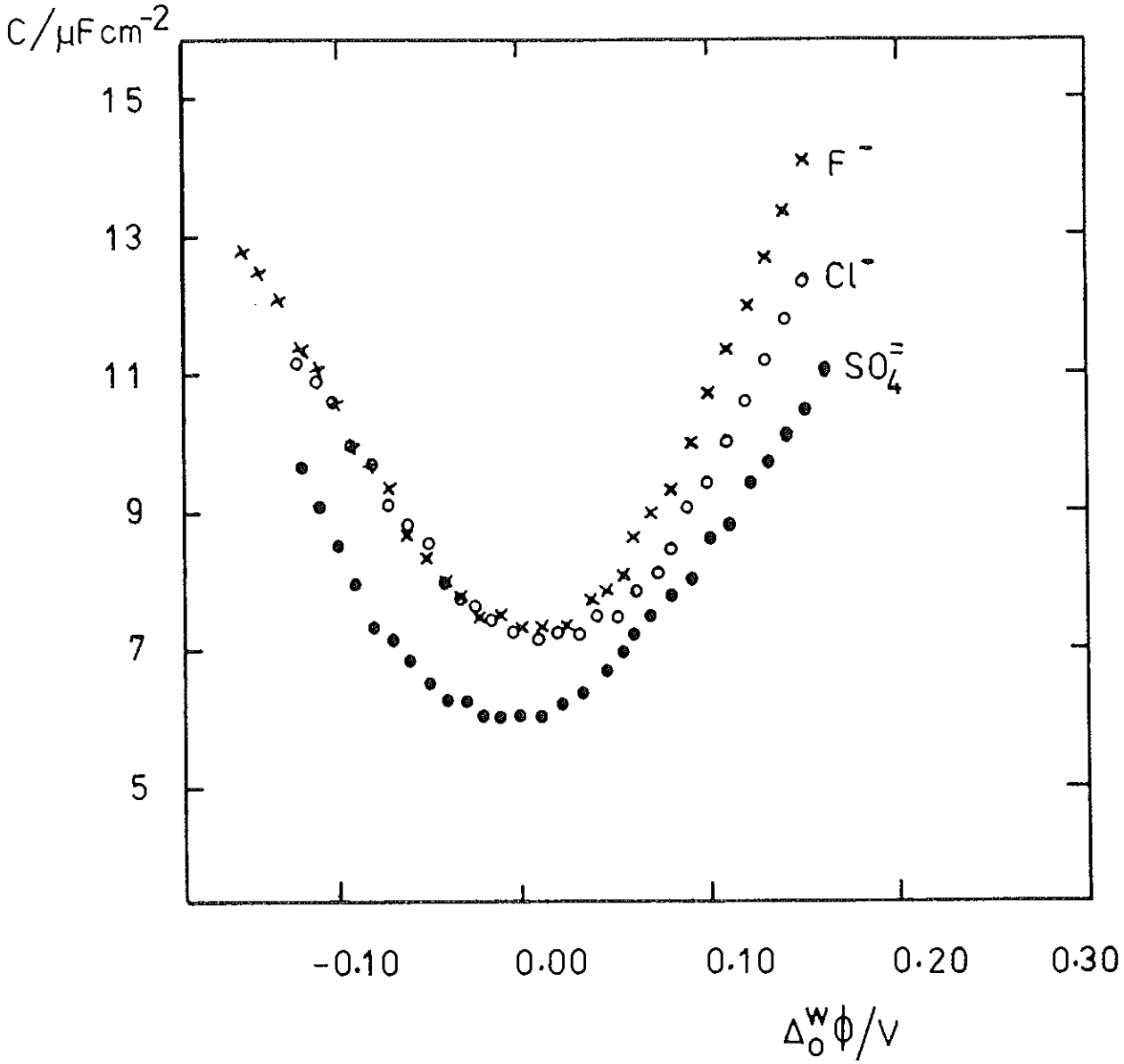

Fig. 5.3.11. Plots of the interfacial capacitance C vs $\Delta^{w}_{o}\phi$ for the water/o-nitrotoluene interface containing 10 mM LiCl, LiF and Li_2SO_4 in the aqueous phase and 10 mM PNPDCC in the organic phase.

Table 5.3.3 Capacitance values obtained at the water/o-nitrotoluene interface containing 10 mM different base electrolytes in the aqueous phase and 10 mM TBATPB in the organic phase.

$\Delta^{w}_{o}\phi$ / V	C/μF cm^{-2} (LiCl)	C/μF cm^{-2} (LiF)	C/μF cm^{-2} (Li_2SO_4)
0.140	15.46	11.38	13.90
0.130	14.43	10.66	13.30
0.120	13.92	10.58	12.55
0.110	12.62	10.21	11.85
0.100	12.00	9.85	11.36
0.090	11.46	9.72	10.92
0.080	10.83	9.51	10.35
0.070	10.17	9.33	10.17
0.060	9.81	9.02	9.92
0.050	9.45	9.40	9.60
0.040	9.31	9.01	9.30
0.030	9.44	9.63	8.60
0.020	9.62	10.26	9.18
0.010	9.80	10.89	9.71
0.000	10.18	11.70	10.22
-0.010	10.35	12.61	10.62
-0.020	11.20	13.72	11.62
-0.030	11.95	15.31	12.41
-0.040	13.00		13.23
-0.050	14.16		14.99

Table 5.3.4 Capacitance values obtained at the water/o-nitrotoluene interface containing 10 mM different base electrolytes in the aqueous phase and 10 mM PNPDCC in the organic phase.

$\Delta^{w_0}\phi$ / V	C/μF cm^{-2} (LiCl)	C/μF cm^{-2} (LiF)	C/μF cm^{-2} (Li_2SO_4)
0.150	12.31	14.00	10.47
0.140	11.79	13.28	10.09
0.130	11.17	12.60	9.72
0.120	10.58	11.90	9.42
0.110	10.00	11.28	8.77
0.100	9.43	10.60	8.63
0.090	9.07	9.91	8.02
0.080	8.45	9.25	7.78
0.070	8.13	8.90	7.47
0.060	7.84	8.58	7.21
0.050	7.49	7.97	6.98
0.040	7.50	7.90	6.83
0.030	7.22	7.70	6.35
0.020	7.23	7.24	6.22
0.010	7.16	7.24	6.03
0.000	7.51	7.24	6.01
-0.010	7.79	7.41	6.01
-0.020	7.75	7.39	6.01
-0.030	7.72	7.71	6.26
-0.040	7.96	7.91	6.26
-0.050	8.56	8.26	6.52
-0.060	8.83	8.57	6.81
-0.070	9.12	9.27	7.10

Table 5.3.4 (cont.)

$\Delta^{w}{}_{o}\phi$ / V	C/μF cm^{-2} (LiCl)	C/μF cm^{-2} (LiF)	C/μF cm^{-2} (Li_2SO_4)
-0.080	9.68	9.58	7.33
-0.090	9.96	9.89	7.90
-0.100	10.57	10.50	8.48
-0.110	10.88	11.00	9.06
-0.120	11.14	11.30	9.62
-0.130		12.00	10.88
-0.140		12.40	11.14
-0.150		12.70	

obtained for the water/o-nitrotoluene interface with the potential of the streaming electrode $\Delta^{w}_{o}\phi_{(str.)}$ also known as the potential of the streaming maximum [52] the streaming method was applied using the cell arrangement described in Chapter 4. The experimentally measured potential value for 10 mM LiCl(w)/10 mM TBATPB(o-nt), $E_{(str.)}$, was found to be equal to 0.175 V. Using the standard Galvani potential value of TBA^+ in this system ($\Delta^{w}_{o}\phi^{0}_{TBA^+}$ =-0.191 V) and Eq. 5.3.4 [52], the Galvani potential difference of the streaming electrode, $\Delta^{w}_{o}\phi_{(str.)}$, was found to be -0.016 V.

$$E_{(str.)} = \Delta^{w}_{o}\phi_{(str.)} - \Delta^{w}_{o}\phi^{0}_{(TBA^+)} \qquad (5.3.4.)$$

In the calculation $\Delta^{w}_{o}\phi^{0}_{TBA^+}$ was obtained from the formal Galvani potential difference ($\Delta^{w}_{o}\phi^{\circ\prime}_{TBA^+}$ =-0.197 V) and the activity coefficient of TBA^+ in o-nitrotoluene($\gamma^{o\text{-}nt}$ =0.79). It can be seen that there is a difference of 55 mV between $\Delta^{w}_{o}\phi_{(str.)}$ and $\Delta^{w}_{o}\phi_{(cap.min)}$ (≈40 mV). In an earlier work deviations between these two quantities were also indicated for several immiscible systems such as the water/1,2-dichloroethane, water/nitrobenzene, water/nitroethane and water/organic mixtures [52]. The observed variations were explained in terms of the experimental conditions of the methods employed. The results obtained by the two methods would be equal only under conditions close to ideal polarisability which could not be achieved experimentally for the system LiCl(w)/TBATPB(o).

In summary no specific ionic adsorption was observed for the studied electrolytes and in many respects the behaviour of the water/o-nitrotoluene interface is similar to that of the water/nitrobenzene.

5.3.2 The Water/o-Dichlorobenzene Interface.

Figure 5.3.12 depicts the ac voltammograms of the in-phase and quadrature components obtained at the water/o-dichlorobenzene interface containing 5 mM LiCl in water and 5 mM PNPDCC in the organic phase. Impedance measurements were carried out in the potential regions where the current is mainly used for charging of the double layer.

Figure 5.3.13 compares the complex plane impedance plots of the system at three concentrations and different potentials. All the impedance measurements were taken in the frequency range between 20 and 200 Hz. The Z'' vs Z' plots for the system containing 5 mM electrolytes at different potentials display predominantly a Warburg like behaviour.

Figure 5.3.14 shows the linear dependence of Z_c on $1/\omega$ from which the values of the capacitance of the interface were evaluated. Table 5.3.5 lists the results of the capacitance measurements at various potentials.

In Fig. 5.3.15 capacitance vs potential curves are shown for three electrolyte concentrations. Unlike the behaviour of the preceding systems the capacitance plots of this system occur in the negative potential regions. Shift in the potential of the capacitance minimums towards more negative potentials is observed with decreasing electrolyte concentration. As can be seen the potential difference between two consecutive capacitance minimums is very large ($\approx$ 0.15 V). In the above figure the magnitudes of the capacitance minimums for 5, 10 and 50 mM concentrations are 3.5, 6 and 10.1 $\mu F\ cm^{-2}$ respectively. A comparison of these data with the results obtained at the water/o-nitrotoluene interface of the same electrolyte composition demonstrates that the above values are lower than the values of the latter system by about 1.6 $\mu F\ cm^{-2}$.

The capacitance of the diffuse double layer was calculated from the Gouy-Chapman theory taking into account the extensive association of PNPDCC in o-dichlorobenzene. As shown by Eqs (2.2.24) and (2.2.25) of Chapter 2, the value

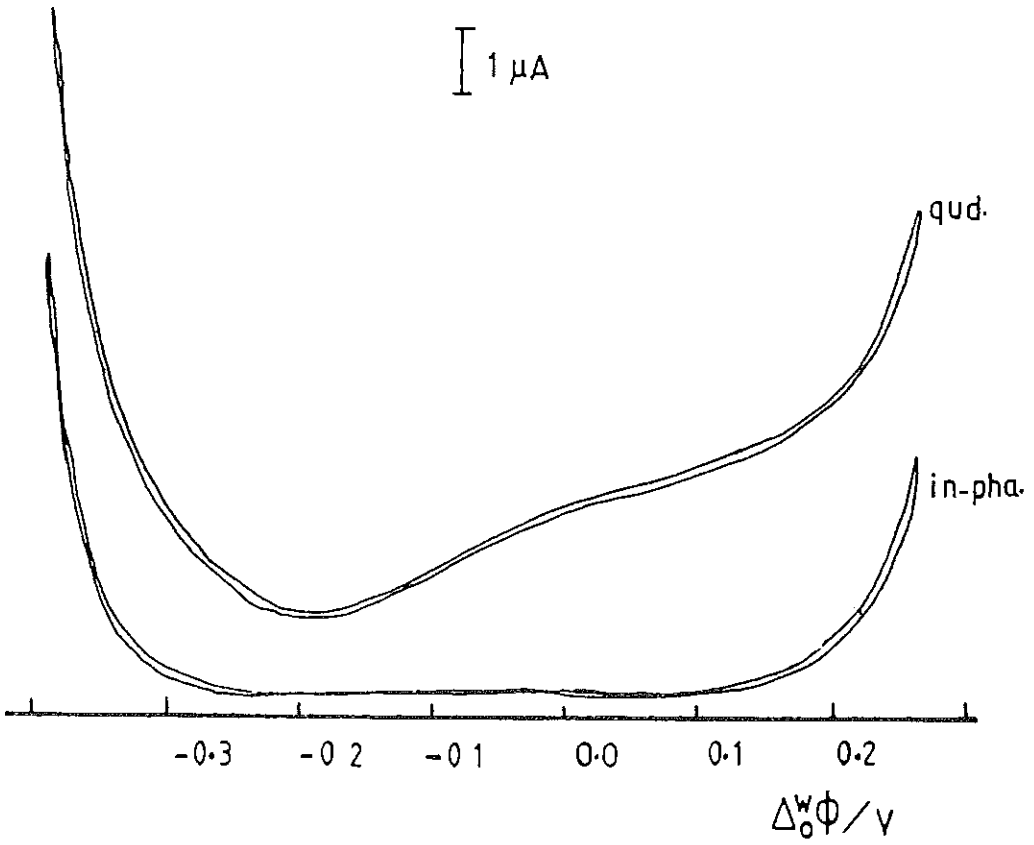

Fig. 5.3.12. Quadrature and in-phase components of ac impedance measurements at the water/o-dichlorobenzene interface. Electrolyte concentration: 5 mM LiCl (aq.) and 5 mM PNPDCC (o-dcb). Sweep rate = 5 mV s^{-1}; f = 35 Hz; ΔE = 5 mV.

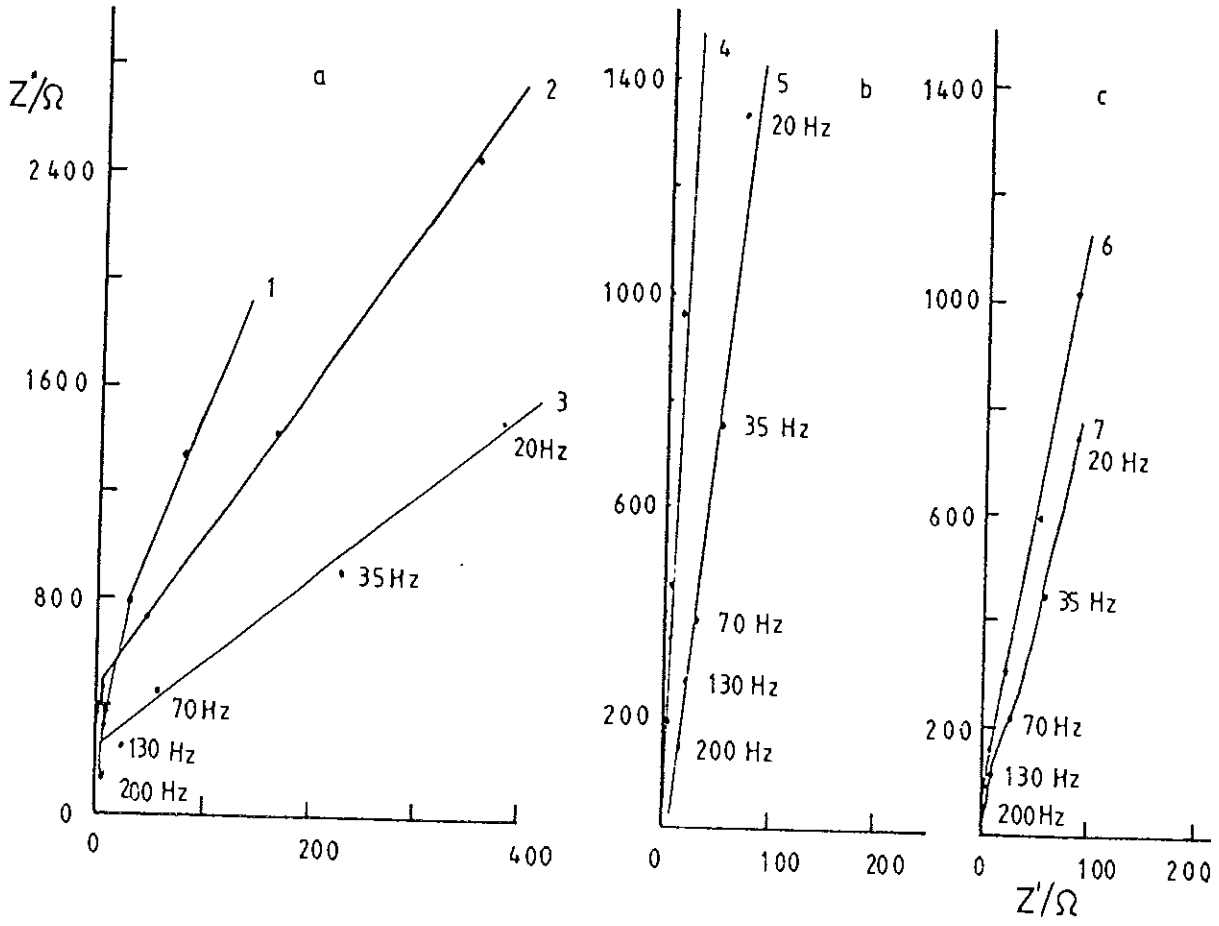

Fig 5.3.13. Complex plane impedance plots of the water/o-dichlorobenzene interface. Electrolyte concentration: LiCl (aq.)/PNPDCC(o-dcb) 5 mM (a), 10 mM (b) and 50 mM (c); $\Delta^{w}_{o}\phi$ (V): -0.13 (1), -0.29 (2), -0.34 (3), -0.20 (4), -0.28 (5), -0.10 (6).and -0.24 (7).

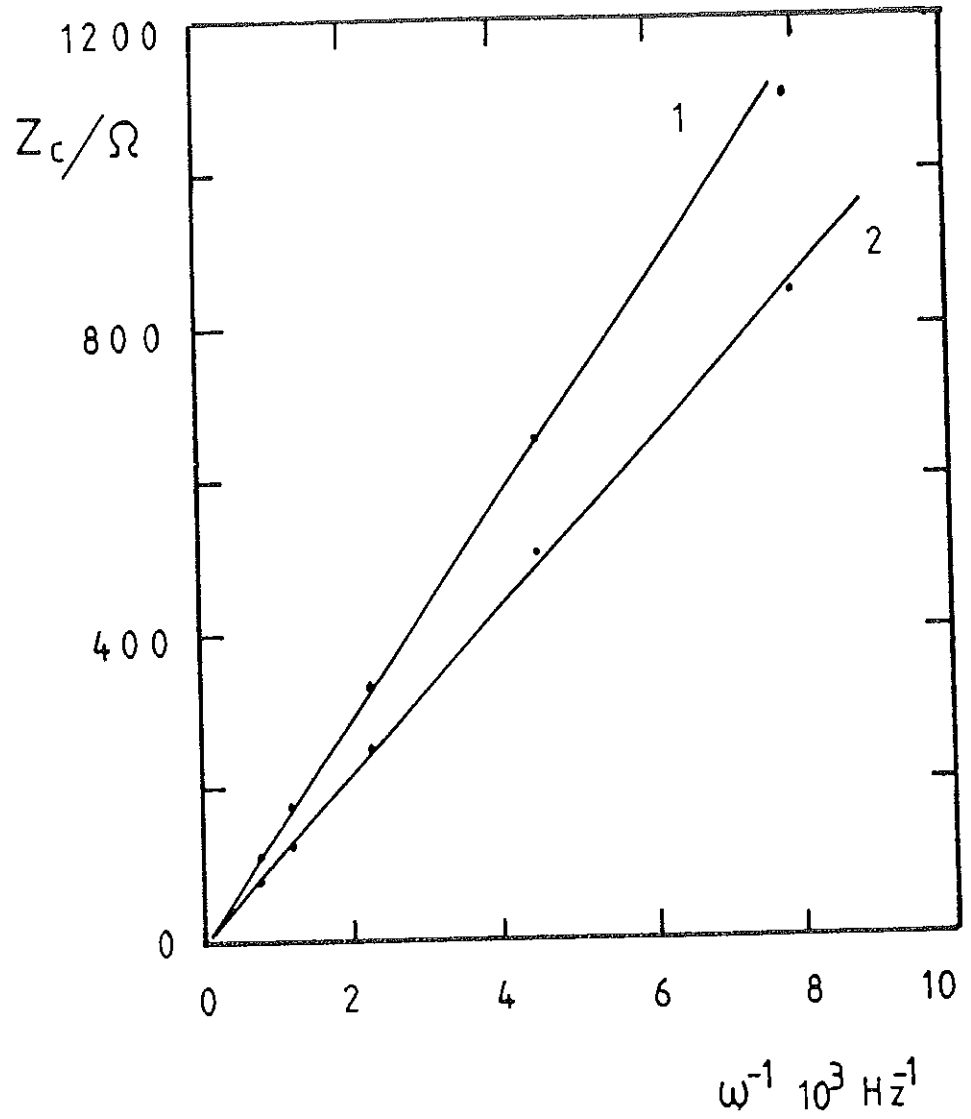

Fig. 5.3.14. Plots of the capacitance impedance Z_C vs $1/\omega$ at $\Delta^w_o\phi$ (V): -0.10 (1), and -0.24 (2). Electrolytes: 50 mM LiCl(w)/50 mM PNPDCC(o-dcb).

Table 5.3.5 Experimental capacitance data obtained at the water/o-dichlorobenzene interface for different concentrations of LiCl/PNPDCC.

$\Delta^{w}_{o}\phi$ / V	C/μF cm^{-2} (5 mM)	C/μF cm^{-2} (10 mM)	C/μF cm^{-2} (50 mM)
0.090			20.93
0.080			19.87
0.070			18.65
0.060			18.14
0.050			16.98
0.040			15.62
0.030			15.13
0.020			14.52
0.010			13.84
0.000			13.34
-0.010		14.32	12.58
-0.020		13.87	11.85
-0.030		13.44	11.83
-0.040		11.92	11.10
-0.050		11.28	10.38
-0.060		10.59	10.40
-0.070		9.94	10.40
-0.080	14.32	8.74	10.21
-0.090	8.05	8.45	10.25
-0.100	7.47	7.70	10.24
-0.110	7.16	7.35	10.08
-0.120	6.85	7.02	10.76

Table 5.3.5 (cont.)

-0.130	6.15	6.63	10.67
-0.140	5.81	6.24	10.95
-0.150	5.53	6.30	11.29
-0.160	4.78	6.27	11.53
-0.170	4.45	6.54	11.77
-0.180	4.12	6.57	12.98
-0.190	4.21	6.96	12.87
-0.200	3.40	7.43	13.55
-0.210	3.50	7.82	14.51
-0.220	3.50	7.78	14.70
-0.230	3.35	8.63	15.88
-0.240	4.23	8.40	
-0.250	3.99	9.35	
-0.260	3.86	9.54	
-0.270	4.40	10.00	
-0.280	5.01	10.83	
-0.290	5.52	11.57	
-0.300	5.63	12.54	
-0.310	5.45		
-0.320	6.32		
-0.330	9.54		
-0.340	10.00		

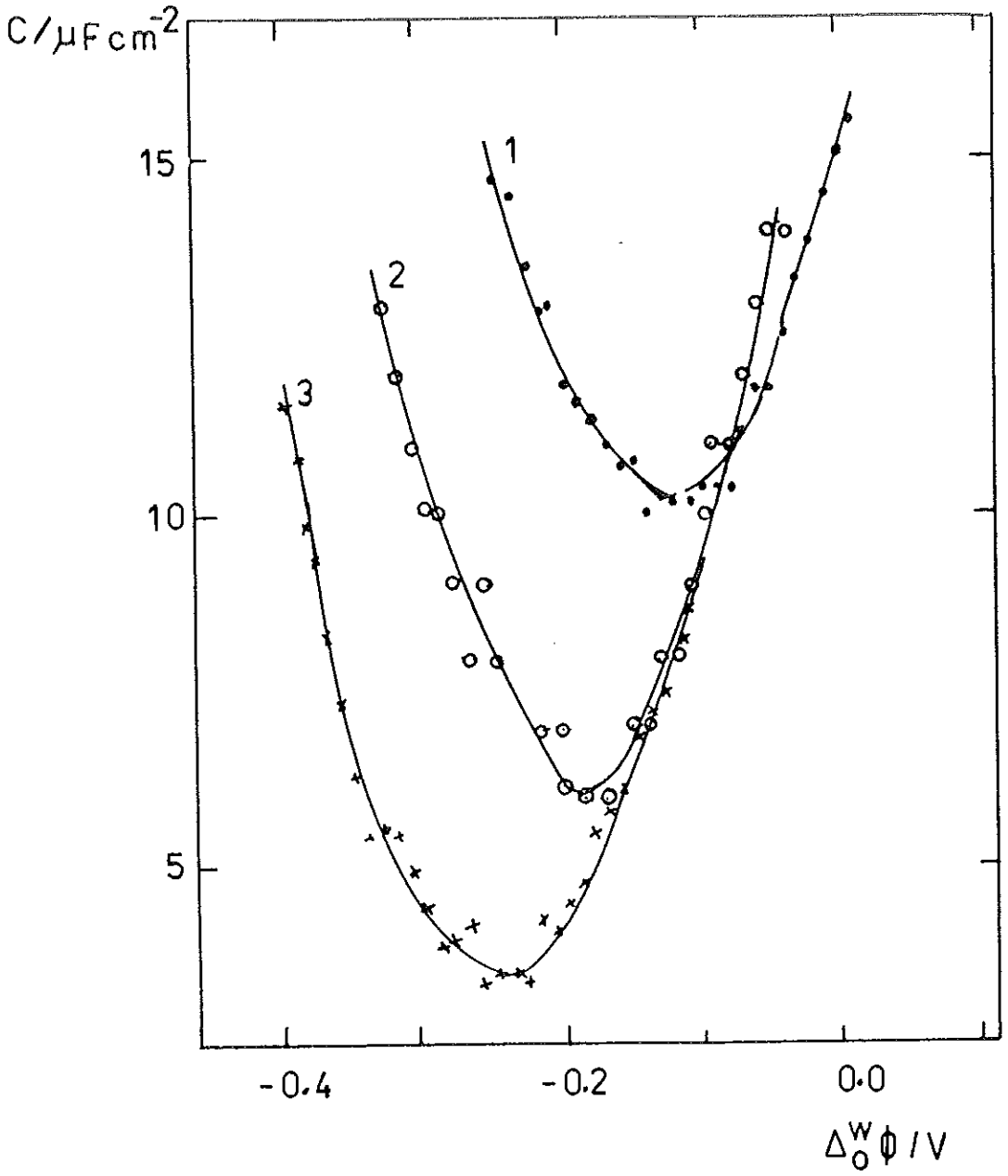

Fig. 5.3.15. Plots of the interfacial capacitance C vs $\Delta^{w}_{o}\phi$ for the system LiCl (w)/ PNPDCC (o-dcb). Electrolyte concentration: 50 mM (1), 10 mM (2), and 5 mM (3).

of C_d in the Gouy-Chapman theory is dependent on the electrolyte concentration. As a result one should take into consideration the effect of ion association which decreases the apparent concentration of the electrolyte. The degree of association of PNPDCC in o-dichlorobenzene was approximated to be 45% [15]. Hence, 2.8, 5.5 and 27.5 mM concentrations of PNPDCC were used in the calculations for the solutions prepared as 5, 10, and 50 mM respectively . For the computations, the assumption $\Delta^{w}_{o}\phi_{i}$ = constant = 0 was employed. The results of the calculation are tabulated in Table 5.3.6.

The calculated theoretical values of the capacitance minimums are in good agreement with the experimental results stressing the influence of ion association in the capacitance measurements. It appears that the observed shift in the capacitance minimums is due to the ion pair associations or adsorption. The adsorption of species at the interface could bring significant changes in the potential of the capacitance minimum since this latter quantity is the sum of the potentials due to the dipole orientation and adsorption [53]

$$\Delta^{w}_{o}\phi_{(cap.min)} = \Delta^{w}_{o}g_{(dipole)} + \Delta^{w}_{o}g_{(ads)} \qquad (5.2.3)$$

The contribution of $\Delta^{w}_{o}g_{(ads)}$ to $\Delta^{w}_{o}\phi_{(cap.min)}$ becomes highly pronounced particularly when ions of large size are employed in the organic phase [53]. The degree of surface adsorption is also enhanced when solvents of low polarity are used [54]. Different phenomena like imperfect adsorption equilibrium state and local concentration variations are also believed to affect the potential of the capacitance minimum [54]. Studies which were made on the adsorption of synthetic phospholipids on ITIES have also indicated the occurrence of a low capacitance minimum at negative potentials due to a strong potential dependent adsorption [55]. All these observations might be evidences for the existence of adsorbed species at the interface of the present system. However the strong shift

Table 5.3.6 Capacitance data obtained from the Gouy-Chapman theory for the water/o-dichlorbenzene interface at different concentrations of LiCl/PNPDCC.

$\Delta^{w}_{o}\phi$ / V	C/μF cm^{-2} 5 mM LiCl/ 2.8 mM PNPDCC	C/μF cm^{-2} 10 mM LiCl/ 5.5 mM PNPDCC	C/μF cm^{-2} 50 mM LiCl/ 27.5 mM PNPDCC
0.160	10.54	14.90	33.32
0.140	8.85	12.51	27.98
0.120	7.44	10.53	23.54
0.100	6.27	8.87	19.82
0.080	5.29	7.48	16.72
0.060	4.49	6.35	14.19
0.040	3.89	5.50	12.29
0.020	3.51	4.97	11.10
0.010	3.42	4.83	10.80
0.000	3.38	4.78	10.70
-0.010	3.42	4.83	10.80
-0.020	3.51	4.97	11.10
-0.040	3.89	5.50	12.29
-0.060	4.49	6.35	14.19
-0.080	5.29	7.48	16.72
-0.100	6.27	8.87	19.82
-0.120	7.44	10.53	23.54
-0.140	8.85	12.51	27.98
-0.160	10.54	14.90	33.32

of the capacitance minimum towards more negative potentials with decreasing electrolyte concentrations is not clear at this stage. Therefore, further work for the future is required to re-investigate the behaviour of the double layer of this system using alternative methodology, such as electrocapillary measurements. Moreover to understand clearly the cause of the potential shift, more quantitative measurements have to be carried out and the effect of different base electrolytes in both phases will have to be investigated systematically.

References

1. J. Koryta, Electrochim. Acta., 29 (1984) 445.
2. B. Hundhammer and T. Solomon, J. Electroanal. Chem., 157 (1983) 19.
3. Z. Samec, V. Marecek and M.P. Colombini, J. Electroanal. Chem., 257 (1988)147.
4. A.J. Bard and L.R. Faulkner, Electrochemical Methods, Fundamentals and Applications, John Wiley and Sons, New York, 1980.
5. M. Bond and J.O. Halloran, Anal. Chem., 48 (1976) 872.
6. R.A. Robinson and R.H. Stockes, Electrolyte Solutions, Butterworths, London, 1959.
7. M.H. Abraham and J. Liszi, J. Inorg. Nucl. Chem., 43 (1981) 143.
8. J.P. Coetzee and G.P. Cunningham, J. Am. Chem. Soc., 87 (1965) 2529.
9. Y. Marcus, Introduction to Liquid State Chemistry, Wiley, London, 1977.
10. F.J. Millero, Chem. Revs., 71 (1971) 147.
11. H. Alemu and T. Solomon, J. Electroanal. Chem., 237 (1987) 113.
12. A.F. Danil de Namor and H.T. Hill and E. Sigstad, J. Chem. Soc., Faraday Trans. 1, 79 (1983) 2713.
13. A.F. Danil de Namor and H. Berroa de Ponce, J. Chem. Soc., Faraday Trans. 1, 83 (1987) 1569.
14. H. Alemu and T. Solomon, J. Electroanal. Chem., 261 (1989) 297.
15. M.H. Abraham and A.F. Danil de Namor, J. Chem. Soc., Farady Trans. 1, 72 (1976) 955.
16. B. Hundhammer, private communication.
17. S. Kihara, M. Suzuki, K. Maeda, K. Ogura, S. Umetani, M. Matsui, and Z. Yoshida, Anal. Chem. 58 (1986) 2954.
18. J. Prasad and N.C. Petrson, Inorg. Chem., 8 (1969) 1627.
19. R. Farina and R.G. Wilkins, Inorg. Chem., 7 (1968) 514.
20. R. Farina and R. Hogg and R.G. Wilkins, Inorg. Chem., 7 (1968) 170.

21. E.S. Kucharski, B.W. Skelton and A.H. White, Aust. J. Chem., 31 (1978) 47.
22. R. Holyer, C. Hubbard, S. Kettle and R. Wilkins, Inorg. Chem., 5 (1966) 622.
23. E. Nakache, M. Dupeyrat, M. Vignes-Adler, Faraday Discuss., Chem. Soc., 77 (1984) 1.
24. The Interface Structure and Electrochemical Processes at the Boundary Between Two Immiscible Liquids, Ed. V.E. Kazarinov, Spriner-Verlag, Berlin, 1987.
25. W. Reiff, W. Bakerjun and N. Erickson, J. Amer. Chem. Soc., 90 (1968) 4794.
26. J.C. Imbeaux and J.M. Saveant, J. Electroanal. Chem., 44 (1973) 169.
27. M. Greness and K.B. Oldham, Anal. Chem., 44 (1972) 1121.
28. Z. Samec, J. Electroanal. Chem., 111 (1980) 211.
29. E.C. Constable, Adv. Inorg. Chem. Radiochem., 30 (1986) 69.
30. D. Homolka and H. Wendt, Ber. Bunsenges. Phys. Chem., 89 (1985) 1075.
31. J. Koryta, Electrochim. Acta, 29 (1984) 445.
32. H. Alemu, B. Hundhammer and T. Solomon, J. Electroanal. Chem., 294 (1990) 165..
33. J. Koryta, Electrochim. Acta, 24 (1979) 293.
34. M.H. Abraham and J. Liszi, J. Chem. Soc., Farady Trans. I, 74 (1978) 1604.
35. Y. Liu and E. Wang, J. Electroanal. Chem., 277 (1990) 305.
36. Handbook of Organic Analytical Reagents. Eds. K.L. Cheng, K. Ueno, T. Imamura, CRC Press Inc., Florida, 1982.
37. Z. Samec, V. Marecek and D. Homolka, J. Electroanal. Chem., 126 (1981) 121.
38. V. Marecek and Z. Samec, J. Electroanal. Chem., 149 (1983) 185.
39. P. Hajkova, D. Homolka, V. Marecek and Z. Samec, J. Electroanal. Chem.,

151 (1983) 277.

40. D. Homolka, P. Hajkova, V. Marecek and Z. Samec, J. Electroanal. Chem., 159 (1983) 233.
41. Z. Samec, V. Marecek and D. Homolka, Faraday Discuss. Chem. Soc., 77 (1984) 197.
42. T. Osakai, T. Kakutani, and M. Senda, Bull. Chem. Soc. Jpn. 57 (1984) 370.
43. Z. Samec, V. Marecek and D. Homolka, J. Electroanal. Chem., 187 (1985) 31.
44. Z. Samec, V. Marecek, K. Holub, S. Racinsky and P. Hajkova, J. Electroanal. Chem., 255 (1987) 65.
45. T.Kakiuchi and M. Senda, Bull. Chem. Soc. Jpn. 56 (1983) 1753.
46. F. Silva and C. Moura, J. Electroanal. Chem., 177 (1984) 317.
47. Southampton Electrochemistry Group, Instrumental Methods in Electrochemistry, Ellis Horwood Publishers, Chichester, 1985.
48. R. Reeves, in J. Bockris, B. Conway and E. Yeager (Eds.), Comprehensive Treatise of Eletrochemistry, Vol. 1, Plenum Press, New York, 1980, p.83.
49. D.M. Mohilner, in A.J. Bard (Ed.), Electroanalytical Chemistry, Vol. 1, Marcel Dekker, Ink, New York, 1966, p.241.
50. E. Gileadi, E. Kirowa-Eisner and J. Penciner, Interfacial Electrochemistry an Experimental Approach, Addison-Wesley Inc.,Massachusetts, 1975.
51. H.H. Girault and D.J. Schiffrin, J. Electroanal. Chem., 161 (1984) 415.
52. Z. Koczorowski, I. Paleska and J. Kotowski, J. Electroanal. Chem., 235 (1987)287.
53. Z. Koczorowski, J. Electroanal. Chem., 190 (1985) 257.
54. I.Paleska and Z. Koczorowski, J. Electroanal. Chem., 280 (1990) 439.
55. Z. Samec, Chem. Rev. 88 (1988) 617.

CHAPTER SIX

CONCLUSIONS

In the first part of these studies ion transfer across ITIES was made using different water/organic solvent systems. The aims of such investigations were:

(i) to screen organic solvents which could serve in the electrochemical studies of ITIES and thereby to examine the transfer behaviour of ions across the interfaces.

(ii) to determine the standard Gibbs energies of transfer of the ions across the interface and compare the results with theoretical values.

The chosen organic solvents were found to meet the necessary requirements such as immiscibility with water, relatively high dielectric constant and different density from that of water. Depending on the nature of the organic solvents, the obtained polarisable potential windows of the systems differ from each other. The relatively narrow potential range of the water/benzonitrile interface did not allow the investigations of hydrophilic ions such as NO_3^- ,I^- etc. On the other hand the water/o-dichlorobenzene system exhibited a wide potential range in which the transfer of many ions could be studied. However, the relatively low dielectric permitivity of o-dichlorobenzene and the limitation on the solubility of the base electrolytes were drawbacks of the system. The water/o-nitrotoluene interface gave a fairly wide potential range. From the studies made on these systems, it has been possible to observe the transfer of several ions and determine their standard Gibbs energies of transfer. The results were found to be in reasonable agreement with theoretical values. Comparisons of the experimental findings with the calculated values have also enabled to explain the states of the ions (hydrated or unhydrated) during the transfer process.

The second part of the studies involved the investigation of complex ion transfer and facilitated ion transfer across the water/organic solvent systems using terpyridine and biquinoline as ligands. The transition metal-terpyridine complexes have exhibited different voltammetric behaviour which depends on

the kind of the complex, metal to ligand concentration ratio and the pH of the solution. It has been possible to establish the relative stability of the complexes from the analysis of the voltammetric responses. The determination of ΔG^{o}_{tr} values of the complexes has also enabled the estimation of the ΔG^{o}_{tr} values of the metal ions by extrapolation. The results obtained have shown the potentiality of the techniques of voltammetry in analysing complex ions which transfer across ITIES.

The facilitated transfer of Cu^{+} across ITIES has also been shown to depend on the metal to ligand concentration ratios from which the transfer mechanisms were inferred.

Investigation of the electrical double layer at the water/o-nitrotoluene and water/o-dichlorobenzene interfaces was the final part of these studies. Analyses of the results of the ac impedance measurements have shown that the behaviour of the double layer at the water/o-nitrotoluene interface to be similar to that of the water/nitrobenzene system. The test which was made to check the existence of specific ionic adsorption has shown the absence of such effect. On the other hand an attempt has been made to explain the capacitance data which were obtained at the water/o-dichlorobenzene interface in terms of ion pair formation and adsorption effects. Nevertheless, it was not possible to give a full account for the observed phenomena. Therefore, it is believed that a further study using other techniques and different base electrolytes is required to reach a well established conclusion.

DECLARATION

I, the undersigned, declare that this dissertation is my work and that all sources of material used for the dissertation have been duly acknowledged.

Name Hailemichael Alemu

Signature 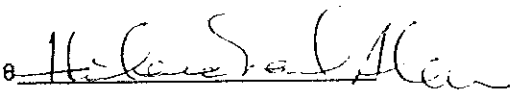

Place and date of submission: Chemistry Department Addis Ababa University, February 1991.